

TOPICAL REVIEW • OPEN ACCESS

Multiscale computational modeling techniques in study and design of 2D materials: recent advances, challenges, and opportunities

To cite this article: Mohsen Asle Zaeem *et al* 2024 *2D Mater.* 11 042004

View the [article online](#) for updates and enhancements.

You may also like

- [Exploring the Role of Molecular Intercalants in Electrochemical Production of Graphene-Based 2D Materials](#)
Zhenyuan Xia, Daheng Zhang, Sankar Sasidharan et al.
- [Ionic 2D Materials](#)
Eliseo Ruiz
- [\(Invited\) Two-Dimensional Phictogens: Van Der Waals Growth, Stability, and Phase Transformation](#)
Oussama Moutanabbir and Matthieu Fortin-Deschênes

2D Materials



TOPICAL REVIEW

OPEN ACCESS

RECEIVED
27 February 2024

REVISED
7 May 2024

ACCEPTED FOR PUBLICATION
16 July 2024

PUBLISHED
9 September 2024

Original content from
this work may be used
under the terms of the
[Creative Commons
Attribution 4.0 licence](#).

Any further distribution
of this work must
maintain attribution to
the author(s) and the title
of the work, journal
citation and DOI.



Multiscale computational modeling techniques in study and design of 2D materials: recent advances, challenges, and opportunities

Mohsen Asle Zaeem^{1,*} , Siby Thomas^{1,2} , Sepideh Kavousi¹ , Ning Zhang³ ,
Tanmoy Mukhopadhyay⁴  and Avik Mahata⁵ 

¹ Department of Mechanical Engineering, Colorado School of Mines, Golden, CO 80401, United States of America

² Department of Chemical Engineering, University of Florida, Gainesville, FL 32611, United States of America

³ Department of Mechanical Engineering, Baylor University, Waco, TX 76706, United States of America

⁴ Faculty of Engineering and Physical Sciences, University of Southampton, Southampton, United Kingdom

⁵ Mechanical and Electrical Engineering, Merrimack College, North Andover, MA 01845, United States of America

* Author to whom any correspondence should be addressed.

E-mail: zaem@mines.edu

Keywords: 2D materials, density functional theory, molecular dynamics, molecular mechanics, phase-field modeling, machine learning, properties, synthesis

Abstract

This article provides an overview of recent advances, challenges, and opportunities in multiscale computational modeling techniques for study and design of two-dimensional (2D) materials. We discuss the role of computational modeling in understanding the structures and properties of 2D materials, followed by a review of various length-scale models aiding in their synthesis. We present an integration of multiscale computational techniques for study and design of 2D materials, including density functional theory, molecular dynamics, phase-field modeling, continuum-based molecular mechanics, and machine learning. The study focuses on recent advancements, challenges, and future prospects in modeling techniques tailored for emerging 2D materials. Key challenges include accurately capturing intricate behaviors across various scales and environments. Conversely, opportunities lie in enhancing predictive capabilities to accelerate materials discovery for applications spanning from electronics, photonics, energy storage, catalysis, and nanomechanical devices. Through this comprehensive review, our aim is to provide a roadmap for future research in multiscale computational modeling and simulation of 2D materials.

Contents

1. Introduction	3
2. Electronic scale calculations: DFT	3
2.1. A short background on DFT	3
2.2. DFT calculations for determining properties of 2D materials	5
2.3. DFT based study and design of 2D materials for different applications	10
2.4. DFT integration with large scale simulations	12
3. MD simulation	13
3.1. Mechanical behavior and properties of 2D materials	13
3.2. Thermal behavior and properties of 2D materials	16
3.3. Oxidation behavior	19
3.4. Desalination behavior	19
4. Lattice and continuum-based molecular mechanics modeling of 2D materials	20
4.1. Mechanical equivalence of atomic bonds and effective elastic moduli	22
4.2. Numerical results and comparative assessment of accuracy	24
5. Artificial intelligence and ML assisted study and design of 2D materials	25
5.1. ML-assisted potentials and force fields	26
5.2. Non-intrusive approaches for ML-assisted prediction of physical properties	26
5.3. Image-based computational mapping using ML	27
5.4. Exploiting ML for probabilistic analysis and uncertainty quantification	28
5.5. ML-based investigation of multi-layer 2D heterostructures	29
6. Multiscale modeling and synthesis of 2D materials	30
6.1. Experimental synthesis techniques	30
6.2. DFT colocations relevant to experimental synthesis of 2D materials	31
6.3. MD simulation facilitated synthesis techniques	34
6.4. Micro/meso scale: PF approach	37
6.5. Continuum modeling and ML in the synthesis of 2D materials	43
7. Evolving trends and future directions	45
7.1. Electronic scale calculations	45
7.2. MD simulations	45
7.3. Molecular mechanics	46
7.4. PF modeling and other microscale models	47
7.5. Artificial intelligent and ML	47
8. Concluding remarks	48
Data availability statement	48
References	48

1. Introduction

Two-dimensional (2D) materials are single atomic or molecular layered materials that exhibit remarkable properties. There exist different 2D lattice structures based on their atomic compositions and arrangement of atoms with one atomic layer (graphene, h-BN, RuC, BP, planar carbon allotropes, BCN, etc), two-atomic layers (silicene, borophene, phosphorene, etc), and three-and more atomic layers (MoS₂, Ti₂C MXenes, Ti₂CF₂, etc) [1]. The exceptional properties of 2D materials, including excellent electrical conductivity, mechanical strength, and optical transparency have positioned them as the building blocks of next-generation of electronic [2], optoelectronic [3], nanomechanical [4], and thermoelectrical [5] devices. Several overview articles exist which described the origin [6–8], synthesis methods [9–12], characterization techniques [9, 13–15], and applications [9, 15–17] of 2D materials. This present article aims to review the recent progress, challenges, and future prospective of multiscale computational modeling techniques in study and design of 2D materials.

Computational models and simulations allow for in-depth exploration of structures, properties, behaviors, and functionalities of materials across various length and times scales. The atomistic scale simulation models consider atoms as the building blocks of the material and study how atoms and molecules interact, move, and form structures. They employ principles from quantum mechanics and molecular dynamics (MD) to describe fundamental mechanisms which give rise to intrinsic material properties [18–20]. Continuum models, on the other hand, consider the material as if it were a continuous homogeneous medium rather than discrete particles [21]. They are described by partial differential equations derived from principles like conservation of mass, momentum, and energy [22–24]. Continuum mechanics describes the material's behavior at scales relevant to the engineering and macroscopic processes [21]. As a result, they fail to predict the complexities of material behavior that is rooted in the interplay between localized chemical composition, environmental/working conditions, and various microstructural features such as voids, cracks, phases, grains, dislocations [25–31]. Mesoscale models are alternative techniques that bridge the timescale and length-scale gaps that exist between atomistic and continuum models. There are different mesoscale modeling techniques, including but not limited to Kinetic Monte Carlo [32, 33], phase-field (PF) and PF crystal models [34–40].

Computational modeling and simulations mostly complement the experimental synthesis, characterization and testing to accelerate the study and design

of materials, explain physics associated with materials phenomena [41, 42], or calculate material properties which are hard, if not impossible, to determine by experiments [43, 44]. They are even capable of designing and optimizing properties of materials which have not been experimentally synthesized yet [45]. Another advantage of computational modeling is the ability to efficiently explore a wide range of structures and properties of materials, which may be challenging, costly and time-consuming through experiments alone [42, 46, 47]. Additionally, they have the unique ability to isolate specific properties or phenomena within complex experimental setup where the limitations on the external factors, such as temperature or humidity, affect the reproducibility and reliability of the results.

The physics driven computational models have proven their potential in predicting the relationship among processing, nano/microstructure, and mechanical properties [48–51]. However, they always suffer from the high computational costs. Recent advancements of data-driven computational models [52–57] and deep learning techniques [58–61] have facilitated acceleration of modeling predictions and improved the computational performance in identifying the specific compositions and nano/microstructures based on the processing methods and target material properties.

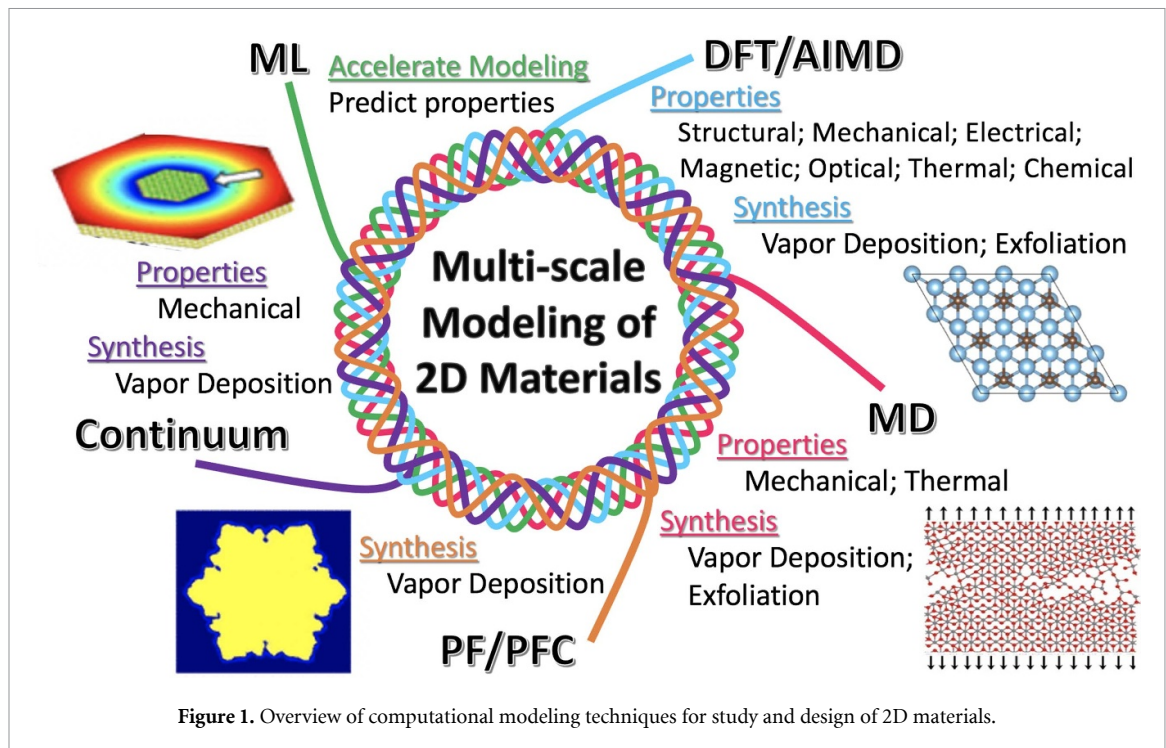
In this comprehensive review, we first discuss the role of computational modeling techniques in accelerating the understanding of structures and properties of 2D materials. Then, we will review different length scale models that can help synthesis of 2D materials. Figure 1 shows a schematic integration of multiscale computational techniques that we considered in this article, including, density functional theory (DFT), ab-initio MD (AIMD), MD, PF, PF crystal (PFC), continuum (continuum-based molecular mechanics), and machine learning (ML).

2. Electronic scale calculations: DFT

DFT technique has emerged as one of the promising tools for analyzing the structures and properties of various classes of materials, including 2D materials. Due to its solid mathematical foundation, DFT opens up paths for material discovery and tailoring material properties for specific applications.

2.1. A short background on DFT

Hohenberg and Kohn established the foundation of DFT [62] which states that by knowing the electron density, one can accurately determine the energy of the ground state, i.e. $E = E[n(\mathbf{r})]$. Later, Kohn and Sham [63] developed the mathematical formulation of DFT using a set of equation, known as Kohn–Sham (KS) equations which serve as the foundation of



the DFT methodology. In this way, the KS equations provide a bridge between the intricate many-electron system and the quantum mechanics described by the Schrödinger equation [64–66]. The key challenge of solving the many-electron problems, which involves addressing the Schrödinger equation through a self-consistent approach [67] is then achieved through the KS approach. In the self-consistent scheme, at first, a tentative electron density $n(r)$ is considered. This density forms an electron cloud and plugs that in an exchange correlation (XC) functional (V_{xc}) and eventually builds the effective potential V_{eff} . This will supply the eigenvalues (ϵ_j) and eigenvectors (ϕ_j) of the KS equations. Having the eigenvectors (ϕ_j), a new set of electron density $n(r)$ can be achieved, and this process is repeated until the convergence is reached [67]. More details on DFT methodology can be found elsewhere [68].

2.1.1. Role of XC functionals in calculating properties by DFT

DFT, although formally exact, requires a series of approximations for practical implementation in solving the KS equations. A series of XC functionals such as local spin density approximation (LSDA or LDA), generalized gradient approximation (GGA), and meta-GGA approximation have been proposed to build an exact DFT method. The LDA is well-suited for computations involving ground-state properties like total energy, and lattice constants. However, LSDA tends to underestimate certain properties, particularly those associated with electronic correlation. The GGA approximation [69] is built from LDA and is notable for its flexibility and is the most used

approach for predicting different properties of 2D materials by balancing the quantitative prediction and computational cost. Further, meta-GGA approximation was introduced that improves upon GGA functionals by introducing the KS kinetic energy as a new component, in addition to the uniform spin densities of an electron gas. The meta-GGA offers enhanced accuracy for molecular properties such as surface energies, reaction barriers and non-covalent interactions [70, 71].

Although the commonly used semi-local LDA, GGA or meta-GGA have been successful in the study of non-magnetic (close shell) molecules and solids, they may fail in systems which involve un-paired and localized electrons due to delocalization error [72], and often leads to misleading prediction regarding magnetic materials [73]. Recently, a hybrid functional was proposed which holds remarkable success in predicting the electronic and magnetic properties of many magnetic systems, including 2D materials [74]. For the electronic properties, this hybrid functional helps overcoming the band-gap underestimation of GGA functional. Studying strongly correlated systems, such as d electrons in transition metal based 2D materials, necessitates the incorporation of auxiliary theories, such as the Hubbard U parameter [75]. The on-site Hubbard-corrected DFT + U approach [75] accounts for d - and f - electron contributions of transition metals-based 2D materials. This approach can effectively remedy the excessive delocalization of d and f electrons in standard LDA or GGA [76] and leads to significant improvement of the description of magnetic properties in 2D materials like MXenes consisting of transition metal atoms such as Ti and V.

Since a detailed understanding of thermal properties such as vibrational properties and heat capacity required the knowledge of anharmonic effects, advanced methods beyond standard DFT, such as density functional perturbation theory (DFPT) and phonon calculations, are often employed [77, 78]. While DFT continues to be the primary method for ab initio modeling of ground-state properties, the cutting-edge approach for elucidating electronic and optical excitations of 2D materials is presently the many-body perturbation theory (MBPT) based on Green's function methodologies [79]. Band structures, incorporating quasi-particle (QP) corrections, are derived using the GW (G: Green's function, W: Coulomb interaction) scheme [80], and absorption spectra, encompassing excitonic effects, are computed through the solution of the Bethe–Salpeter equation (BSE) [81]. It should also be noted that traditional DFT methods, which do not explicitly include van der Waal's (vdW) interactions, can lead to inaccurate predictions of interlayer distances, binding energies, and other properties of 2D materials. To overcome this limitation, vdW corrections can be introduced into the DFT calculations to capture the non-local, long-range correlation effects associated with vdW forces [82, 83]. From the aforementioned details, it is clear that selection of an ideal DFT functional is important when considering different properties and diverse applications of 2D materials.

2.2. DFT calculations for determining properties of 2D materials

2D materials, such as graphene [84], transition metal dichalcogenides (TMDs) [85], and MXenes [86], have garnered significant attention due to their unique properties and characteristics [87]. DFT, as a first-principles quantum mechanical approach, can provide accurate prediction of ground-state properties and offer valuable insights into the diverse applications of 2D materials. In the following, we summarize previous DFT calculations for determining different properties of 2D materials, and in section 2.3 we provide some insights into study and design of 2D materials for different applications.

2.2.1. Stability of 2D structures

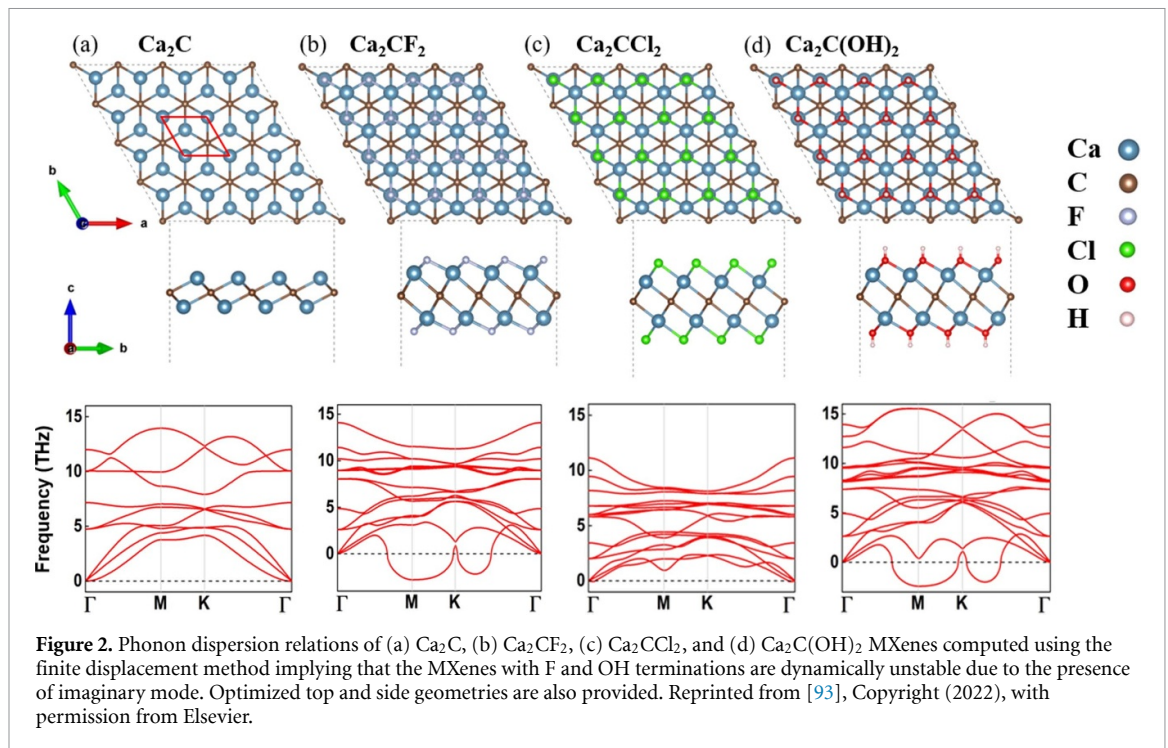
The stability analysis of 2D materials is crucial for any type of applications. The structural arrangement of atoms in a material directly influences its physical and chemical properties, and the ground state energy from DFT gives first-hand information about the most stable atomic configurations. By computing the cohesive energy (E_C), one can estimate the stability of a structure, and this can be used as the first step in designing 2D materials. A higher (negative) cohesive energy generally indicates stronger intermolecular or interatomic forces, leading to more stable structures. E_C of a 2D material containing two elements,

say A and B , can be calculated using this relation:

$$E_C = (E_{2D} - aE_A - bE_B) / (a + b) \quad (1)$$

where E_{2D} is the total energy of the 2D simulation cell, a and b are the number of atoms in A and B , and E_A and E_B are the total energies of free A and B atoms, respectively. Among 2D materials, graphene is considered as the most stable one with E_C in this range 7.5–7.9 eV atom⁻¹, which was calculated by DFT using different functionals [88–90]. The E_C of some other important 2D materials were calculated by DFT, such as MoS₂ (4.98 eV atom⁻¹), RuC (7.31 eV atom⁻¹) [91], Si₂BN (6.22 eV atom⁻¹), and phosphorene (3.30 eV atom⁻¹) [92]. From the above details it is evident that MoS₂ possesses higher stability compared to phosphorene, i.e. a higher E_C indicates the higher stability and feasibility of the material for synthesis and further utilization. Since E_C analysis is the first step in establishing the structural stability of a material, more detailed analysis based on phonon and mechanical stability is also important and are discussed below.

Phonon analysis stands as a crucial criterion for assessing the stability of 2D materials. In the equilibrium state, the potential energy of the system consistently rises concerning any combination of atomic movements. This characteristic allows us to leverage vibrational spectra as a filter to validate material stability, with the presence of imaginary frequencies implying that the material is unstable, as shown in figure 2. It is noteworthy that the phonon filter stands as the most widely employed method in the stability analysis of 2D materials, and a wealth of phonon spectra is now publicly accessible through the Materials Cloud database [94]. Despite its widespread use, phonon analysis alone is insufficient to demonstrate the dynamic stability of a material [93]. This limitation arises from the fact that phonon analysis primarily deals with small atomic displacements, rendering it incapable of capturing phase transitions coupled with intricate lattice reconstructions [95]. However, to ensure dynamical stability, it is essential to demonstrate that a material, particularly at the first-principles level, remains structurally stable without undergoing energy-reducing changes. This verification is typically achieved through AIMD simulations. To assess the dynamic stability of 2D materials, AIMD simulations incorporating annealing steps at a fixed temperature are employed. Various temperature protocols, such as quenching steps, may be utilized. Given that AIMD simulations are constrained by the limited size of modeled systems (typically a few hundred atoms), energy fluctuations can overshadow those associated with structural changes. Furthermore, DFT is instrumental in exploring phase diagrams by predicting the thermodynamic stability of different phases of a material under varying conditions of temperature and pressure [96, 97].



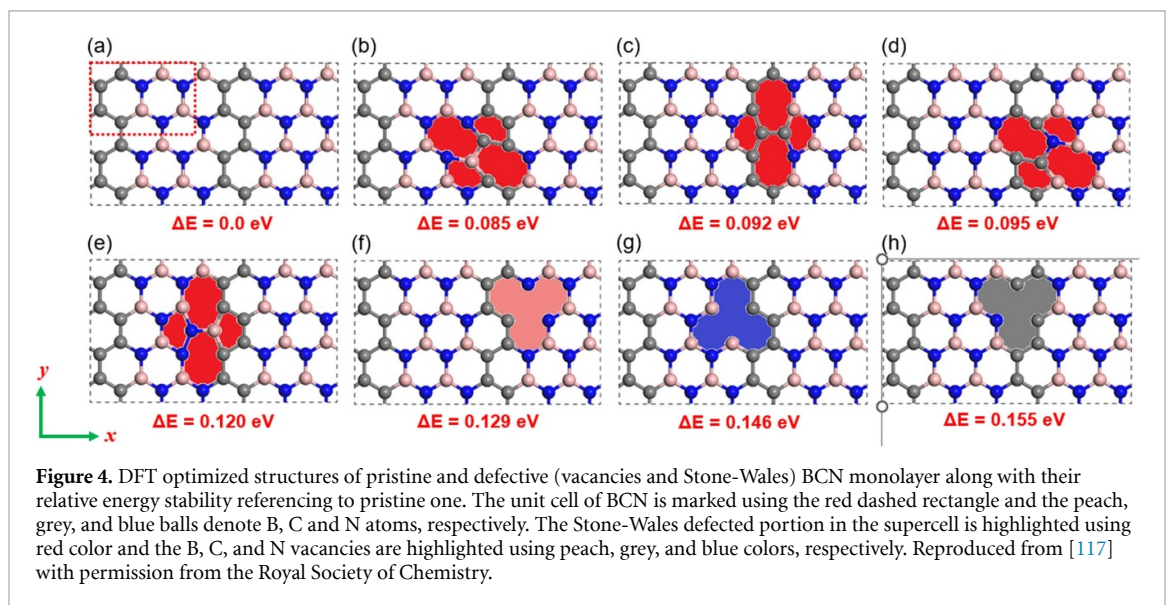
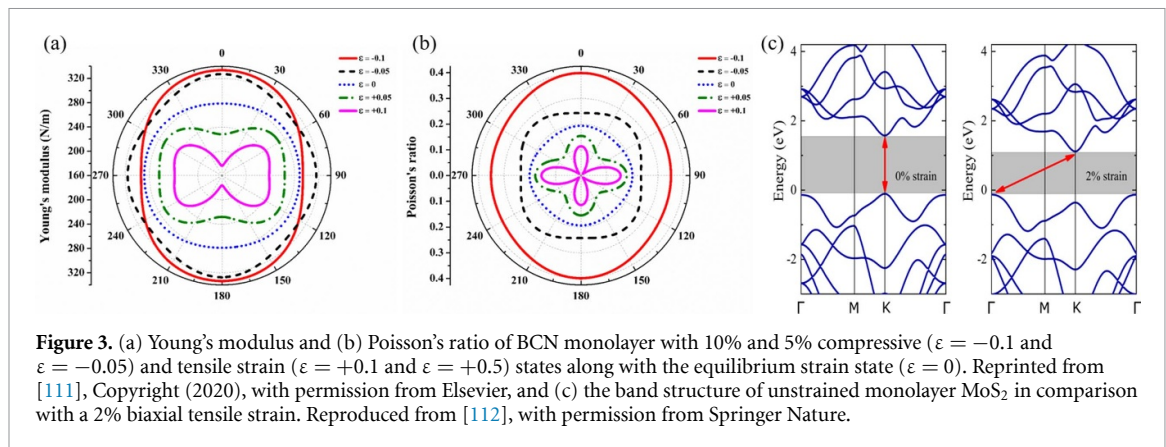
However, relying solely on the potential energy profile is inadequate as a criterion for dynamic stability. Nonetheless, this analysis provides valuable insights into the material's stability, and the pace of material development can be accelerated significantly, reducing the time and cost associated with experimental synthesis and characterization.

Mechanical property analysis is another key criterion in establishing the stability of a 2D material. In 2D materials, the high surface area [7, 98] leads to the formation of strong in-plane bonds, providing exceptional structural features, including bond strength, which contributes to the high mechanical strength of most 2D materials [99]. In order to establish the mechanical stability of a 2D material, the Born stability criterion [100] can be utilized which forms a set of necessary and sufficient conditions to determine whether a given unstressed material is stable or not. For the case of 2D materials, the mechanical stability criterion is represented using the Voigt representation as: $C_{66} > 0$ and $C_{11}C_{22} - C_{12}^2 > 0$ [101], whereas C_{11} and C_{22} are the in-plane elastic constants along the x and y directions, and C_{12} is the shear strain along the xy plane. In an study using DFT, the elastic properties of 90 different 2D MXenes were determined, producing useful data with respect to mechanical stability for the synthesis of 2D MXenes [102]. DFT has proven as a useful tool in predicting the tensile strength of novel 2D materials, predicting similar strengths to that of experiment [103–108]. Besides, to establish the isotropic or anisotropic characteristics of a 2D material, the angular dependent polar diagram can be used. For example, figure 3, shows the results of a previous study establishing that the BCN monolayer

possesses both isotropic (anisotropic) characteristics and is evident in the circular (non-circular) behavior of the polar diagram. Predictions of ideal strength are made using variations of the DFT method, such as DFPT to study phonons in 2D materials as the material is strained [105]. Using DFT, 2D materials can be systematically strained, observing the stability of the phonons as strain is applied. When they grow unstable, the material is considered to have reached peak stress [105, 109, 110]. The prediction of strength and strength trends among 2D materials is valuable in the efforts of developing improved 2D materials, and one of the important contributions that the DFT method provides.

2.2.2. Influence of electronic scale defects

Like any other material, 2D materials contain crystalline imperfections in their structure, both native defects and extrinsic defects, ranging from vacancies and substitutions to interstitials. Point defects, such as vacancies, emerge as omnipresent entities significantly shaping the characteristics of crystalline materials, as shown in figure 4. For example, in the case of MXenes, these defects originated from either the precursors (the bulk MAX phases) or during their processing by chemical wet etching or exfoliation [113]. In contrast to non-planar 2D materials like TMDs and MXenes, planar 2D materials such as graphene, h-BN, BCN, Si_2BN , etc, exhibit a unique lattice property which is the ability to reconstruct by forming non-hexagonal rings, leading to the creation of topological defects [114]. A notable example is the Stone-Wales (SW) defect (see figures 4(b)–(e)), where four hexagons transform into two pentagons and two



heptagons [SW (55–77) defect] through the rotation of one C–C bond by 90°, without any added or removed atoms [115]. DFT provides a valuable understanding of the effects of defects in 2D materials and elucidates how these defects influence their structural, electronic, and optical properties. This makes DFT an indispensable tool for interpreting experimental results on the effects of defects, including (magneto-)optical experiments [116]. However, the complexity of defect calculations poses a major challenge, even in low-throughput mode, involving considerations of large supercells, local magnetic moments, and electrostatic corrections. By analyzing the vacancy formation energy (E_{VFE}) [117–119], one can establish the favorable formation of different 2D materials with the presence of defects. The VFE can be computed using this relation:

$$E_{VFE} = E_{defect} - E_{perfect} + n_i \mu_i \quad (2)$$

where E_{defect} and $E_{perfect}$ are the total energies of a defective and pristine 2D surface, respectively. n_i is the total number of vacancies in the 2D material, and μ_i is the chemical potential of the atoms present

in the system which are taken as the bulk energy of their most stable state. As it is a common convention, most of the studies assumed that the chemical potential is equal to the total energy of the bulk systems. Although most DFT results are strictly valid for the zero Kelvin case [120, 121], the thermodynamic associated properties including thermal expansion and thermoelasticity at finite temperatures within the DFT perspective can be estimated from DFPT by using the quasiharmonic approximation (QHA) to account for the anharmonicity of the lattice vibrations [122]. Comparing the formation energies of different defect types allows researchers to identify the most stable defects under specific conditions. For example, in 2D Si₂BN, it was reported that Si (3.25 eV) and B (2.27 eV) monovacancies possess the highest and lowest formation energies, respectively. However, these values indicate that they are both lower than that of graphene (7.5–7.84 eV) [114] and BCN monolayers (6–8 eV) [111], therefore both are thermodynamically favorable defects in 2D Si₂BN. Since defects can introduce new energy levels within the band structure, influencing electrical conductivity and other electronic characteristics, a

detailed and fundamental understanding of defects becomes inevitable. DFT emerges as a powerful tool for unraveling the intricate effects of defects.

2.2.3. Electronic properties and role of lattice strain

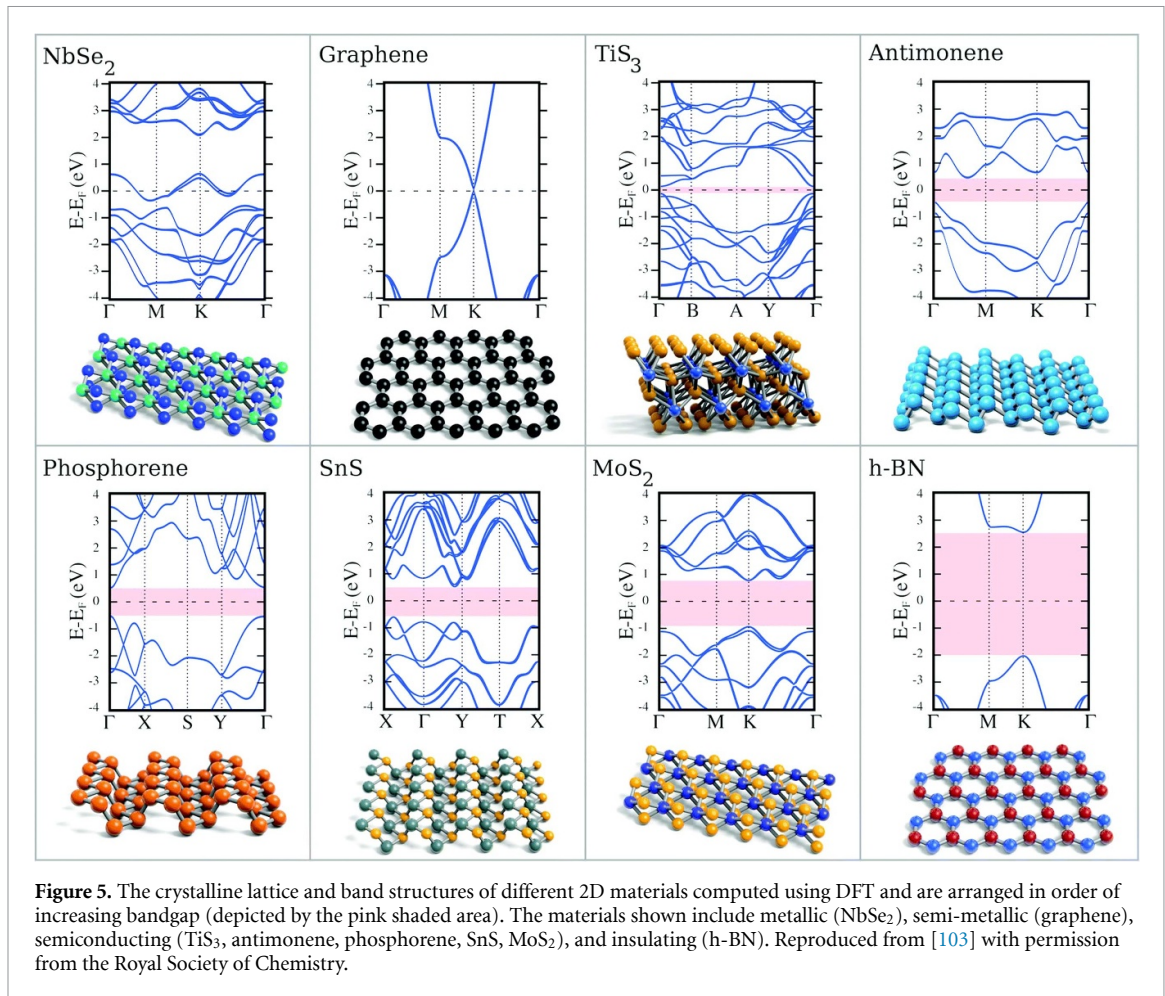
Due to the layered nature of 2D materials, quantum confinement effects become prominent, leading to electron accumulation at the surface, enabling effective tuning and control of electronic properties [123]. Band structure and density of states (DOS) are the two important electronic properties obtained from DFT calculations, providing fundamental insights for designing electronic devices and understanding transport properties. For most ground-state properties, GGA functionals, available in both *ab initio* and semi-empirical variants, offer sufficient accuracy [124]. Additionally, expensive hybrid functionals, incorporating some exact Hartree–Fock exchange, prove effective in describing the bandgap of materials with experimental accuracy. However, the hybrid functional is unsuitable for metals due to the unphysical logarithmic singularity of Hartree–Fock band energies at the Fermi level—the energy level that separates occupied from unoccupied states [125]. In metals, where occupied states exist around the Fermi level, this artifact leads to the generation of fictitious charge and spin density waves [126]. The on-site Hubbard-corrected DFT + U approach [75] accounts for d- and f- electron contributions of transition metals-based 2D materials. This approach can effectively remedy the excessive delocalization of d and f electrons in standard LDA or GGA [76] and leads to significantly improve the description of electronic properties in 2D materials like MXenes consists of transition metal atoms such as Ti and V.

DFT + U represents a refined yet more cost-effective version of the hybrid XC functional, introducing exact exchange only for localized open-shell electrons, where the ‘self-interaction error’ (arising from approximate exchange) is most significant, as opposed to applying it to all electrons, as in hybrid XC. Delocalized electrons are handled with standard XC density functionals [127]. DFT + U theory significantly enhances the description of materials exhibiting this mixed type of electron distribution, particularly mid-to-late first-row transition metal oxides and sulfides [128]. DFT remains a valuable tool for studying electronic properties, providing insights that are difficult or impossible to obtain experimentally. Figure 5 represents the band structures of different planar and buckled 2D materials such as metallic NbSe₂, semi-metallic graphene, semiconducting TiS₃, antimonene, phosphorene, SnS, MoS₂, and insulating h-BN [103] computed using the Perdew–Burke–Ernzerhof (PBE) [69] functional. The PBE functional implemented using GGA approach is the most used approach for predicting different properties of 2D materials by balancing the quantitative prediction and computational cost.

A key factor affecting electronic properties is lattice strain in 2D materials [111]. Unlike 3D traditional materials, 2D materials can withstand remarkably large mechanical strain, up to 10%. Tailoring strain levels enables control over electronic, mechanical, and optical properties, making it essential for applications in sensors, flexible electronics, and strain-engineered devices. Our prior research using PBE functional demonstrated that Young’s modulus and Poisson’s ratio in a BCN monolayer exhibit significant anisotropy under strain (see figures 4(a) and (b)), showing an increase during compressive strain and a decrease with tensile strain. This effect of strain is also responsible for altering the direct equilibrium bandgap of 2D materials, and an example for MoS₂ is shown in figure 4(c). Peto *et al* used DFT to study the band structure of monolayer MoS₂ for with no strain and under 2% biaxial tensile strain [112]. The comparison reveals a reduction in the bandgap of 0.46 eV and a transition from a direct to an indirect bandgap, as shown in figure 4(c). This shift is attributed to the downward movement of bands near the K point concerning the Fermi energy due to the strain-induced modification of orbital overlaps. By employing DFT calculations, López-Galán *et al* studied the electronic structure and transport properties of Van der Waals multilayer and multi/single-layer of MoS₂/MoSe₂ and MoSe₂/MoS₂ heterostructures with a zigzag and chalcogen–chalcogen interlayer alignment [129]. This study shows that the shift in bandgap at the interfaces is strongly related to the interlayer coupling due to induced strain and subsequent reallocation of metallic d-orbital and chalcogen orbitals in energy levels inside the band gap. In another case, it has been reported that the compressive and tensile strains alter the direct equilibrium bandgap in the BCN monolayer (1.18 eV) to 0.59 eV and 1.53 eV along the zigzag direction [111]. Corresponding variations in the armchair direction are 1.47 eV and 0.76 eV under compressive and tensile strains, respectively. It is evident that DFT can predict strain effects on electronic properties of 2D materials and identify critical points where the material undergoes changes under specific strain conditions.

2.2.4. Magnetic and optical properties

The magnetism in 2D materials has been an emerging and rapidly growing research field. First-principles DFT calculations, with or without considering spin-orbit coupling (SOC) [130], is an efficient approach in computing the magnetic parameters, such as magnetic moment, exchange integral, Magnetic Anisotropy Energy (MAE), and Curie temperature (T_C) of 2D magnetic materials. Furthermore, a combination of DFT and Monte Carlo (MC) simulations employing the Heisenberg model [131] allows for the tracking of magnetization variation with temperature, enabling the determination of the magnetic



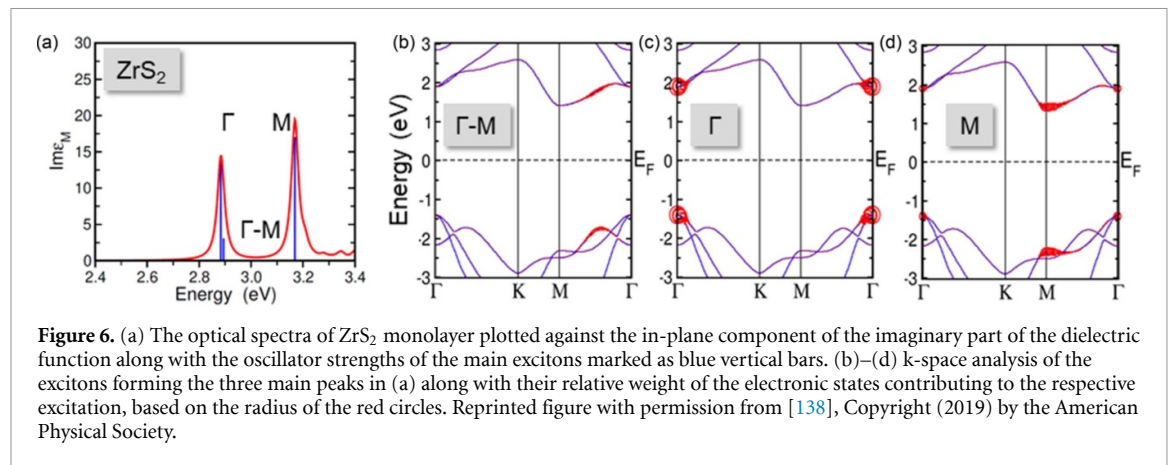
transition temperature for 2D materials. For instance, DFT calculations [132–134] determined the ferromagnetic (FM) nature of 2D CrI₃, and this behavior was later experimentally verified [135]. The DFT reported magnetic moment and Curie temperature ranged from 3 to 3.44 μ B per formula unit and 61–107 K, respectively. Notably, the magnetic behaviors of single- or few-layer sheets of α -RuCl₃, VSe₂, VTe₂, NbTe₂, and CrGe(Si)Te₃ have also been explored through DFT calculations [136]. In addition, DFT analysis can provide an in-depth understanding of effects of dopants and defects on magnetic properties, and this can efficiently accelerate the screening of 2D magnetic materials [45].

To accurately estimate the optical spectra of materials, precise prediction of excited states is essential. While DFT is the cornerstone for determining ground-state properties (as discussed in section 2.2.1), the most advanced method for describing electronic and optical excitations relies on MBPT based on Green's function approaches [79]. Despite its computational cost, MBPT is indispensable for establishing the band gap in semiconductor systems, particularly when accounting for electron-electron correlations through the GW approach. This advanced theory, when integrated with DFT, unravels photon absorption, electron-hole interactions, and

electron-photon scattering mechanisms in semiconductors, including 2D materials.

By employing DFT simulations using GGA-PBE functional, it was shown that the hydrogenated penta-Pt₂N₄ monolayer significantly enhances the electronic bandgap from 1.10 eV to 2.70 eV. This study also demonstrated that hydrogenated Pt₂N₄ displays a weak and strong optical absorption in the visible and ultraviolet regions, respectively [137]. In a separate work [138], the optical property analysis of monolayer ZrS₂ (bandgap: 2.8 eV) using the GW approach shows two intense peaks formed by bound excitons with large oscillator strengths, as shown in figure 6(a). Here, the lowest-energy peak is observed at 2.68 eV, and the k-space analysis of the excitons forming the three main peaks is shown in figures 6(b)–(d). This study also suggests that replacing the ZrS₂ component within the ZrS₂/HfS₂ heterostructure significantly enhances the dissociation of intralayer excitons in ZrS₂, resulting in a higher photoelectron generation rate. Such quantitative analyses of electronic and optical properties using DFT offer a comprehensive understanding of material properties, opening avenues for next-generation optoelectronic device applications [138].

The Moiré pattern, or Moiré superlattice, is another key property of 2D materials, characterized



by the overlapping of two analogous layers, resulting in a distinct periodicity [139]. Variations in lattice constants, translational shifts, or twisted angles between the layers can alter the periodicity of the Moiré superlattice [140]. In the case of magnetic 2D materials, these superlattices can significantly influence the magnetic properties of the system, such as magnetic anisotropy, spin polarization, or magnetic coupling between layers. By precisely controlling the stacking configuration and interlayer interactions of magnetic materials, these magnetic properties can be effectively tuned through the manipulation of the Moiré pattern. Notably, Ramos *et al* demonstrated a rapid transition from a semiconductor state to a metallic state of 2 H-MoS₂ at approximately 10° of rotation [141]. Additionally, their analysis of the band structure within the range of 0° < θ < 90° revealed a reversal state from metallic to semiconductor upon rotation reaching 90°.

2.3. DFT based study and design of 2D materials for different applications

Most promising applications of 2D materials, including batteries, catalysis, and sensing, belong to the category of host-guest chemistry (HGC). Most types of HGCs are governed by the physisorption of the guest atoms or molecules on the surface of the 2D materials, in which the adsorbates are held onto the surface of the absorbent by weak Van der Waals forces. This type of analysis is beneficial for many applications, including alkali-ion battery electrodes [142], and bio and gas sensing [143, 144]. On the other hand, during chemisorption, the adsorbates are bound to the host material by chemical bonds as mostly seen in catalysis [145].

The DFT is an ideal tool for estimating the adsorption capability of a guest atom or molecule on the surface of a 2D material by computing the adsorption energy using this relation:

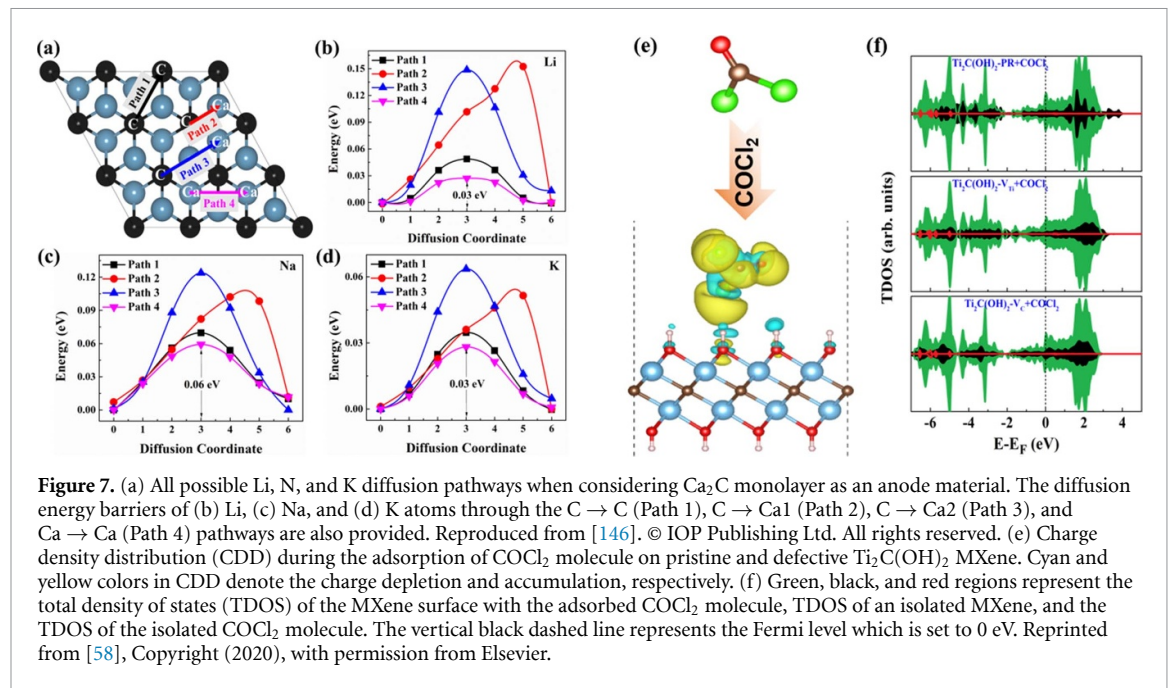
$$E_{ads} = E_{2D+guest} - (E_{2D} + E_{guest}) \quad (3)$$

where $E_{2D+guest}$ is the total energy of the lowest energy configuration of the 2D material with the adsorbed

guest entity, E_{2D} is the total energy of the 2D structures without the adsorbed guest entity, and E_{guest} is the total energy of the individual guest atom or molecule. By analyzing the adsorption energy, one can find the most stable geometries of the host-guest configurations. According to equation (3), a negative value of adsorption energy shows that the adsorption process is spontaneous and exothermic, which is crucial for deciding the feasibility of a host material for an HGC application. DFT is the most suitable approach in estimating the distinct adsorption behaviors of different types of guest atoms and molecules on surfaces of 2D materials by analyzing the degree of chemisorption and physisorption, as well as different levels of charge transfer, electronic properties, and host-guest distance [142].

2.3.1. Metal ion batteries

DFT approach is widely used in estimating the properties of different materials for metal-ion battery (MIB) electrode applications. In the case of 2D materials for use in MIBs, the HGI occurs when guest alkali atoms are absorbed onto the surface of a 2D material, and DFT can determine the adsorption energy. However, adsorption energy is not the sole determinant for estimating the potential of a 2D material in MIB applications. Charge transfer processes between the electrode and electrolyte as well as electrode and the metal-ions, essential for battery operation, can be studied through DFT by examining electronic structure changes during charge and discharge cycles. Additionally, DFT predicts open-circuit voltage by calculating the electrochemical potentials of redox couples. The method also simulates volume expansion upon ion intercalation, offering crucial information about structural stability during cycling. Moreover, DFT assesses the impact of defects, such as vacancies, on the electronic and structural properties of 2D materials, contributing to a comprehensive understanding of their performance in battery applications. DFT is instrumental in evaluating diffusion barriers and the nudged elastic band (NEB) approach ensures the proper understanding of the diffusion



properties of alkali atoms, and utilizing this capability, a previous study investigated the diffusion barrier of Li/Na/K on Ca_2C MXenes [146], as shown in figure 7. This study considered all the possible metal adatom diffusion kinetics pathways as shown in figure 7(a) and revealed ultra-low diffusion barriers of Li, Na, and K adatoms on Ca_2C MXenes ensuring superionic mobility. This can effectively reduce the charging time and thus making Ca_2C MXenes to be potentially excellent anode materials for MIBs. Studies also demonstrated that defects such as vacancies, SW defects, and other topological defects in 2D materials act as a potential trap with active sites for the adsorption of alkali-metal atoms, thus enhancing the metal-ion conduction, suitable for battery performance [147]. In the case of 2D MXenes, the vacancy defect can enhance the adsorption of Lithium ion near the defective region [148]. In 2D BC_3 monolayer, the SW defect incorporation provided an enhanced capacity of 1287 mAhg^{-1} , compared to its pristine form (1144 mAhg^{-1}) [142] and conventional MIB electrodes, such as graphite with a capacity of 372 mAhg^{-1} [149].

2.3.2. Gas and bio sensors

The gas and bio sensing applications of 2D materials are another notable area in which DFT can be effectively used. The primary distinction between sensing applications and battery technologies lies in the specific property of interest that can enable efficient sensing technologies. In sensing, the focus is often on properties such as conductivity, resistivity, or changes in electrical characteristics. The conductivity of a material may change when exposed to certain gases and calculation related to electronic structure, energy levels, desorption time, and charge transport

properties are crucial in understanding and predicting these changes for effective sensor design. On the other hand, in battery technologies, the primary property of interest is the electrochemical behavior of 2D electrode materials. This involves calculations related to energy storage capacity, redox potentials, ion diffusion rates, and structural stability during charge-discharge cycles. Understanding these properties is essential for designing batteries with optimal energy density, charge/discharge rates, and cycle life. The key entity for determining the capability of 2D materials for efficient sensing technology is the adsorption energy. From the adsorption energy, the desorption time or the recovery time of the gas molecule can be completed, and a faster recovery time indicates that the sensor can be used as a multi-use sensor. There have been several studies which used DFT calculations to study and design toxic gas sensors. For example, Thomas and Asle Zaeem [118] demonstrated that the interaction between both the pristine and defective $\text{Ti}_2\text{C}(\text{OH})_2$ sheet and the COCl_2 gas molecule is primarily governed by physisorption with a stable adsorption energy, and there is charge transfer from the molecule to the MXene, which is desirable for superior sensing performance (see figure 7(e)). This study also reported a notable improvement of DOS contributions at the Fermi level with the presence of COCl_2 molecule adsorbed on $\text{Ti}_2\text{C}(\text{OH})_2$ MXenes, as shown in figure 7(f). These DFT analyses show that the sensing mechanism of the COCl_2 molecule on a $\text{Ti}_2\text{C}(\text{OH})_2$ sensor is influenced by both defects and surface functional groups. It should also be noticed that since diverse types of gas molecules are present in the atmosphere, the adsorption properties of specific gas molecules can be influenced, or not, by the presence of other molecules.

The selective sensing aspect is crucial, particularly for the accurate detection of specific target molecules. Previous research indicated that the presence of water molecules (humidity) and other gases might not significantly impact the gas sensing properties of 2D materials [150, 151]. Similar to gas sensing, DFT is used to extract sensing performance of biomolecules when interacting with 2D materials. In recent studies [143, 144], new insights were provided about the adsorption mechanism, charge transfer, and electronic properties of 2D layered double hydroxides such as NiFe and NiCo for glucose and dopamine selective sensing applications, respectively. The insights obtained from DFT further provided valuable information to narrow down the experimental efforts. These DFT studies clearly underscore the role of fundamental analysis in designing 2D materials for sensing applications.

2.3.3. Catalysis

Heterogeneous catalysis is another critical HGC problem involving the discovery and development of practical catalysts with excellent selectivity and activity for various electrochemical reactions, including the hydrogen evolution reaction (HER), oxygen evolution reaction (OER), oxygen reduction reaction (ORR), CO₂ reduction reaction (CO₂RR), nitrogen reduction reaction (NRR), and C-H activation, among others. DFT calculations can determine reaction pathways, predict active sites, delineate the roles of reaction intermediates such as CO or formate, and assess the overpotentials [152]. For C-H Activation, DFT calculations provide a detailed understanding of the role of various geometrical and chemical descriptors such as vacancy formation energy (VFE) and Bader charges for efficient catalytic activity [153]. DFT calculations have been utilized to study a wide variety of 2D materials including MXenes [154] for their HER catalytic capabilities such as adsorption energies, Gibb's free energy, and surface reactivity. Among the many MXenes which have never been synthesized in a laboratory setting yet, DFT simulations revealed which MXenes were viable without costly synthesis [155]. By employing DFT, Kumar *et al* studied the oxidative dehydrogenation (ODH) of light alkanes such as ethane (C₂H₆), propane (C₃H₈), and butane (C₄H₁₀) over oxygen functionalized hexagonal boron nitride (h-BN) [153]. In this work, the DFT helps to understand the role of O functionalization, the reactivity of O atoms, electronic properties, and catalytic descriptors such as Bader charge and O vacancies for establishing the most selective catalyst. Previous DFT studies also established that the presence of defects, dopants, and large number of edges in 2D materials, such as in graphene [156] and MoS₂ [157], create active sites for catalytic activities. For example, in

the case of OER, it is a complex multistep process, initiated by a hydroxyl group (OH⁻) adsorption at the catalytic site which is considered the activation step. In view of this, understanding the catalyst activation step following OH⁻ adsorption on the surface-active site is crucial in providing detailed insights into the catalytic activities. DFT was used in computing the OH⁻ adoption energy, electronic properties, and charge transfer of NiSe, NiTe, and NiSeTe slab models to obtain their catalytic performance to support the experimental observations [145]. This study provided new understanding of structure-property-performance relationships of these catalysts for the improved OER performance.

2.4. DFT integration with large scale simulations

While DFT and AIMD simulations supply accurate insights, obtaining a quantitative understanding compared to experiments can be challenging. This is primarily due to the computational demands, system size limitations, and the level of theory employed for DFT and AIMD computations. Overcoming the length-scale limitations of DFT is possible through nano- and mesoscale atomistic simulations, including MD and phase field (PF) simulations. The physical insights gained from DFT simulations, coupled with relevant experimental data, can effectively aid in developing and fine-tuning accurate empirical potentials [158] for nano-scale MD simulations. The significance of empirical interatomic potentials and nano- and mesoscale simulations for modeling significantly larger systems is discussed in section 3.

Despite their remarkable physical and chemical properties, it should be noted that most 2D materials own unique features that cannot be fully captured using the standard DFT approach. This is associated with the fundamental limitation of DFT that stems from its mathematical foundation, which exclusively addresses the ground state density. Consequently, the exploration of excited states encounters obstacles within this method, although alternative approaches like time-dependent DFT (TDDFT) [159, 160] have been proposed. Furthermore, despite being commonly interpreted as physical quantities, the KS eigenvalues and eigenvectors do not formally correspond to the energy levels and eigenstates of the system. Similarly, as mentioned before, the hybrid DFT calculations [161] have been employed for accurate bandgap predictions, based on the specific material of interest [162]. Besides, as DFT is inherently a zero Kelvin approach, the incorporation of temperature can be achieved through AIMD techniques. However, certain critical material properties, like thermal expansion, thermal conductivity, and temperature effects on mechanical deformation, cannot be accurately analyzed using AIMD due to limitations in system size with current DFT standards.

3. MD simulation

MD simulation is based on classical mechanics and Newton's equation of motion. It is a powerful tool for nanoscale understanding of the mechanical and physical behaviors of materials and determining different material properties. The typical procedure to perform MD simulations includes defining the material system, selecting or developing the appropriate force field (i.e. interatomic potential), performing energy minimization, integrating the equation of motion, post-processing and visualization, validation and/or uncertainty quantification, and result interpretation. Amongst them, utilizing an appropriate force field is a crucial component that directly affects the accuracy and reliability of the simulation results. Based on whether they explicitly account for chemical reactions, the force field can be broadly categorized into reactive and non-reactive ones. For MD simulations of 2D materials, some commonly used reactive potentials include ReaxFF [163] and the REBO [164] potentials. In the context of non-reactive force fields, empirical (e.g. Lennard-Jones potential [165]) and semi-empirical (e.g. Embedded Atom Method (EAM) [166], and Tersoff Potential [167]) potentials are commonly used to describe the structural and thermodynamic properties of 2D materials. In the following, we will briefly discuss the previous efforts in determining the mechanical, thermal, oxidation, and desalination properties of 2D materials by MD simulations and discuss some technical and/or physical issues associated with these works that have affected the reliability of the results. Also, we provide potential future directions in advancing MD simulations for the study and design of 2D materials.

3.1. Mechanical behavior and properties of 2D materials

MD simulations offer several advantages when it comes to simulating the mechanical properties and deformation behavior of 2D materials compared to experimental or other numerical techniques. As mentioned before, 2D materials often have a layered structure, which is essentially one atom or a few atoms thick, and the individual layers are weakly bound to each other. Such a unique structure endows 2D materials with exceptional mechanical flexibility, making them suitable for applications in flexible electronics and coatings. Meanwhile, the thin layered structure presents several challenges to experimental studies including accurate determination of layer thickness, defects characterization, limited interaction cross-section, susceptibility to strain and mechanical stability, and *in situ* dynamic behavior characterization. MD simulations can accurately capture the interactions within and between layers, which is essential for studying properties such as interlayer sliding and stacking configurations. Additionally,

various defects can form in the synthesis of 2D materials, and understanding the nature and impact of these defects is crucial for tailoring the properties of 2D materials for specific applications.

3.1.1. Elasticity and strength

MD simulations are capable of calculating the elastic properties (e.g. elastic modulus and Poisson's ratio) and strength of 2D materials by subjecting them to different deformation conditions (e.g. uniaxial tension or nanoindentation) and observing their force-displacement or stress-strain response. For example, uniaxial tension simulations with Tersoff potential was conducted to study the effect of point defects, grain boundaries (GBs), and lattice defects on the elasticity of single-layer and polycrystalline hexagonal boron-nitride (h-BN) [168, 169]. Simulation results suggested that an extremely high tensile strength of 80 GPa could be reached in polycrystalline h-BN with grain sizes ranging from 5 nm to 10 nm. Hence, it is speculated that the experimentally fabricated polycrystalline h-BN films can exhibit ultra-high elastic modulus and tensile strength. The revealed failure mechanisms uniaxial tension, namely boron-nitrogen bonds breaking leads to voids growth and crack propagation along GBs, are similar to experimental observations [170].

MD simulations were also applied to conduct uniaxial tensile, tribological, nanoindentation, and bending tests to study the fracture toughness, friction, and wear reduction behavior of various 2D materials, such as graphene [171–173], h-BN [104, 169, 174], MoS₂ [175, 176], and MXenes [158, 177, 178]. Most of the simulation results, such as elastic modulus, hardness and failure mechanisms, agree well with the experimental testing outputs and match the *in-situ* TEM characterization of strengthening and toughening mechanisms.

Since MD calculations are based on classical mechanics, the reliability and accuracy of the predicted mechanical properties and deformation behaviors rely on the accuracy of the force fields used. For example, in the study of single crystalline MXenes, different interatomic potentials were employed, namely a combined EAM, LJ and Axilrod-Teller (AT) potential [179], Charge Optimized Many Body (COMB) potential [180], ReaxFF potential [181, 182], and Tersoff-style bond-order potential [158]. Through a comparison of failure modes, force-displacement curves, and stress-strain curves in figure 8, one can conclude that the selected force fields directly affect the calculated mechanical properties and deformation behaviors of MXenes. Therefore, it is critical and essential to perform uncertainty quantification and validate the MD simulation results to ensure the reliability and accuracy of the simulated outcomes.

In a recent review paper by Nayir *et al* [1], the progress of ReaxFF force field developments

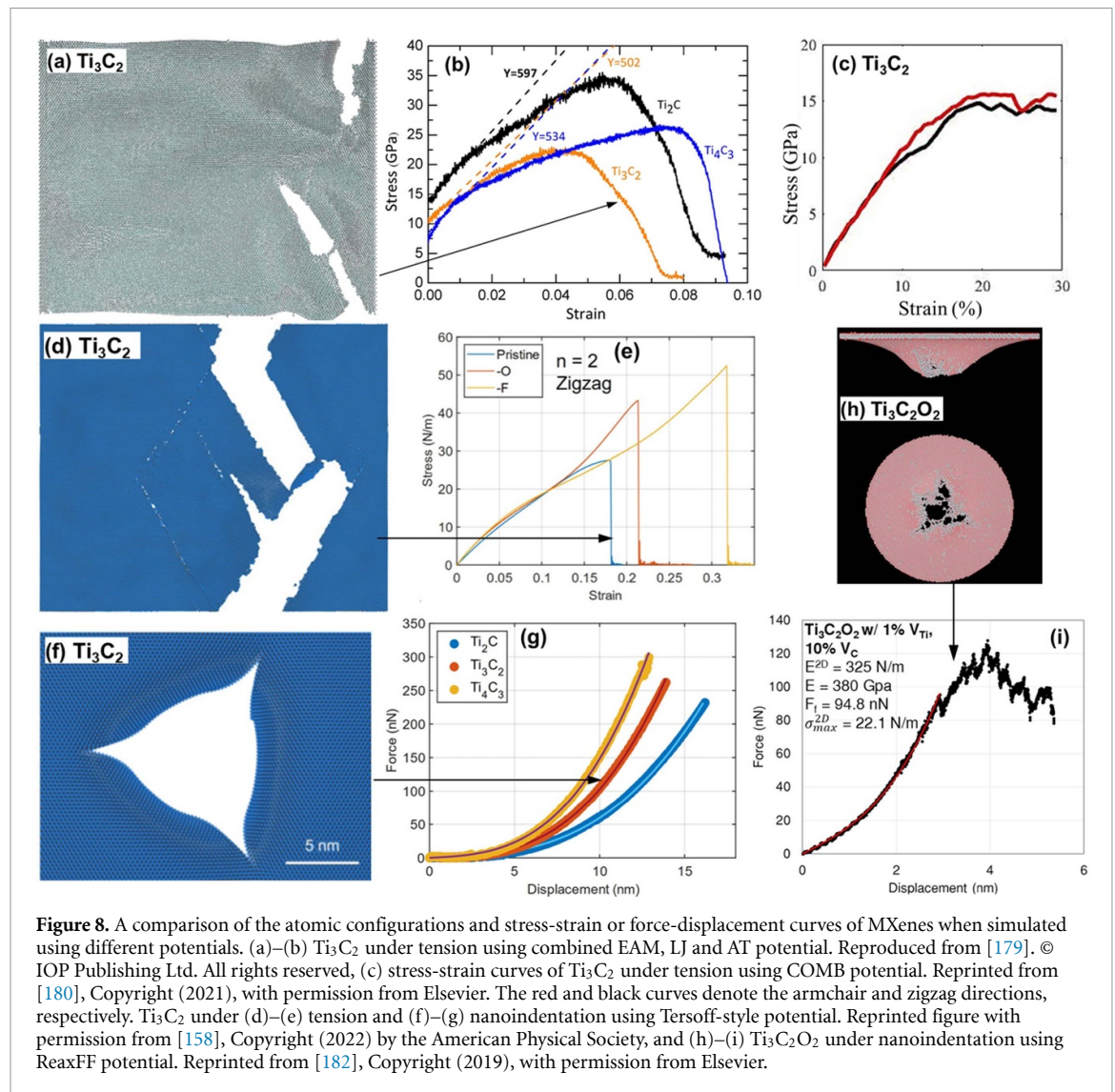


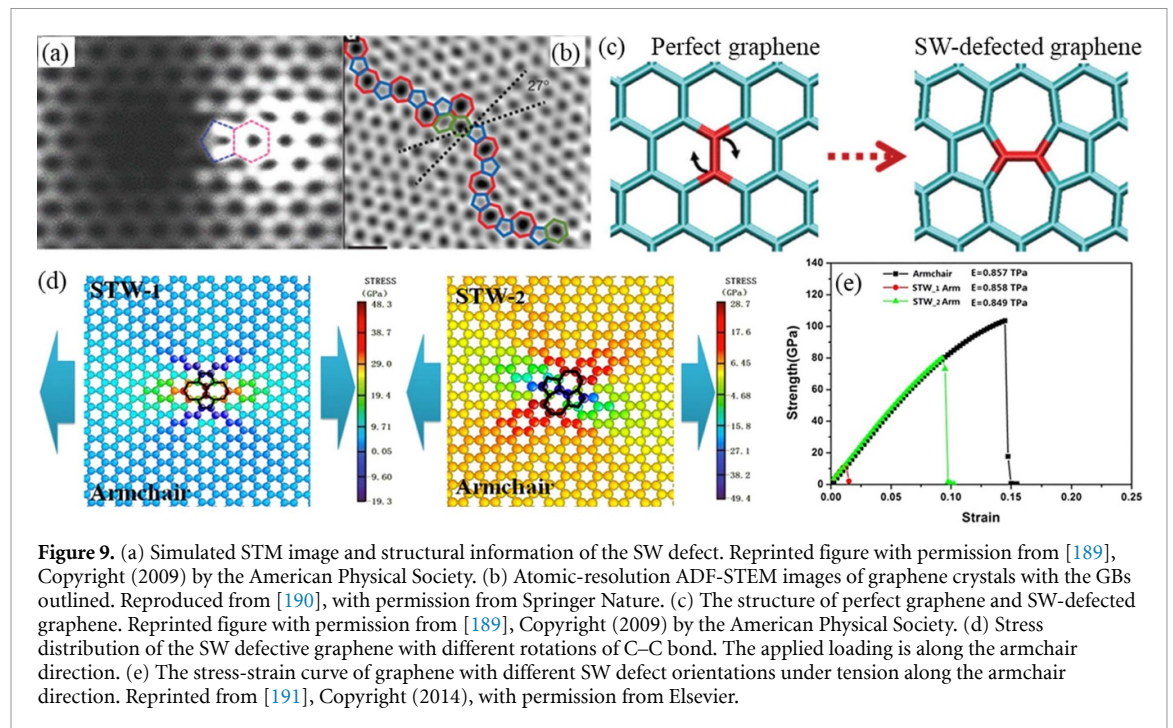
Figure 8. A comparison of the atomic configurations and stress-strain or force-displacement curves of MXenes when simulated using different potentials. (a)–(b) Ti_3C_2 under tension using combined EAM, LJ and AT potential. Reproduced from [179]. © IOP Publishing Ltd. All rights reserved, (c) stress-strain curves of Ti_3C_2 under tension using COMB potential. Reprinted from [180], Copyright (2021), with permission from Elsevier. The red and black curves denote the armchair and zigzag directions, respectively. Ti_3C_2 under (d)–(e) tension and (f)–(g) nanoindentation using Tersoff-style potential. Reprinted figure with permission from [158], Copyright (2022) by the American Physical Society, and (h)–(i) $\text{Ti}_3\text{C}_2\text{O}_2$ under nanoindentation using ReaxFF potential. Reprinted from [182], Copyright (2019), with permission from Elsevier.

for 2D materials was extensively discussed. In the current work, we focus on evaluating the influence of different potentials on material properties and exploring their common applications. Several commonly used validation approaches include direct comparison with experimental data, benchmarking against theoretical prediction [183, 184], and performing sensitivity analysis of key simulation parameters [185]. Validation can not only help assess the performance of the chosen force field but also identify the discrepancies between simulation results and experimental or theoretical data, which could help in understanding the limitations of the simulation approach. Reliable MD simulations can complement experimental studies in providing a comprehensive understanding of the mechanical behavior of 2D materials under various loading conditions. However, it is worth recognizing the aspects of agreement and disparity when validating MD simulation results against the experiment data. In general, MD technique, when properly parameterized, can capture the inherent material behavior, resulting

in agreement in the general trends of stress-strain curves with experimental ones. However, there can be quantitative differences in strength, toughness and ductility between experimental and simulated results, although the elastic modulus and hardness predicted from MD simulation have been reported to be well consistent with the experiment results [186, 187]. The reasons behind inconsistencies include limited size scale ($\sim\text{nm}$), time scale ($\sim\text{ps}$) and high strain rate ($>10^7 \text{ s}^{-1}$) of MD simulations, and mismatched temperature and environmental conditions in simulations and experimental setups. Additionally, MD simulations might oversimplify or misrepresent defects, leading to different responses when compared to real-world experiments.

3.1.2. Defects behavior

Fabrication of perfect single-layer sheets both at the lab scale experiments and commercial scale is very challenging because the produced materials by any method consist of some specific defects [188]. Also, defects can form during operation and use of 2D



materials. The multiscale defects in 2D materials include vacancies, interstitials, insertion of foreign elements, edge distortions, and lattice deformation, and twisting and bulking of sheets. They often deteriorate the uniqueness of materials and impact their thermal, mechanical, electronic, photonic, and surface properties. Considering the ultra-thin character of 2D materials, studying the atomic or nanoscale dynamic processes, such as the initiation and propagation of defects, can be challenging in real-time experiments.

MD technique has been extensively adopted to investigate the formation of defects and their effects on the mechanical properties of 2D materials. SW lattice defects are often found in graphene, which is characterized by a 90° rotation of a pair of atoms. They are created when four hexagons are converted into two heptagons and two pentagons, as shown in figures 9(a)–(c) [189–191]. MD-simulation-based studies have been conducted to inspect and analyze the influence of SW defects and vacancies on the mechanical and chemical features of graphene [192–194], graphene/epoxy nanocomposites [195], and h-BN [196]. SW defects were observed to annihilated with increasing stress levels and strain rate, resulting in an impairment of the strength of the 2D materials. It was revealed that the orientation of the SW defect with respect to the chirality governs the strength of graphene while has negligible effect on the elastic modulus, as exhibited in figures 9(d) and (e) [191].

The effect of GBs on the mechanical behavior of 2D materials, such as graphene [171], h-BN [169, 197], and MoS₂ [198], was also investigated by MD simulations. The elastic modulus and tensile strength exhibited a decline with the growing number of

crystal grains, denoting an increased presence of GBs. This trend contradicts the conventional Hall-Patch relation commonly observed in bulk materials. GBs in 2D h-BN were identified as primary sites for crack initiation, demonstrating a higher sensitivity to the number of boundaries rather than their respective sizes [169, 197]. Additionally, MD simulations have been applied to study the impact of point defects on the mechanical properties of 2D materials, such as graphene [199], h-BNs [200], MoS₂ [176], and MXenes [201]. Take MoS₂ for instance, vacancies exhibit various forms, with some occupying only one sulfur site and others extending to occupy up to six sulfur sites. These vacancies may also accommodate alternative atomic species, such as a molybdenum substitutional atom. MD simulations demonstrated that the presence of single sulfur vacancy can increase the failure strain due to phase transformation [176]. The atomistic capabilities of MD simulations enabled exploration of specific sulfur vacancy compositions, elucidating the intricate mechanisms governing the observed alterations in properties.

3.1.3. Fatigue behavior

MD is also an integral tool in studying fatigue behavior of 2D materials. MD simulations can provide a deep understanding of nanoscale mechanisms governing fatigue, such as the evolution of dislocations, crack initiation and propagation, and interactions between defects. Moreover, it allows for the prediction of fatigue behavior under conditions that may be difficult to replicate in experiments. This knowledge is crucial for designing fatigue-resistant 2D materials. Using AFM (figures 10(a)–(c)), graphene was found to exhibit a fatigue life of more than 10^9 cycles

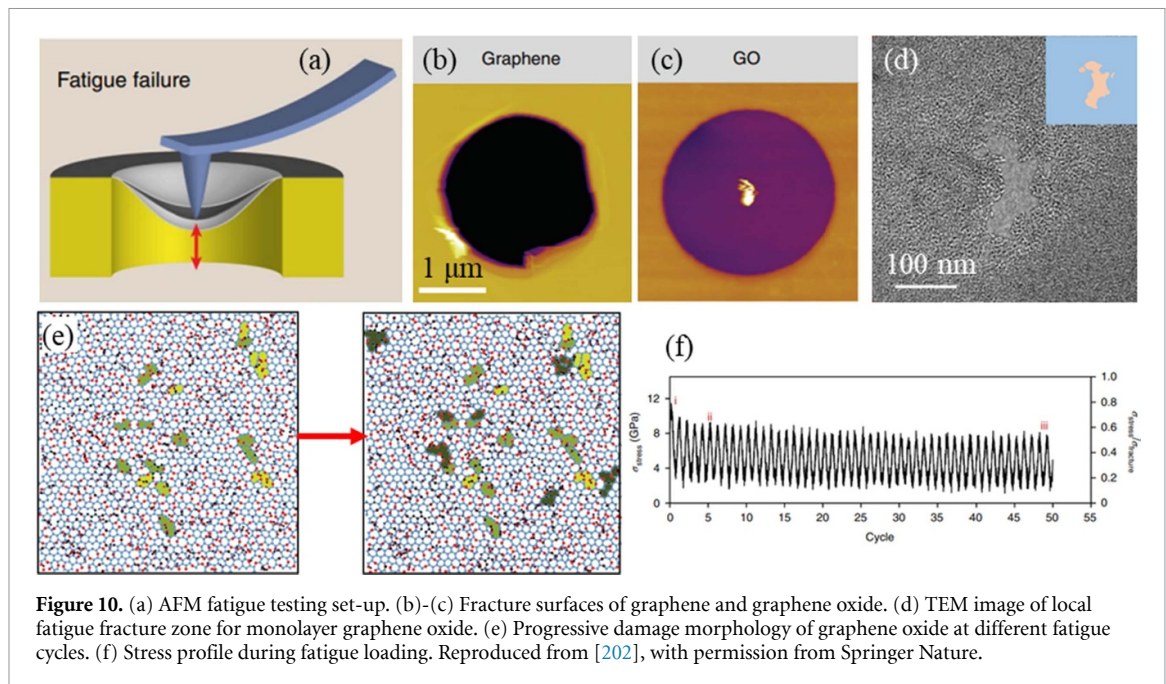


Figure 10. (a) AFM fatigue testing set-up. (b)–(c) Fracture surfaces of graphene and graphene oxide. (d) TEM image of local fatigue fracture zone for monolayer graphene oxide. (e) Progressive damage morphology of graphene oxide at different fatigue cycles. (f) Stress profile during fatigue loading. Reproduced from [202], with permission from Springer Nature.

in uniaxial cyclic tensile loading, and this is higher than any other materials so far. MD simulations with ReaxFF potential were conducted to understand the atomistic mechanisms underpinning the fatigue failure of graphene and graphene oxide [202]. Bond reconfiguration was observed prior to catastrophic failure, which is consistent with the observation from TEM (figures 10(d)–(f)). MD simulations were also performed to study the fatigue behavior of 2D MoS₂ containing a crack under a uniaxial cycle tensile loading. The strain range, strain ratio, initial crack length, and temperature could significantly affect the fatigue life of the material [203]. By employing models or fatigue laws derived at a macroscopic scale to fit MD simulation results, a surprising consistency was observed, indicating the universal nature of the relations between fatigue life and the four influencing factors. This study implies that fatigue behavior in 2D materials display specific features at the atomic scale while concurrently sharing common characteristics observed at the macroscopic scale.

It is worth discussing several shortcomings of MD simulations in the study of the fatigue properties. First, the timescale achievable in MD simulations may be insufficient to capture long-term fatigue behavior. Second, MD simulations may overlook the thermodynamic aspects of fatigue, such as temperature effects and thermal fluctuations. Specifically, in fatigue, the repetitive cycles of deformation and relaxation cycles can induce heat generation, thereby affecting the overall thermodynamic behavior of materials. However, the classical force fields typically work under the assumption of constant temperature. Hence, MD simulations based on classical mechanics might not capture these temperature effects and thermal fluctuations accurately. In contrast, some

advanced simulation techniques, such as AIMD and temperature-accelerated MD (TAMD), can address these limitations by considering quantum mechanical effects or by explicitly incorporating temperature changes. However, the use of these methodologies is hindered by their computational demands, leading to notable restrictions on the scale of the simulation system. Besides, it is challenging to use MD simulations to simulate large-scale systems that represent real-world structures. The simplified models in MD simulations can potentially disregard the presence of defects, impurities, or environmental factors. Thus, more advanced modeling strategies, such as utilizing multiscale modeling or coupling MD with other large-scale simulation methods, may be necessary to address these limitations and provide a more comprehensive understanding of fatigue properties of 2D materials.

3.2. Thermal behavior and properties of 2D materials

MD simulation has emerged as a powerful tool for predicting thermal behaviors and properties of materials at the atomic scale including thermal conductivity, interfacial thermal conductance, temperature distribution phonon dispersion relations, thermal expansion coefficient, thermal diffusivity, and heat capacity. In the following subsection, we will briefly assess the role of MD simulations in advancing our knowledge of the thermal properties of 2D materials.

3.2.1. Thermal conductivity

In MD simulations, thermal conductivity is calculated using either the Green-Kubo method [204] in equilibrium MD (EMD) or the direct method in non-equilibrium MD (NEMD) [205]. The Green-Kubo

method calculates thermal conductivity (κ) from the integral of the heat current autocorrelation function during the equilibrium phase of the MD simulation with respect to a given correlation time t [206]:

$$\kappa = \frac{V}{(3K_B T^2)} \int_0^\infty \langle J(0) \cdot J(t) \rangle dt \quad (4)$$

where V is the system volume, K_B is the Boltzmann's constant, and T is the system temperature. The term within the brackets represents the heat flux autocorrelation and are represented as:

$$J = \frac{1}{V} \left(\sum_i e_i v_i - \sum_i S_i v_i \right) \quad (5)$$

where e_i is the total energy of atom i and v_i is the velocity vector. S_i is the per atom stress tensor. This EMD method provides a detailed understanding of the contribution of different types of interactions to thermal conductivity [207]. However, it requires a long equilibration time, which can be computationally expensive.

On the other hand, the direct method used in NEMD involves creating a non-equilibrium state by adding and subtracting equal amounts of energy, resulting in a steady linear temperature profile in the intervening region. The NEMD can be implemented in two distinct manners: by generating a temperature gradient across the two ends of the system (T-NEMD) or by maintaining a constant heat flux (Q-NEMD). In T-NEMD, the temperatures of the hot and cold reservoirs are designated as $T + \Delta T/2$ and $T - \Delta T/2$, respectively, where T is the equilibrium temperature and ΔT is the temperature difference. After reaching a stable temperature gradient, the thermal conductivity is determined by applying the Fourier's law of heat conduction [208]:

$$\kappa_{MD} = - \frac{J}{(dT_{MD}/dz)} \quad (6)$$

where dT_{MD}/dz is the temperature gradient along the nanowire longitudinal axis. The Q-NEMD closely resembles the T-NEMD method, differing only in the boundary conditions. T-NEMD utilizes the Dirichlet boundary condition, specifying temperatures at the cold and hot reservoirs, whereas Q-NEMD employs the Neumann boundary condition, specifying added and removed heat flux in the hot and cold reservoirs. Although the NEMD method can be more efficient than EMD, it demands a substantial perturbation to manifest a discernible response, thereby introducing additional complexities. A noteworthy benefit of EMD lies in its decreased sensitivity to size effect compared to NEMD. Both methods have advantages and disadvantages, and the choice between them depends on the specific requirements of the simulation.

Furthermore, it is essential to select an appropriate potential to ensure the reliability of the obtained

thermal conductivity. Take graphene for instance, Si *et al* [209] conducted non-equilibrium MD (NEMD) simulations to examine the applicability of four potential models, i.e. Tersoff, REBO, opt-Tersoff and AIREBO, in study the thermal transport of graphene. It was found that the Tersoff, REBO and AIREBO potentials greatly underestimated the thermal conductivity of single-layer graphene. While, the Opt-Tersoff potential was noted to be the most suitable one in predicting the thermal properties of graphene, and it has been demonstrated to be able to well reproduce the experimental results. The thermal conductivities, phonon spectrum and phonon dispersion predicted by these four types of potential are compared in figure 11. Tersoff, REBO, and AIREBO force fields are found to significantly underestimate the thermal conductivities of single-layer graphene, although they qualitatively capture the temperature-dependent trend, as indicated in figure 11(a). Conversely, the opt-Tersoff potential outperforms in providing more accurate thermal conductivities and effectively represents phonon scattering in multi-layer graphene, as demonstrated in figures 11(b) and (c). Table 1 provides a comprehensive summary of the thermal transport properties of graphene utilizing different potentials and methods. The considerable discrepancies in thermal properties observed, which underscores the importance of a cautious selection of potential in calculations to ensure precision in reflecting the thermal properties and behavior of 2D materials.

3.2.2. Phonon dispersion

Phonon localization has a great potential for improving the existing energy applications including thermoelectric materials and thermal barriers by reducing thermal conductivity. According to the theory of Anderson localization [223], the electrons in 3D systems are only partially localized while those in 2D systems can be entirely localized. Inspired by this deduction, NEMD and EMD simulations with Tersoff potential were conducted to investigate the effects of dimensionality on phonon localization in graphene/h-BN superlattice [224]. It was found that the 2D system exhibits more prominent phonon localization behavior than the 3D system. Moreover, stronger phonon localization was observed in random multilayer (RML) model when compared to the superlattice (SL) model, as illustrated in figure 12. When studying phonon transport, atomistic and time-dependent simulations naturally incorporate phonon anharmonicity using semi-empirical parameters that can be derived from ab-initio methods [225], all within systems constrained to thousands of atoms. Moreover, the computational load is significantly increased when the phonon dispersion is implemented in anharmonicity [226]. The accuracy of phonon dispersion relations can be impacted by the size of the simulated system, particularly

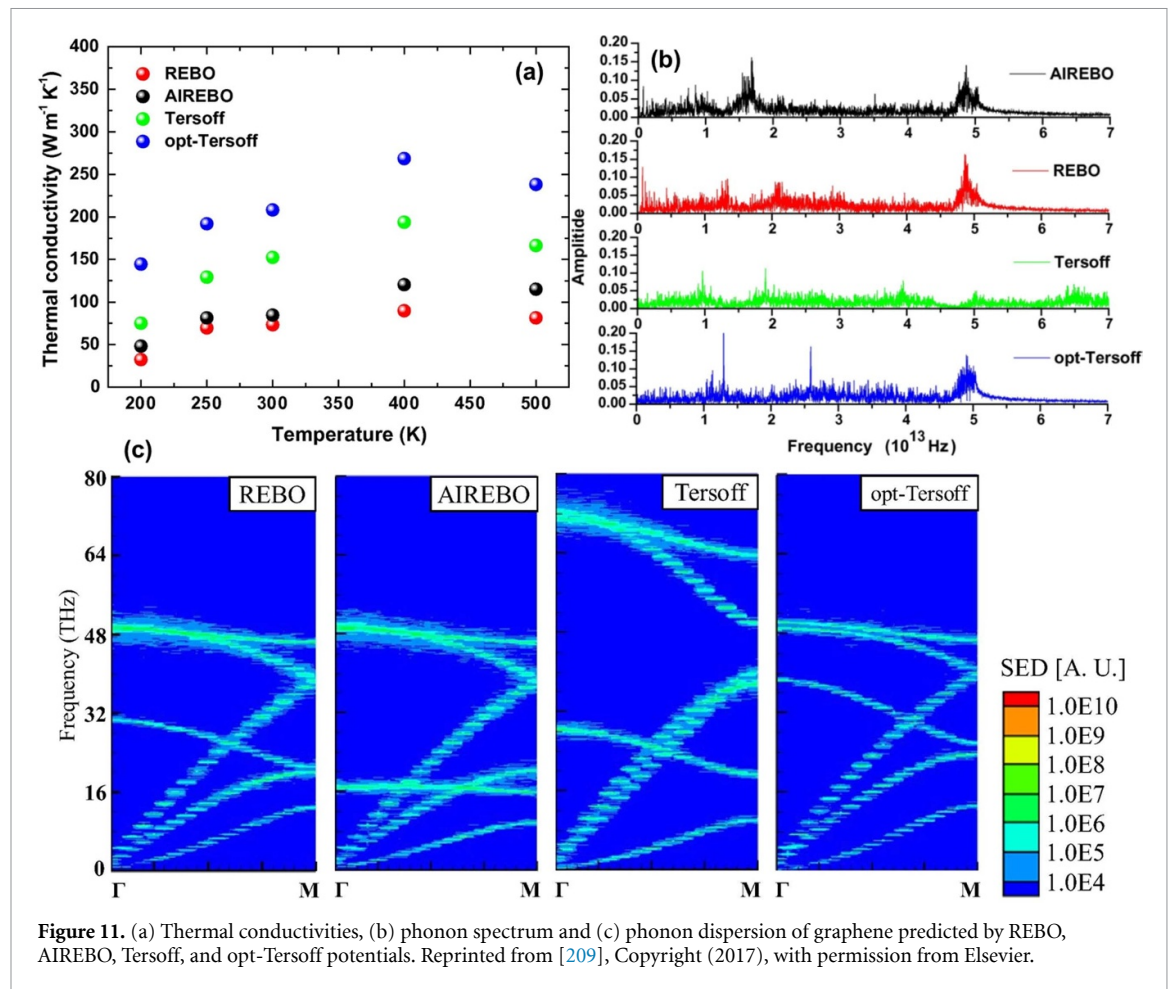


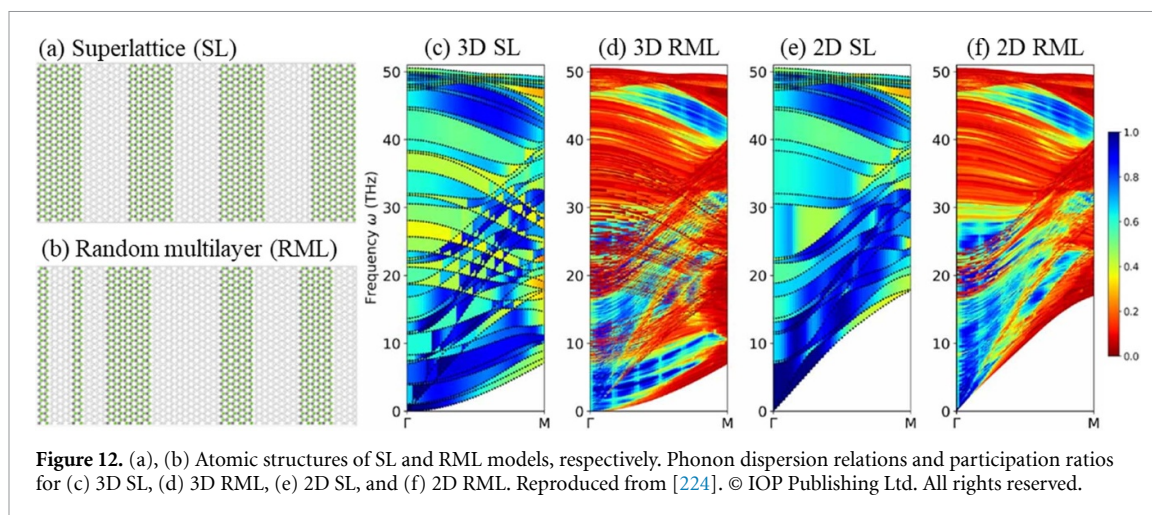
Figure 11. (a) Thermal conductivities, (b) phonon spectrum and (c) phonon dispersion of graphene predicted by REBO, AIREBO, Tersoff, and opt-Tersoff potentials. Reprinted from [209], Copyright (2017), with permission from Elsevier.

Table 1. Thermal transport properties predicted using different types of potentials. Reprinted from [209], Copyright (2017), with permission from Elsevier.

Type	References and years	Thermal conductivity (W m ⁻¹ K ⁻¹)	Typical size	Potential model	Methodology
Single-layer graphene	[210] (2009)	~1300	1.5 × 5.7 nm ²	REBO	NEMD
	[211] (2011)	~2900	2.4 × 2.5 nm ²	Opt-REBO	EMD
	[212] (2011)	77.3	10.2 × 10.2 nm ²	AIREBO	NEMD
	[213] (2012)	53.6	2.2 × 10.2 nm ²	AIREBO	NEMD
	[214] (2012)	400 ~ 1600	5.2 × (45 ~ 2280) nm ²	Opt-Tersoff	NEMD
	[215] (2012)	78	2.13 × 10.5 nm ²	AIREBO	NEMD
	[216] (2012)	3200 ~ 5200	(9 ~ 27) × (4 ~ 18) nm ²	AIREBO	NEMD
	[217] (2013)	370 ~ 580	10.4 × (100 ~ 650) nm ²	Tersoff	NEMD
	[218] (2014)	400 ~ 1800	5 × (0.2 ~ 15) nm ²	Opt-Tersoff	NEMD
	[219] (2016)	910 ~ 1655	(10 ~ 300) × 5.2 nm ²	Opt-Tersoff	NEMD
[220] (2016)	128.4	11.9 × 18.2 nm ²	REBO	NEMD	
Multi-layer graphene	[221] (2011)	580 ~ 880	5 × (7.5 ~ 20) nm ² × (1 ~ 5) layers	Tersoff-LJ	NEMD
	[222] (2012)	200 ~ 1100	(1 ~ 10) × (10 ~ 20) nm ² × (1 ~ 5) layers	Tersoff-LJ	NEMD

for low-frequency modes. Long-wavelength phonons may not be fully sampled due to finite size issues [227]. Numerous improvements to the method have been proposed thus far [228]. A novel method, utilizing the energy density of the phonon spectrum,

has been formulated and evaluated to directly estimate phonon dispersion relations and lifetimes based on atomic velocities in a crystal [228]. It is also suggested to employ methodologies that go beyond classical MD to accurately incorporate quantum phenomena,



such as path integral MD or quantum Monte Carlo techniques.

3.3. Oxidation behavior

The vulnerability of 2D materials to oxidation upon exposure to air, characterized by a chemical reaction involving electron loss and the introduction of oxygen, has a profound impact on their functional properties and the performance of devices utilizing 2D materials [229]. It is crucial to unravel the intricate dynamics of oxidation at the atomic scale, but this is challenging for experiments. MD simulations can provide insights into the oxidation characteristics, such as the rate of oxygen adsorption and charge distribution [230]. ReaxFF potentials are commonly used for oxidation simulations since they are able to simulate bond breaking and reforming. The oxidation behavior of a range of 2D materials, encompassing graphene, TMD, MXenes, and h-BN, has been extensively reviewed in a recent paper leveraging the ReaxFF [1]. This work, we use 2D MXenes as a model to illustrate the capabilities of MD in studying material oxidation behavior. Employing the ReaxFF potential, the interactions of $\text{Ti}_3\text{C}_2\text{T}_x$ MXene layers with intercalated pure water and metal ions was first studied [231]. Thereafter, Lotfi *et al* employed ReaxFF MD simulations to investigate the oxidation behavior of MXenes under different environments, in terms of humidity and temperature, as shown in figure 13(a) [230]. They revealed that by increasing the temperature, the oxidation rate increases, and depending on the oxidant the rate is in the order of: $\text{H}_2\text{O}_2 > \text{wet air} > \text{dry air}$. Recently, a neural network potential (NNP) was developed to study the oxidation behavior of the V_2CO_2 MXenes in aqueous environment [232]. The entire oxidation process can be approximately divided into two stages: H_2O adsorption and proton release, as shown in figure 13(b). The energy predicted by MD is almost equivalent to that calculated by DFT, demonstrating the effectiveness of

the NNP. Besides, MD simulation revealed that free protons and oxides greatly inhibit oxidation reactions, leading to the degradation of oxidation, which is consistent with the oxidation rate measured from experiment.

Conducting MD simulations for oxidation reactions can be computationally intensive because of the strict demand for specific potentials, particularly such as the ReaxFF. If simplified potentials were adopted, it may result in inaccuracies, especially when attempting to capture the intricate chemistry of oxidation. Despite existing challenges, ongoing progress in force field development, simulation methodologies, and computational capacities offers the potential to significantly improve the precision and utility of MD simulations in elucidating the intricate dynamics of oxidation in 2D materials.

3.4. Desalination behavior

Desalination, a crucial process in combating global water scarcity, has recently witnessed the investigation of novel materials, with a focus on 2D materials, to enhance overall performance. The desalination procedure typically consist of two stages: the extraction of pure water from saline water and the recovery of the draw solution, which separate the pure water from the diluted draw solution [233]. With their atomically thin structure, substantial surface area, and mechanical robustness, 2D materials like graphene and MXenes are being explored as viable options for replacing existing membrane materials in desalination and water purification [234]. By employing MD simulations, researchers can explore the dynamics of ion transport within 2D materials, gaining important insights into the mechanisms underpinning desalination processes. The water desalination behavior through hydrogen or hydroxyl functionalized nanoporous graphene membranes were investigated by MD simulations, as shown in figures 14(a) and (b) [235]. The results show

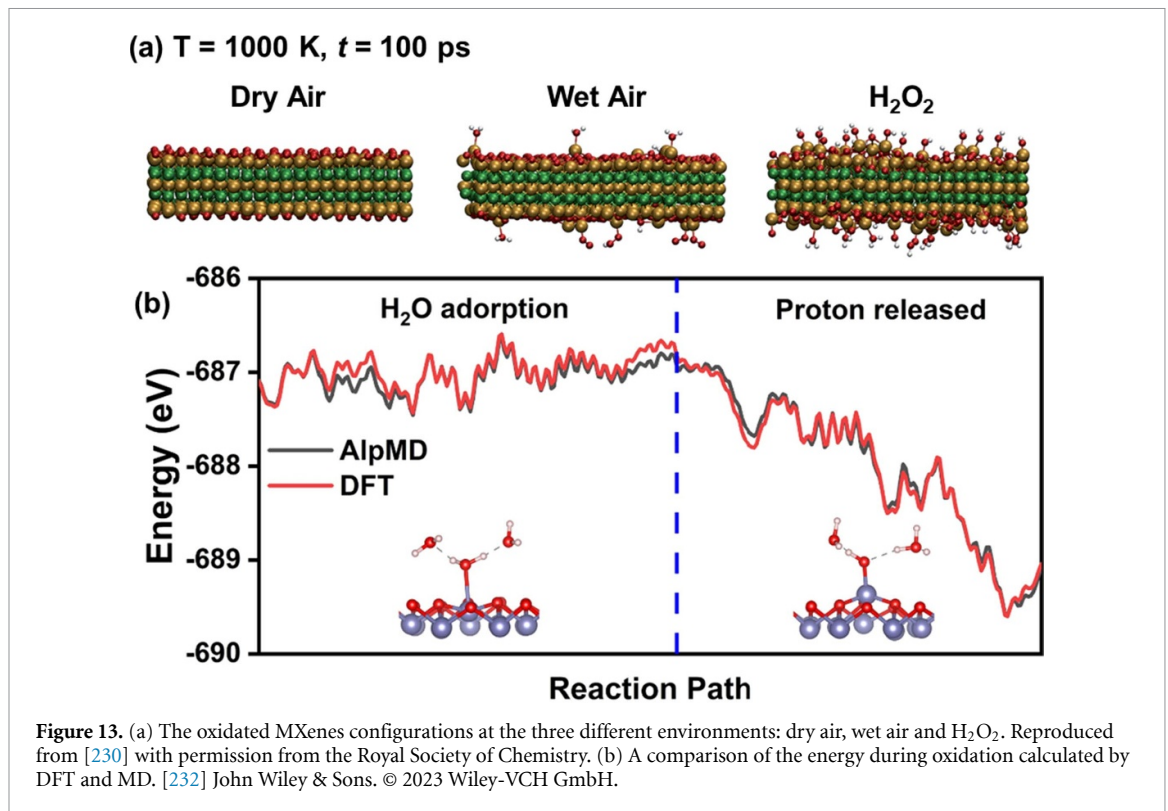


Figure 13. (a) The oxidated MXenes configurations at the three different environments: dry air, wet air and H_2O_2 . Reproduced from [230] with permission from the Royal Society of Chemistry. (b) A comparison of the energy during oxidation calculated by DFT and MD. [232] John Wiley & Sons. © 2023 Wiley-VCH GmbH.

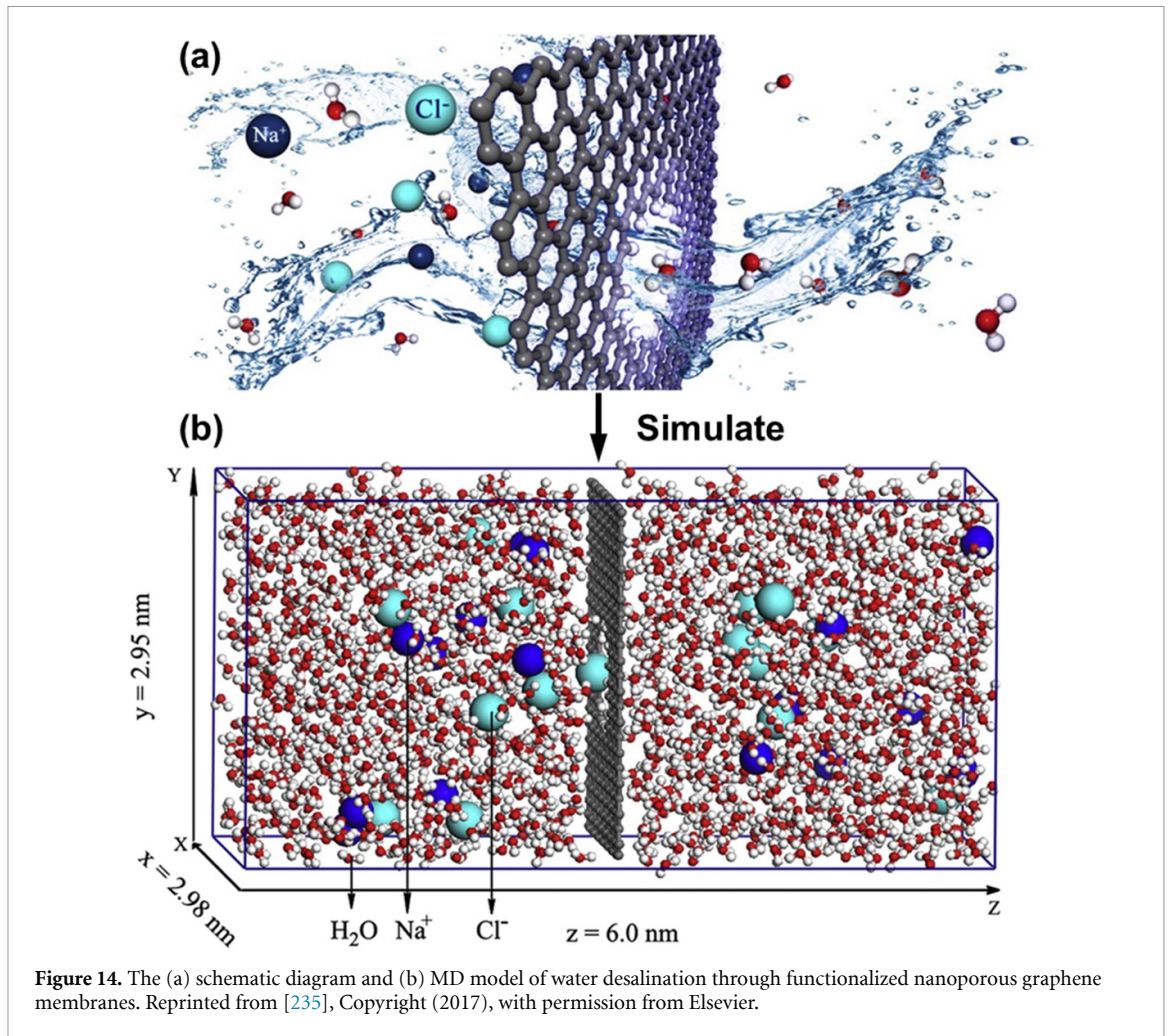
that external pressure facilitates the water desalination. The functionalized graphene membrane exhibits excellent performance for both salt rejection and water transport. This study provides a microscopic insight into water desalination and reveals governing mechanisms for water flux. In a recent study, Priya *et al* developed a ML model by training it with approximately 260 results from MD simulations, enabling the prediction of desalination performance, in terms of maximum water flux and salt rejection rates, for 2D membranes documented in existing literature. It is found that the presence of a transition metal around the pore can increase the average salt rejection rates, while nonmetals like halogens and chalcogens are prone to enhance the average water flux. The effective desalination potential is foreseen in 2D transition metal oxides, carbides, nitrides (MXenes), and their complexes. Therefore, one may conclude that well-validated statistical frameworks can serve as valuable tools for directing experiments within the domain of functional materials for various applications.

4. Lattice and continuum-based molecular mechanics modeling of 2D materials

Hexagonal lattice-like structural forms are present in the nano-structures of several 2D materials [236–238]. The effective mechanical properties of these materials can be expressed on the basis of an equivalent continuum-based assumption. Though, in principle, a range of other physical properties can be

explored based on the efficient continuum-based analyses (as discussed later in this section briefly), the main focus in the literature has been the exploration of effective elastic properties. We focus on nano-scale analysis of the structures of these 2D materials based on an efficient generalized analytical approach that leads to closed-form formulae for the elastic moduli. Two different classes of single-layer materials from a structural point of view, monoplanar [237] and multiplanar [239, 240] as shown in figure 15(a), are considered to demonstrate the results using these analytical formulae. The physics-based high-fidelity analytical models discussed in this section are capable of obtaining the elastic properties of single-layer 2D materials in a computationally efficient manner for a wide range of materials with hexagonal nanostructures. We have further demonstrated an approach to extend such efficient continuum-based approaches for characterizing the elastic moduli of multi-layer 2D heterostructures, as shown in figure 16(b).

From a structural viewpoint, single-layer nanostructures can be of either monoplanar (where all the atoms are in a single plane such as graphene and hBN) or multi-planar (where the constituent atoms lie in multiple planes such as stanene and MoS_2) configuration. Further, from the atomic configuration viewpoint the 2D materials could be homogeneous or heterogeneous based on the atoms that constitute the nano-lattices. For example, graphene consists of only carbon atoms to form a honeycomb like hexagonal lattice in a single plane, while hBN consists of boron and nitrogen atoms to form the hexagonal



lattice in a single plane. Similarly, stanene consists of only Sn atoms that stay in multiple planes, while MoS₂ consists of two different atoms (Mo and S) resting at different planes. Thus there could eventually be four different classes of single layer 2D materials [241]. Figure 15(b)I shows the top and side views of single-layer hexagonal nanostructures where all the constituent atoms are same and they are in a single plane (e.g. graphene [242]). Figure 15(b)II shows the top and side views of single-layer hexagonal nanostructures where the constituent atoms are not same but they are in a single plane (e.g. hBN [243], BCN [244]). Figure 15(b)III shows the top and side views of single-layer hexagonal nanostructures where the constituent atoms are same but they are in two different planes (e.g. silicone [245], germanene [246], phosphorene [247], stanene [248], borophene [249]). And, figure 15(b)IV shows the top and side views of single-layer hexagonal nanostructures where the constituent atoms are not same and they are in two different planes (e.g. MoS₂ [250], WS₂ [251], MoSe₂ [252], WSe₂ [253], MoTe₂ [254]). The generic structural configuration of a 2D multi-planar nano-lattice is shown in figures 15(a) and (b)V, where depending on the value of out-of-plane angle α and the nature

of the atoms (same or different), all the above four classes of 2D material nanostructures can be realized.

For understanding the structural performance of 2D material nanostructures from a mechanical strength and stiffness viewpoint, intended for use as nanoelectromechanical systems such as resonators or nanosensors, it is of utmost importance to evaluate their Young's moduli, in-plane shear modulus and Poisson's ratios [241]. The common computational approaches to investigate 2D nanomaterials are first principle studies/ ab-initio [105, 255–259], MD [260] and molecular mechanics [261–263], which are capable of reproducing the results of experimental analysis. First principles studies and ab-initio and MD-based material characterization approaches are normally expensive and time-consuming. The molecular mechanics-based analytical approach of evaluating elastic moduli is computationally very efficient, yet it produces accurate results.

In this section, we present molecular mechanics based closed-form analytical formulae for Young's moduli, in-plane shear modulus and Poisson's ratios of monoplanar and multiplanar 2D materials. Further, similar continuum-based idealizations are discussed for nano-heterostructures. Here we collate

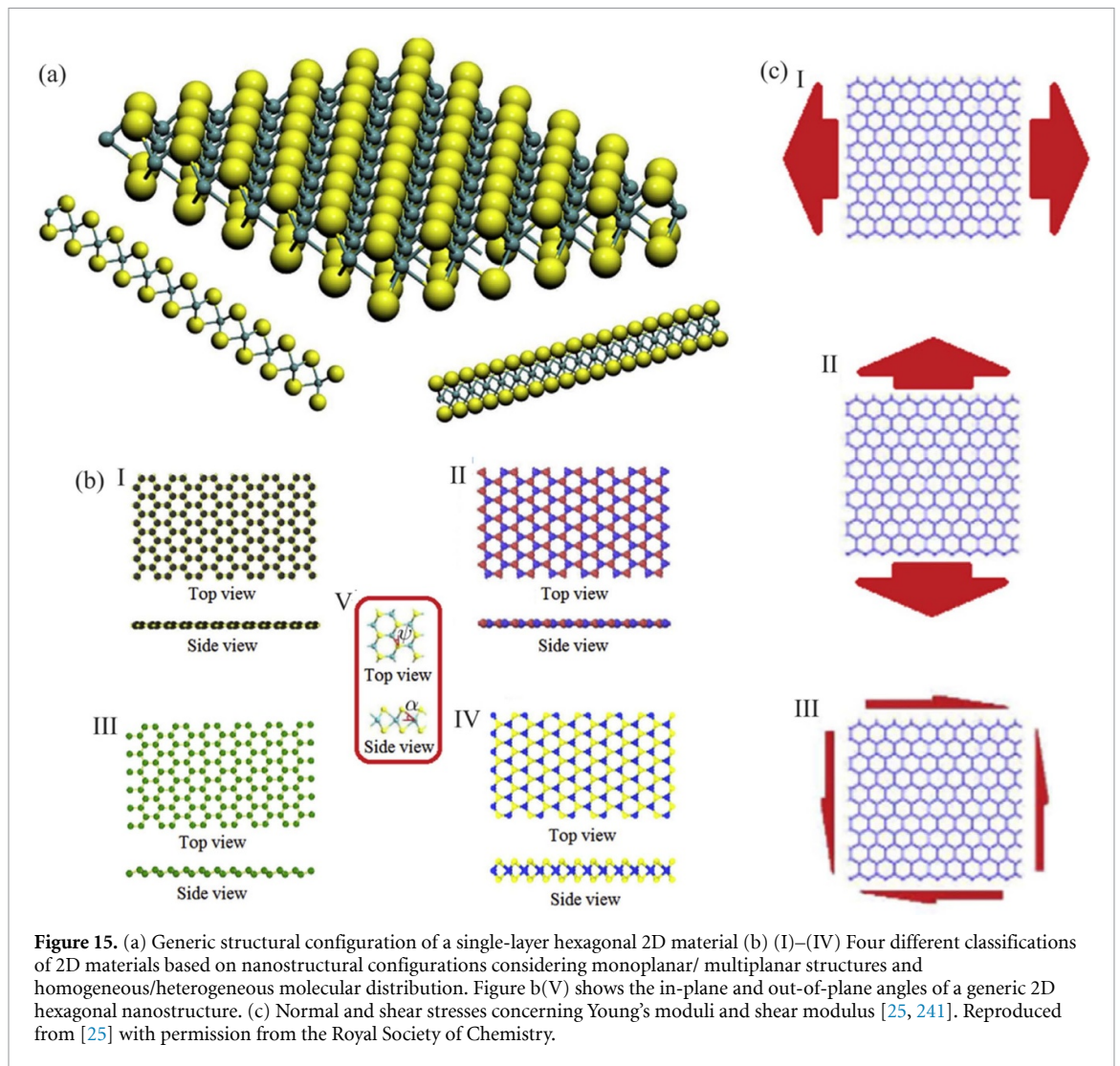


Figure 15. (a) Generic structural configuration of a single-layer hexagonal 2D material (b) (I)–(IV) Four different classifications of 2D materials based on nanostructural configurations considering monoplanar/ multiplanar structures and homogeneous/heterogeneous molecular distribution. Figure b(V) shows the in-plane and out-of-plane angles of a generic 2D hexagonal nanostructure. (c) Normal and shear stresses concerning Young's moduli and shear modulus [25, 241]. Reproduced from [25] with permission from the Royal Society of Chemistry.

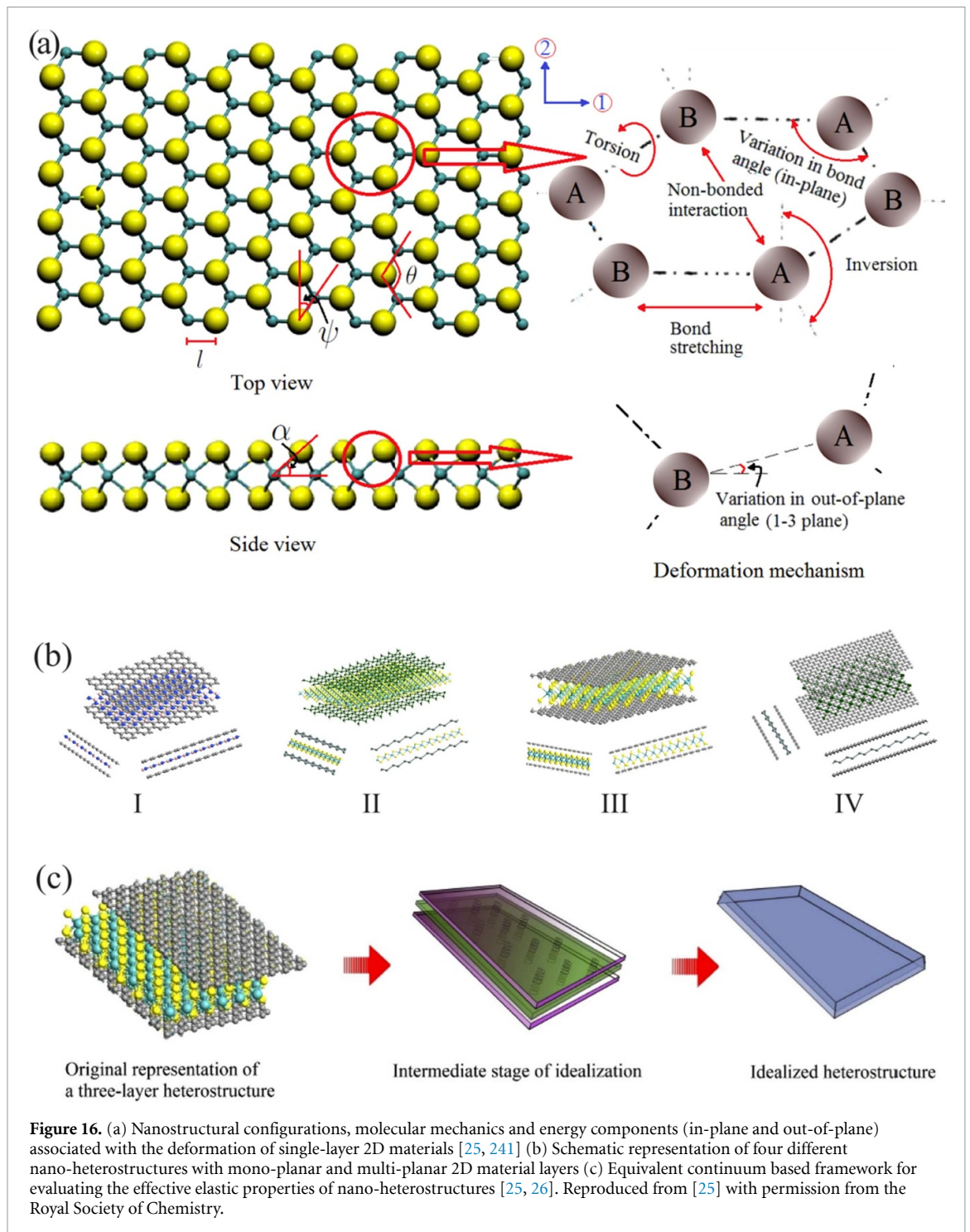
and review the analytical formulae from existing literature with a brief description of the philosophy behind their derivation [25, 26, 241]. The elastic moduli are obtained using a unit cell-based approach, wherein the mechanical equivalence of the atomic bonds is exploited in the form of a beam element. Two different materials, graphene and MoS_2 (along with their multi-layer heterostructures), are chosen to present the numerical results that fall in the two categories of monoplanar and multiplanar structures, respectively.

4.1. Mechanical equivalence of atomic bonds and effective elastic moduli

As discussed in the preceding section, the single layer 2D materials can be broadly classified into four classes. However, from a mechanics point-of-view, two separate categories are required to be recognized: monoplanar structures and multiplanar structures. This is because of the fact that the equivalent properties of the bonds are important in evaluating the elastic properties of materials, rather than the similarity or dissimilarity of two adjacent atoms. It can

be noted in this context that the monoplanar structural form can be treated as a special case of multiplanar structures. The top view and side view of a general multi-planar hexagonal nanostructure are shown in figure 16(a). From this figure, it is evident that a multiplanar structure reduces to monoplanar form when the out-of-plane angle becomes zero (i.e. $\alpha = 0$).

For atomic level behavior of nano-scale materials, the effective interatomic potential energy can be evaluated as a sum of various individual energy components related to bonding and non-bonding interactions [261]. Total strain energy consists of the contributions from bending of bonds, bond stretching, torsion of bonds and energies associated with non-bonded terms such as the van der Waals attraction, the core repulsions and the coulombic energy. However, among all the energy components, effect of bending and stretching are predominant in case of small deformation [264, 265]. For multiplanar hexagonal nanostructures (such as stanene and MoS_2), the strain energy pertaining to bending consists of two components: in-plane component



and out-of-plane component. The predominant deformation mechanisms for a multiplanar nanostructure are depicted in figure 16(a). It can be noted that the out-of-plane component becomes zero for monoplanar nanostructures such as graphene and hBN.

The force constants concerning the atomic bonds, k_r and k_θ (for bond stretching and bending respectively) can be idealized as beams (having length l , cross-sectional area A , second moment of area

I and Young's modulus E) with equivalent bending and axial stiffness [241] (i.e. structural equivalence), as: $k_\theta = EI/l$ and $K_r = EA/l$. On the basis of the established mechanical equivalence between the molecular mechanics parameters (k_r and k_θ) and structural mechanics parameters (EA and EI), the effective elastic moduli (two Young's moduli, two poisson's ratios and shear modulus [266, 267]) of monolayer 2D nanostructures can be obtained in closed form [241]:

$$E_1 = \frac{\cos \psi}{t(1 + \sin \psi) \left(\frac{l^2}{12k_\theta} (\sin^2 \psi + \cos^2 \psi \sin^2 \alpha) + \frac{\cos^2 \psi \cos^2 \alpha}{k_r} \right)} \quad (7)$$

$$E_2 = \frac{1 + \sin \psi}{t \cos \psi \left(\frac{l^2}{12k_\theta} (\cos^2 \psi + \sin^2 \psi \sin^2 \alpha + 2 \sin^2 \alpha) + \frac{\cos^2 \alpha}{k_r} (\sin^2 \psi + 2) \right)} \quad (8)$$

$$\nu_{12} = \frac{\sin \psi \cos^2 \psi \cos^2 \alpha l^2}{12k_\theta (1 + \sin \psi) \left(\frac{l^2}{12k_\theta} (\sin^2 \psi + \cos^2 \psi \sin^2 \alpha) + \frac{\cos^2 \psi \cos^2 \alpha}{k_r} \right)} \quad (9)$$

$$\nu_{21} = \frac{\sin \psi (1 + \sin \psi) \cos^2 \alpha l^2}{12k_\theta \left(\frac{l^2}{12k_\theta} (\cos^2 \psi + \sin^2 \psi \sin^2 \alpha + 2 \sin^2 \alpha) + \frac{\cos^2 \alpha}{k_r} (\sin^2 \psi + 2) \right)} \quad (10)$$

$$G_{12} = \frac{k_r k_\theta \cos \psi (1 + \sin \psi)}{t \left(k_\theta \sin \psi (1 + \sin \psi)^2 \cos \alpha + \frac{k_r l^2}{6} \cos^2 \psi (\cos \alpha + 2) \right)} \quad (11)$$

In the presented expressions of elastic moduli $\psi = 90 - \frac{\theta}{2}$, as shown in figure 16(a), and t is the single layer thickness of a 2D material. In the special case for the hexagonal nanostructures with monoplanar configuration (e.g. graphene and hBN) α becomes 0.

The expressions for elastic moduli of single-layer 2D materials can be extended to derive closed-form expressions for nano-heterostructures, which are applicable for any stacking sequence of the

constituent single layers and any 2D material (refer to figure 16(b)). Such heterostructures essentially open up an entire domain of research with an exceptional promise of multi-functional nano-material invention. Based on a continuum-based layer-wise idealization [25–27], as presented in figure 16(c), the equivalent effective elastic properties of a generic n -layer configuration of nano-heterostructure can be obtained as

$$E_1 = \frac{1}{t} \sum_{i=1}^n \frac{\cos \psi_i}{(1 + \sin \psi_i) \left(\frac{l_i^2}{12k_{\theta i}} (\sin^2 \psi_i + \cos^2 \psi_i \sin^2 \alpha_i) + \frac{\cos^2 \psi_i \cos^2 \alpha_i}{k_{r i}} \right)} \quad (12)$$

$$E_2 = \frac{1}{t} \sum_{i=1}^n \frac{1 + \sin \psi_i}{\cos \psi_i \left(\frac{l_i^2}{12k_{\theta i}} (\cos^2 \psi_i + \sin^2 \psi_i \sin^2 \alpha_i + 2 \sin^2 \alpha_i) + \frac{\cos^2 \alpha_i}{k_{r i}} (\sin^2 \psi_i + 2) \right)} \quad (13)$$

$$\nu_{12} = \frac{\sum_{i=1}^n \frac{\cos \psi_i}{(1 + \sin \psi_i) \left(\frac{l_i^2}{12k_{\theta i}} (\sin^2 \psi_i + \cos^2 \psi_i \sin^2 \alpha_i) + \frac{\cos^2 \psi_i \cos^2 \alpha_i}{k_{r i}} \right)}}{\sum_{i=1}^n \frac{12k_{\theta i}}{\sin \psi_i \cos \psi_i \cos^2 \alpha_i l_i^2}} \quad (14)$$

$$\nu_{21} = \frac{\sum_{i=1}^n \frac{1 + \sin \psi_i}{\cos \psi_i \left(\frac{l_i^2}{12k_{\theta i}} (\cos^2 \psi_i + \sin^2 \psi_i \sin^2 \alpha_i + 2 \sin^2 \alpha_i) + \frac{\cos^2 \alpha_i}{k_{r i}} (\sin^2 \psi_i + 2) \right)}}{\sum_{i=1}^n \frac{12k_{\theta i}}{\sin \psi_i \cos \psi_i \cos^2 \alpha_i l_i^2}} \quad (15)$$

$$G_{12} = \frac{1}{t} \sum_{i=1}^n \frac{k_{r i} k_{\theta i} \cos \psi_i (1 + \sin \psi_i)}{\left(k_{\theta i} \sin \psi_i (1 + \sin \psi_i)^2 \cos \alpha_i + \frac{k_{r i} l_i^2}{6} \cos^2 \psi_i (\cos \alpha_i + 2) \right)} \quad (16)$$

In the above equations, t denotes the total thickness of the heterostructure, and the subscript i is used as an index for a particular 2D material layer.

4.2. Numerical results and comparative assessment of accuracy

The expressions of elastic moduli can be adopted to readily obtain the elastic moduli of both

Table 2. Results for two Young's moduli (E_1 and E_2 , in TPa) and two in-plane Poisson's ratios (ν_{12} and ν_{21}) of graphene-MoS₂ (G–M) heterostructures with different stacking sequences and the respective mono-layers. The thickness of single layer graphene and MoS₂ are considered as 0.34 nm and 0.6033 nm, respectively. The results obtained using separate MD simulations are from [26].

Configuration	Continuum results			Continuum results		
	E_1	E_2	References ($E_1 = E_2$)	ν_{12}	ν_{21}	References ($\nu_{12} = \nu_{21}$)
G	1.0419	1.0419	1.05 [255] 1 ± 0.1 [275]	0.2942	0.2942	0.34 [276], 0.195 [277]
G/G	1.0419	1.0419	1.06 [255], 1.04 ± 0.1 [278]	0.2942	0.2942	0.2798 [26]
M	0.1778	0.3549	0.16 [255], 0.27 ± 0.1 [279]	0.0690	0.1376	0.1376 [26], 0.21 [280]
M/M	0.1778	0.3549	0.27 [255], 0.2 ± 0.1 [279]	0.0690	0.1376	0.1018 [26]
G/M	0.4893	0.6025	0.53 [255], 0.49 ± 0.05 [256]	0.1672	0.2059	0.2153 [26]
G/M/G	0.6357	0.7189	0.68 [255], 0.56 [105]	0.2058	0.2328	0.1805 [26]
M/G/M	0.3678	0.5059	0.45 [255]	0.1318	0.1813	0.1859 [26]

Table 3. Results for shear modulus (G_{12} , in TPa) of graphene-MoS₂ (G–M) heterostructures with different stacking sequences and the respective mono-layers. The thickness of single layer of graphene and MoS₂ are considered as 0.34 nm and 0.6033 nm, respectively. The results obtained using separate MD simulations are from [20].

Configuration	Continuum results	Reference results
G	0.3689	0.28 ± 0.036 [281], 0.493 [282]
G/G	0.3689	0.3730 [25]
M	0.1192	0.1310 [25]
M/M	0.1192	0.1205 [25]
G/M	0.2092	0.2400 [25]
G/M/G	0.2515	0.2430 [25]
M/G/M	0.1741	[25]

monoplanar and multiplanar 2D nanostructures, and their heterostructural forms. Two different 2D materials with hexagonal nano-structures are considered (graphene and MoS₂) here for showing the effectiveness of the closed-form formulae. Graphene belongs to the monoplanar configuration, wherein all the atoms are carbon, and they are in a single plane. The molecular mechanics parameters k_r and k_θ can be obtained from literature using AMBER force field [268] as $k_r = 6.52 \times 10^{-7}$ Nnm⁻¹ and $k_\theta = 8.76 \times 10^{-10}$ Nnm rad⁻². The out-of-plane angle for graphene is $\alpha = 0$ and the bond angle is $\theta = 120^\circ$ (i.e. $\psi = 30^\circ$), while bond length and thickness of single layer graphene can be obtained from literature as 0.142 nm and 0.34 nm, respectively [262]. MoS₂ belongs to the multiplanar configuration, wherein two different atoms Mo and S form the 2D material nanostructure and they are in different planes. The molecular mechanics parameters k_r and k_θ can be obtained from literature as $k_r = 1.646 \times 10^{-7}$ Nnm⁻¹ and $k_\theta = 1.677 \times 10^{-9}$ Nnm rad⁻², and the out-of-plane angle, bond angle, bond length and thickness of single layer of MoS₂ are $\alpha = 48.15^\circ$, $\theta = 82.92^\circ$ (i.e. $\psi = 48.54^\circ$), 0.242 nm and 0.6033 nm, respectively [269–274].

The elastic moduli of mono-layer and multi-layered 2D nanostructures predicted by the analytical formulae are compared with previous studies reported in scientific literature. Tables 2 and 3 show that the results obtained based on the computationally efficient molecular mechanics-based closed-form

formulae are well-aligned with the results available in literature, establishing the accuracy of this approach.

In summary, generalized closed-form molecular mechanics based analytical formulae for the elastic moduli of hexagonal mono- planar and multiplanar 2D nano-structures are discussed in this section. The dependence of the elastic moduli on length, angles and stiffness parameters of atomic bonds are explicitly demonstrated. Subsequently, it is also shown that an efficient continuum-based framework can be developed for the effective elastic properties of multi-layer heterostructures. This method's accuracy aligns with experimental and literature data, proving its efficacy in predicting mechanical properties critical for applications in nanoelectromechanical systems. Future research will likely focus on hybrid multiscale simulation approaches to comprehensively investigate the mechanical, thermal, and electrical properties of 2D materials, addressing the need for effective property mapping across different length scales and exploring properties defined at molecular, atomistic, and electronic levels.

5. Artificial intelligence and ML assisted study and design of 2D materials

With tremendous recent progress in the field of ML and artificial intelligence (AI), the materials science community has developed a legitimate interest in integrating the physics-based computational approaches with data-driven approaches for achieving computational efficiency and to explore

previously unexplored design domains. The field of 2D materials, with the vast scope of combining their different variants with numerous possibilities of stacking sequences along with design parameters like twisting angle, strains, introduced defects and translations [283], has embraced such data-driven approaches for identifying target combinations of the parameter space that would be impossible to explore solely using conventional methods of simulations and experiments. Besides efficient prediction, the emerging ML and AI algorithms can be useful in feature identification, sensitivity analysis, optimum design for multi-objective goals and uncertainty quantification. In this section, we have discussed the recent trends of adopting ML for analyzing and designing 2D materials (including the development of ML potential and characterization of different internal and external influencing parameters of 2D materials and their heterostructures) along with prospective future directions.

5.1. ML-assisted potentials and force fields

For MD simulations, interatomic potentials such as AIREBO [164], REAX [285], Tersoff [286] and associate LJ potential have been very successful in predicting various physical, chemical, and electronic properties of graphene and different 2D heterostructures. Gaussian approximation potential (GAP) method was utilized to construct a ML potential for graphene [287], which was trained using energies, forces, and virial stresses calculated using high-quality van der Waals (vdW) inclusive DFT calculations. While the GAP model quantitatively predicts specific properties of graphene, it falls short compared to the predictive capabilities of REBO/AIREBO potential across a comprehensive range. However, GAP-based ML potential has a significant advantage over AIMD simulations [287] as it enables faster MD simulations.

ML has also been used to construct force-fields for other 2D materials other than graphene, such as Mxenes [288], Stanene [289], MoS₂ heterostructures [289], Hexagonal Boron Nitride [290, 291] and their heterostructures. In short, these works (and other related reports) involve designing strategies for efficient parameter optimization for thermal, mechanical, and other physical properties. Also, MD simulation utilizing ML-based potentials can also be used in combination with ML-based data analysis and experiments for achieving better prediction accuracy. For example, a combination of ML with MD simulations and in-situ high-resolution transmission electron microscopy was able to explore the evolution of defects in TMDs, where ML provided information for structural optimization and evolution of defects to help understand the structural transition in 2D TMDs [201]. Figure 17 demonstrates that ML potential (MLP) can be used to accurately predict classical interatomic potential. Figure 17(a) shows MLP's strong correlation with DFT reference energies

in training and testing datasets. Figure 17(b) indicates that the majority of errors in both datasets were within target accuracy. Figure 17(c) demonstrates MLP's effective prediction of metastable atomic structures with minimal deviation. Figure 17(d) illustrates energy conservation in MD simulations of graphene, with minor energy fluctuations, except for a slight drift in longer time steps.

A practical method to explore hybrid 2D materials was developed by coupling ML with DFT calculations [292]. The structural and electronic properties of different hybrid 2D materials were provided and various parameters for vdW heterostructures were screened. A ML model with force-field-inspired descriptors in material screening for complex systems was introduced to discover exfoliated 2D-layered materials [292]. In another work, an artificial neural network for titanium dioxide systems was trained based on a DFT calculated database, where a novel quasi 2D titanium dioxide structure was revealed [293]. Similarly, new 2D materials with high magnetic moments were found using a ML model trained by first-principles data [294]. ML methods have also been used to aid the development of force fields for classical simulations of materials. For instance, a force field for classical simulations of stanene was developed using a ML method trained by data sets from ab-initio results to calculate the mechanical and thermal properties of stanene [259].

5.2. Non-intrusive approaches for ML-assisted prediction of physical properties

Several ML based models have been developed to study the mechanical properties, electronic properties, and chemical properties of 2D materials. Support Vector Mechanics (SVM) were used to study the fracture strength of graphene [295, 296], MoS₂ [297], and MoSe₂ [298]. The mechanical properties of WS₂ [299], Graphene Oxides [300], hBN [301] were evaluated using a Random Forest (RF) regression algorithm. Other ML algorithms that have been implemented in the context of different 2D materials for understanding mechanical properties include least absolute shrinkage and selection operator (LASSO) [302], recursive feature elimination (RFE) [303], extreme gradient boosting (XGBoost) [298, 301], long short-term memory (LSTM) [298], and feed forward neural network (FFNN) [298]. The underlying ideas of all above mentioned ML approaches are comparable to each other. In the above-mentioned works, the general approach for investigating the mechanical properties is the following. In the first step, sufficient training data for ML needs to be obtained by performing uniaxial tensile tests using MD simulations under various conditions. This data can be also complied with available experimental data as well. The input conditions (e.g. chirality, strain rate, and density of defects) of the MD simulations and the corresponding outputs (e.g. fracture

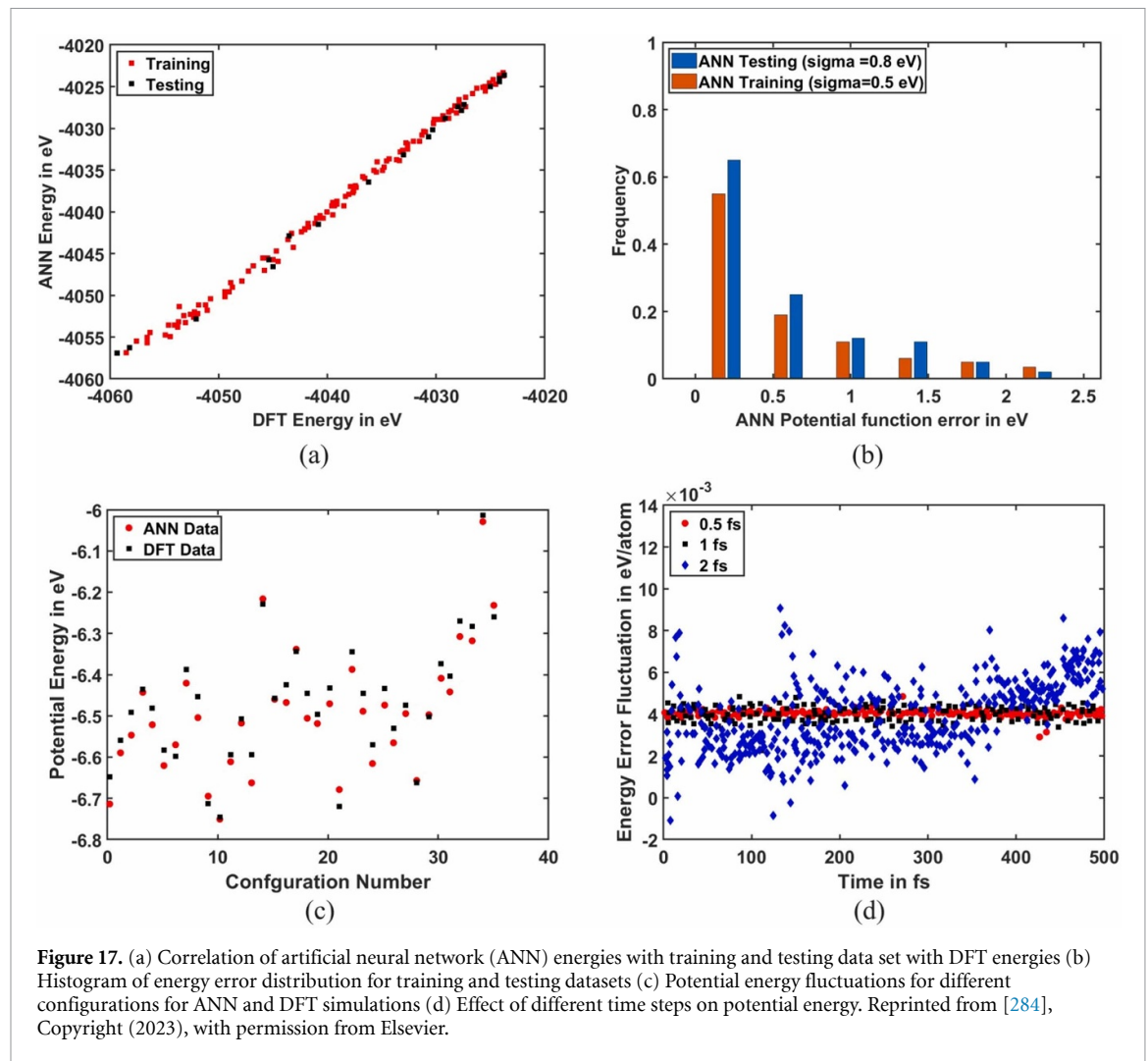


Figure 17. (a) Correlation of artificial neural network (ANN) energies with training and testing data set with DFT energies (b) Histogram of energy error distribution for training and testing datasets (c) Potential energy fluctuations for different configurations for ANN and DFT simulations (d) Effect of different time steps on potential energy. Reprinted from [284], Copyright (2023), with permission from Elsevier.

strain, strength, and Young's modulus) serve as input features and labeled outputs, respectively. At the next stage, a computational mapping is established between the set of input and output features using a suitable ML algorithm. The predictive capability of the constructed ML model is verified thoroughly based on unseen data points using several measures such as Root Mean Square Error (RMSE), Mean Absolute Error (MAE), Mean Absolute Percentage Error (MAPE), and scatter plots. If the error is within acceptable limits, the ML model can be further utilized for prediction corresponding to any combination of the input features within specified bounds. The application of these ML algorithms in understanding electronic properties follows a very similar approach. ML has been employed utilizing kernel ridge (KRR), support vector (SVR), Gaussian process (GPR), and bootstrap aggregating regression algorithms to extract band gaps of 2D Mxenes [304].

5.3. Image-based computational mapping using ML

The training data for ML can also be image-represented objects. Problems such as defects,

dislocations, and vacancies can be studied using deep convolutional neural network (CNN). CNN has been implemented in studying the mechanical properties of h-BN [307]. The input for CNN can be a set of RGB images rendered from atomistic modelling for the subject material. The output of the neural network is a number predicting either Young's modulus or strength (while studying mechanical properties). As CNN is a kind of network architecture for deep learning algorithms and is specifically used for image recognition and tasks that involve the processing of pixel data, it is beneficial to supplement results available from electron microscopy for 2D materials [308, 309]. Sterbentz *et al* [305] presented an image processing ML program, as demonstrated in figure 18, which advances image segmentation by utilizing unsupervised clustering algorithms to automatically discern the thickness of 2D materials in optical microscopy images with $\sim 95\%$ pixel accuracy. This approach maintains all three RGB color channels and applies Gaussian mixture models to cluster analysis, enhancing generality across various substrates. Figure 18 depicts the process from initial image cropping and optical contrast-based thickness

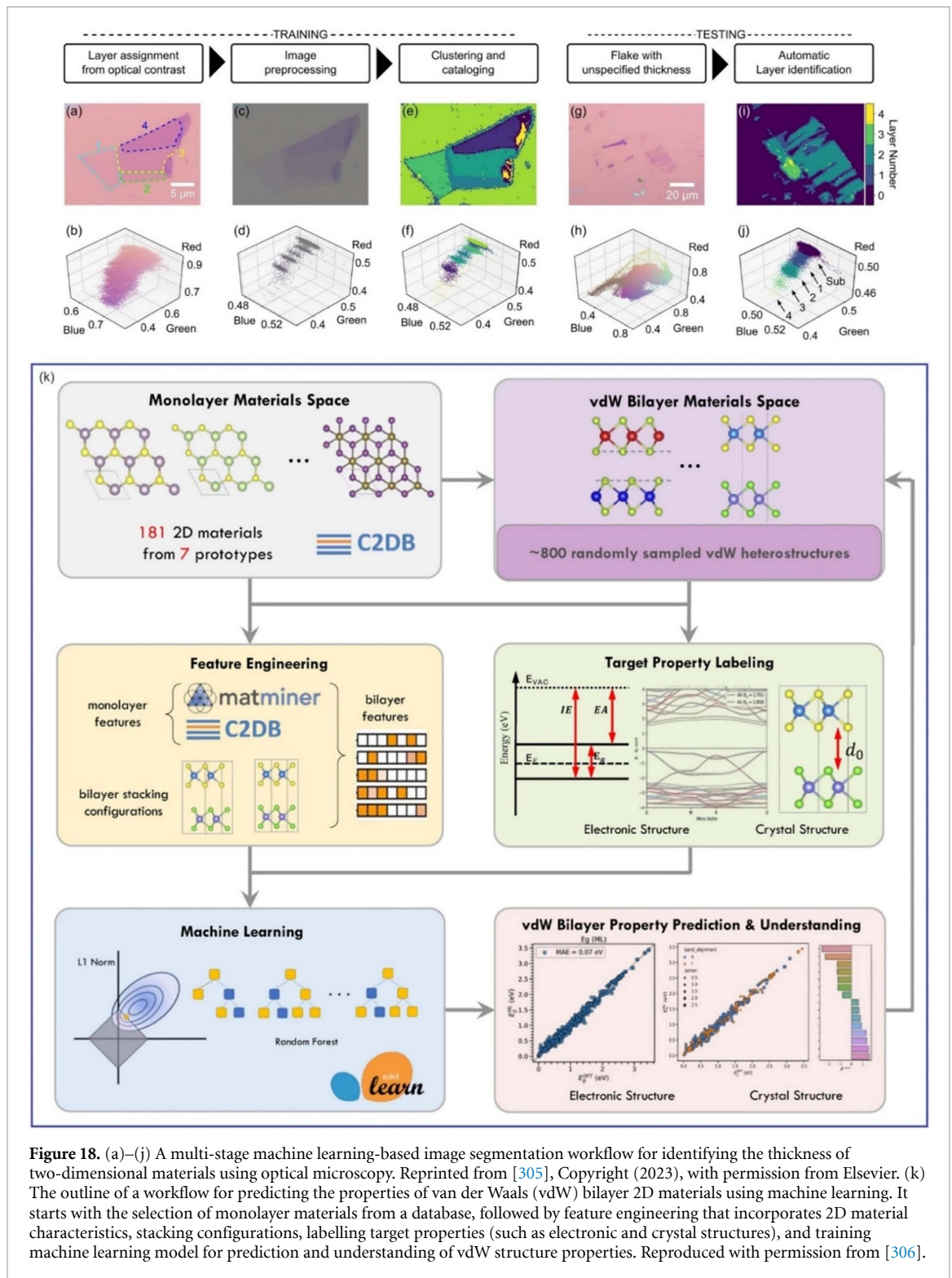


Figure 18. (a)–(j) A multi-stage machine learning-based image segmentation workflow for identifying the thickness of two-dimensional materials using optical microscopy. Reprinted from [305], Copyright (2023), with permission from Elsevier. (k) The outline of a workflow for predicting the properties of van der Waals (vdW) bilayer 2D materials using machine learning. It starts with the selection of monolayer materials from a database, followed by feature engineering that incorporates 2D material characteristics, stacking configurations, labelling target properties (such as electronic and crystal structures), and training machine learning model for prediction and understanding of vdW structure properties. Reproduced with permission from [306].

labeling (figure 18(a)) to noise reduction and cluster differentiation (figures 18(c) and (d)). Cluster centers are pinpointed via mean shift and density-based clustering, with Gaussian mixture models further defining cluster traits (figures 18(e) and (f)). A master catalog correlating these clusters to known thicknesses is then created and tested against new images for thickness verification (figures 18(g)–(j)), showcasing the program's efficacy in assigning layer thicknesses and

promising universal applicability for different materials and substrates.

5.4. Exploiting ML for probabilistic analysis and uncertainty quantification

Recently the efficient predictive capabilities of ML have been exploited in simulation-extensive analyses such as uncertainty quantification and sensitivity analysis concerning different influencing factors in

the mechanical responses of 2D materials [60, 287, 310, 311]. For example, the reliability of the results derived from MD simulations depends on the adopted interatomic potential, which is mathematically fitted to the data obtained from first principles approaches or experiments. There exists a significant scope of uncertainty associated with the interatomic potential parameters. Such internal uncertainties, together with the effect of stochastic external parameters like temperature and strain rate can trigger an augmented random deviation in the output mechanical responses [284, 312, 313]. With the aim of developing an inclusive analysis and design paradigm, the effect of uncertainties associated with the internal parameters (Tersoff interatomic potential parameters) and external parameters (temperature and strain rate) along with their respective sensitivity was quantified on the mechanical properties of graphene [312].

In establishing the complete probabilistic descriptions of the response quantities corresponding to different levels of source uncertainties, a coupled ML-based Monte Carlo simulation approach was shown to achieve significant computational efficiency without compromising the accuracy of the results. A similar approach was extended further by coupling artificial neural networks, MD and Monte Carlo simulations for probing the stochastic fracture behavior of twisted bilayer graphene [315]. Further, the effects of intrinsic defects and doping on the stochastic mechanical properties of graphene were investigated based on ML assisted MD simulations [316]. A Gaussian process based ML approach in conjunction with MD simulations has been proposed to investigate the high-velocity ballistics of twisted bilayer graphene under stochastic disorder [314]. Notably, the stochastic analysis and uncertainty quantification concerning 2D materials following the ML approach, as discussed here, follow a non-intrusive approach, rather than developing the potential for MD simulations.

5.5. ML-based investigation of multi-layer 2D heterostructures

The data-orientated AI/ML-based approach can present an unprecedented opportunity and flexibility to test existing as well as hypothetical materials. The heterostructures of these single-layer materials (obtained by stacking different 2D materials on top of each other) are often even more interesting from the multi-functionality viewpoint than the single-layer 2D materials. Strong covalent bonds provide in-plane stability of 2D crystals, whereas relatively weak, van-der-Waals-like forces are sufficient to keep the stack together. The possibility of making multilayer van der Waals heterostructures was demonstrated experimentally, leading to various extraordinary physical, chemical, optical properties [317].

Unlike traditional heterostructures, vdW heterostructures are not limited by lattice mismatch.

Their properties may be strongly influenced by the interlayer twist angle and stacking order, which can provide a large material design space. Given the growing number of 2D monolayers, the vdW heterostructures space grows exponentially. Fabrication and characterization of vdW heterostructures via trial-and-error become an increasingly difficult task, as well as resource-intensive. Even high-throughput first-principles approaches become extremely expensive. Scalability is also another issue in first principle calculations, as the number of atoms that can be considered for each simulation is limited to around 100 atoms. Recently, ML methods have been applied to circumvent this problem. Tawfik *et al* [292] constructed 267 bilayers out of 53 different monolayers and trained ML models to predict the interlayer distance and band gap by using the property-labeled materials-fragments (PLMF) descriptors. Their best-performing models achieve a testing R^2 score of 0.96 and a mean-squared error (MSE) of 0.005\AA^2 for predicting the interlayer distance using 267 training data. Choudhary *et al* [318] leveraged a 2D material database in the JARVIS-DFT [319] library to predict the band edges and work function of monolayers by using classical force-field inspired descriptors (CFID). Their model predicts the monolayer valence band maximum (VBM) and conduction band minimum (CBM) with a mean-absolute-error of 0.67 eV and 0.62 eV, respectively. Dong *et al* [320] recently proposed a low-cost method of obtaining the electronic band structure of bilayers via band-folding. They applied their model to 703 vdW bilayer heterostructures based on 1 T and 2 H prototype structures and performed a comprehensive analysis of their electronic structures. A recent ML based model developed by Willhelm *et al* [306] predicts the atomic and electronic structure of vdW heterostructures of nearly 4000 unique bilayer structures from seven different hexagonal monolayer prototypes. The developed ML models were found to predict the bilayer band-gap, interlayer binding energy, interlayer distance etc. with low error, providing a valuable tool for screening the vast vdW heterostructure material space with a significantly reduced computational cost for a wide range of optoelectronic applications. In general, such studies establishes the fact that it is highly desirable to establish accurate ML models that can predict a rich set of material properties for a large number of vdW heterostructures with a variety of stacking configurations and prototype structures from the existing 2D material database. This would lead to the identification of optimum heterostructure configurations efficiently (based on thousands of realizations which would have been otherwise impossible using experiments or traditional simulation techniques) that can possess application-specific multi-objective capabilities.

Overall the idea of ML-based models has been shown in figure 18(k) [306]. First, material data and

ground-state crystal structures are mined from 2D material databases or obtained suitably using conventional simulation or experimental methods. The ground-state monolayer structures are stacked vertically to create a large material design space of unique heterostructures. We then sample the vdW heterostructure design space, and the corresponding physical properties are calculated using high-throughput DFT calculations, experiments, or MD simulations. In the next stage, the ML models are constructed based on a suitable algorithm ensuring adequate prediction accuracy through a series of measures. In the literature, ML has been also used to predict band gaps concerning several heterostructures such as HfS₂-MoTe₂, HfS₂-WTe₂, MoSe₂-TiS₂, MoTe₂-HfS₂, HfS₂-WTe₂, TiS₂-WSe₂, TiS₂-ZnO, and TiSe₂-WTe₂ [292].

In this section, we discussed some of the recent progress in applying ML approaches for study and design of 2D materials. After development of predictive and computationally efficient ML models for 2D materials and their heterostructures, the natural progression is to exploit those for identifying optimum configurations for achieving multiple, often conflicting objectives. In doing so, the notion of inherent uncertainty, direct image-to-image correlations, reinforcement learning, and Bayesian approaches are being pursued actively [267, 321, 322]. The future trajectory of 2D materials research is poised for an exciting convergence with physics-based ML methodologies [323, 324]. Integrating physics principles into ML models is anticipated to revolutionize material science by fostering a deeper understanding of the fundamental physics governing 2D materials.

6. Multiscale modeling and synthesis of 2D materials

6.1. Experimental synthesis techniques

The synthesis strategies of 2D materials are divided into two main classes, known as top-down and bottom-up methods. Mechanical/liquid exfoliation and etching are well-known techniques based on the top-down approach in which the three-dimensional (3D) crystal is isolated into single- or multi- atomic layers. Depending on their robust geometric and bonding criteria, there are various 3D materials that appear layered and have the potential to be synthesized by top-down methods. Materials such as MoS₂ [325], h-BN [326], WS₂ [325] and graphene [327], consist of layers connected with weak van der Waals (vdW) forces (shown in figure 19(a)). These materials are mostly manufactured by exfoliation techniques. The strong three-dimensional covalent/ionic bonding makes top-down approaches such as mechanical exfoliation a highly unlikely synthesis method. Hence, most of the strategies employed for the 2D synthesis of these materials are bottom-up methods. However, in a very recent approach Puthirath Ballan

et al [328] showed non-layered (non-vdW) materials such as metal oxides [329] with ionic bonds can also be exfoliated. They used the concept of cleavage planes along which intrinsic isotropic covalent/ionic crystals tend to be unstable [330, 331]. The bottom-up synthesis method is a scalable approach building the material atom by atom. This technique facilitates achieving high levels of thickness uniformity, which makes this method a suitable choice for manufacturing electronics and optoelectronics materials [332].

6.1.1. Top-bottom method: mechanical and liquid exfoliation and etching

Exfoliation synthesis method can be divided into two main categories: mechanical and liquid exfoliation. As shown in the schematic representations of liquid exfoliation in figure 19(b), ultrasound or electrical current helps overcoming the binding energy between the atomic layers [333–335]. In ultrasonic liquid exfoliation, the bulk material is placed into organic solvent or water and ultrasonic waves are applied to the system [336]. The high-frequency sound waves and the resulting intense shear forces break the interlayer bonds and form individual layers from bulk material. Similar to ultrasonic liquid exfoliation, electrochemical liquid exfoliation starts from placing the bulk layered material inside a liquid medium. An electric potential is applied across the dispersion that causes ionic intercalation within the layers of bulk material. This induces force that weakens the interlayer forces [336, 337].

The sticky tape is the traditional mechanical exfoliation approach, where the peeling or pulling of an adhesive taped on top of bulk material separates some layers from bulk material [338]. Wedge technique is an advanced variation of mechanical exfoliation which used a sharp wedge-shaped object to separate a thin layer from the bulk material [339]. Ball milling is a relatively simple and scalable approach for exfoliating 2D material [340]. This method places bulk material into a milling container filled with balls. The rotating container creates the mechanical shear force needed to exfoliate individual layers. Another group of 2D materials known as MXenes [341] are ternary carbides and nitrides with a layered, hexagonal structure. MXenes are obtained from 3D MAX phases [342], where M is an early transition metal, A is an A-group (mostly IIIA and IVA) element and X is either carbon and/or nitrogen. The transformation of a 3D MAX phase into a 2D layered MXene is performed via the top-bottom chemical wet etching method, as shown in figure 19(b) [343, 344].

6.1.2. Bottom-up method: chemical and physical vapor depositions

The basis for describing the surface morphology and studying the dynamics of bottom-up growth of 2D material is by creating steps, as shown in figure 19(c). Steps separate different height terraces, and they

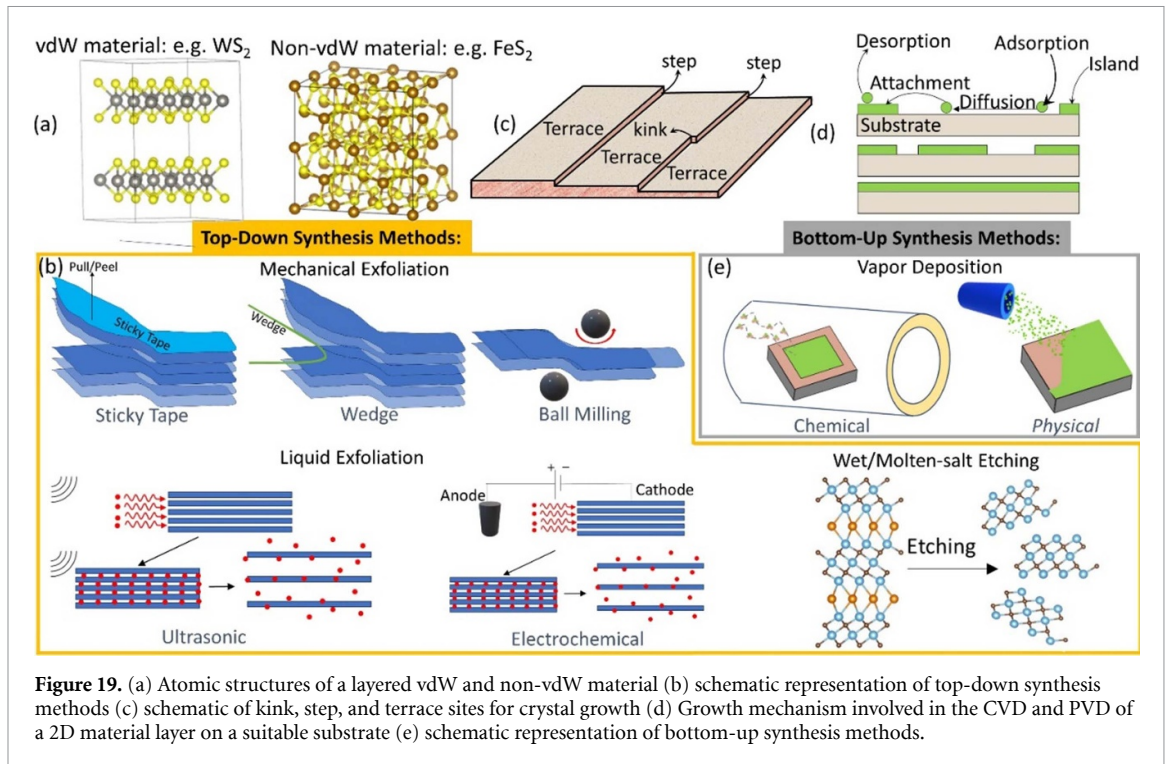


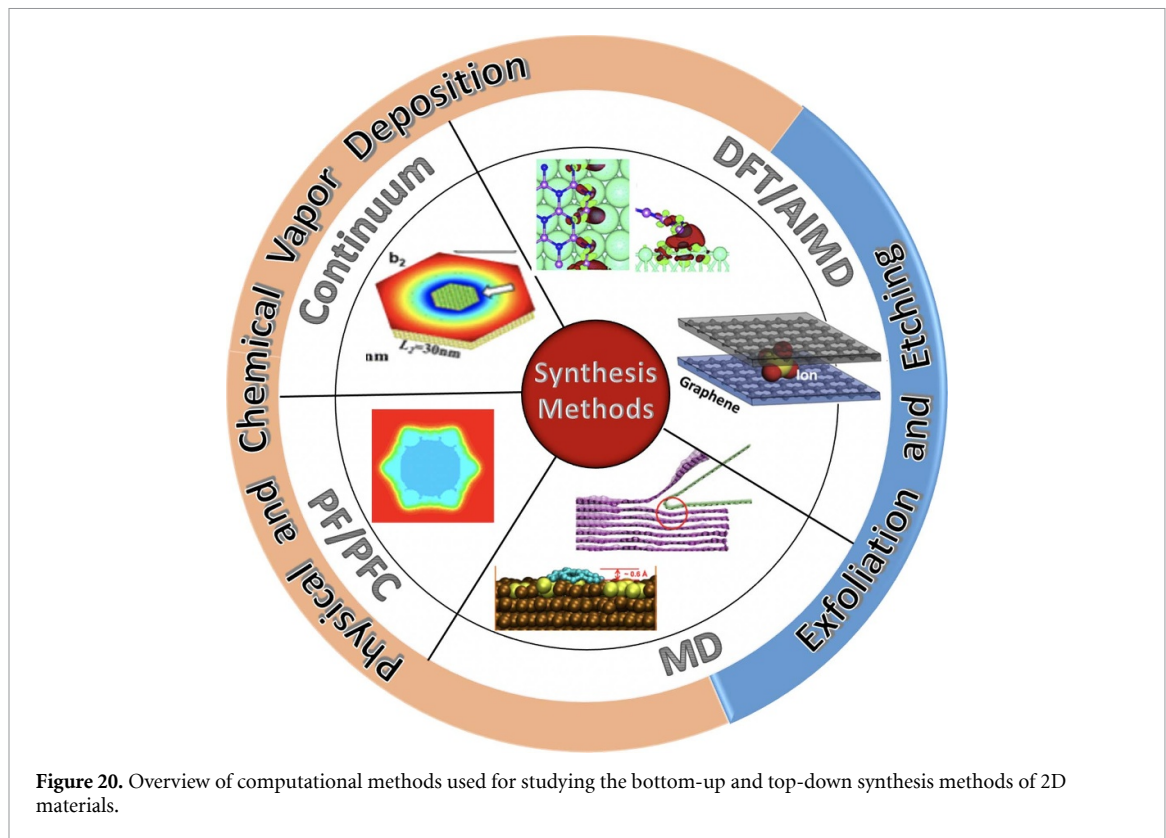
Figure 19. (a) Atomic structures of a layered vdW and non-vdW material (b) schematic representation of top-down synthesis methods (c) schematic of kink, step, and terrace sites for crystal growth (d) Growth mechanism involved in the CVD and PVD of a 2D material layer on a suitable substrate (e) schematic representation of bottom-up synthesis methods.

provide kink sites for the incorporation of new atoms into the crystal. As the atoms adsorb onto the surface of the growing crystal, they move across the surface via diffusion seeking for the most energetically favorable position. Given by figure 19(d), the diffusion and attachment of adatoms can result crystal growth by (i) nucleation and growth of new steps, or (ii) advancement of existing steps, or (iii) annihilation of steps by merging of islands and terraces. As the layer thickness increases, the substrate will also be covered which will hinder further deposition of layers. Chemical vapor deposition (CVD) and physical vapor deposition (PVD) techniques, as shown in figure 19(e), are two popular bottom-up synthesis. CVD produces a thin film by a chemical reaction between the precursor gases that contains the required elements. The desired material is a product of this chemical reaction and is deposited on the substrate. CVD has been widely used to produce various 2D materials, including graphene [345], h-BN [346], and TMDs [347]. However, during the PVD, the vaporized form of the desired material enters the chamber and is condensed on the substrate forming thin films. In this paper we mainly focus on the applications of different computational approaches to investigate 2D material synthesis, and the details of each synthesis technique are not covered here, and they are described in detail in other works [9–12]. Figure 20 summarizes the computational methods used to study each bottom-up and top-down synthesis technique.

6.2. DFT collocations relevant to experimental synthesis of 2D materials

2D materials research has garnered considerable attention, notably following the successful exfoliation of single-layer graphene from its bulk graphite counterpart through the scotch tape method [327]. In theoretical work, it has become customary to designate 2D compounds as single freestanding layers. However, it is crucial to recognize that while some 2D materials like phosphorene [348, 349], h-BN [350, 351], and MoS₂ [352], can be exfoliated as freestanding single layers, many others like silicene [353] can only adopt a 2D structure when cultivated on a substrate or possessing a substantial thickness. Previous experimental studies have reported that silicene can only be stabilized on a specific substrate, and all attempts to stabilize it as a freestanding 2D layer were unsuccessful [353]. Since the formation of a 2D material involves breaking weak interlayer vdW bonds present in the bulk compound, in the case of 2D materials on a substrate, the substrate acts as a stabilizing agent, often fostering chemical bonding between the substrate and the 2D material [354]. Thus, if the isolation energy of the 2D material surpasses a specific threshold, achieving the compound in a freestanding form becomes less probable [355].

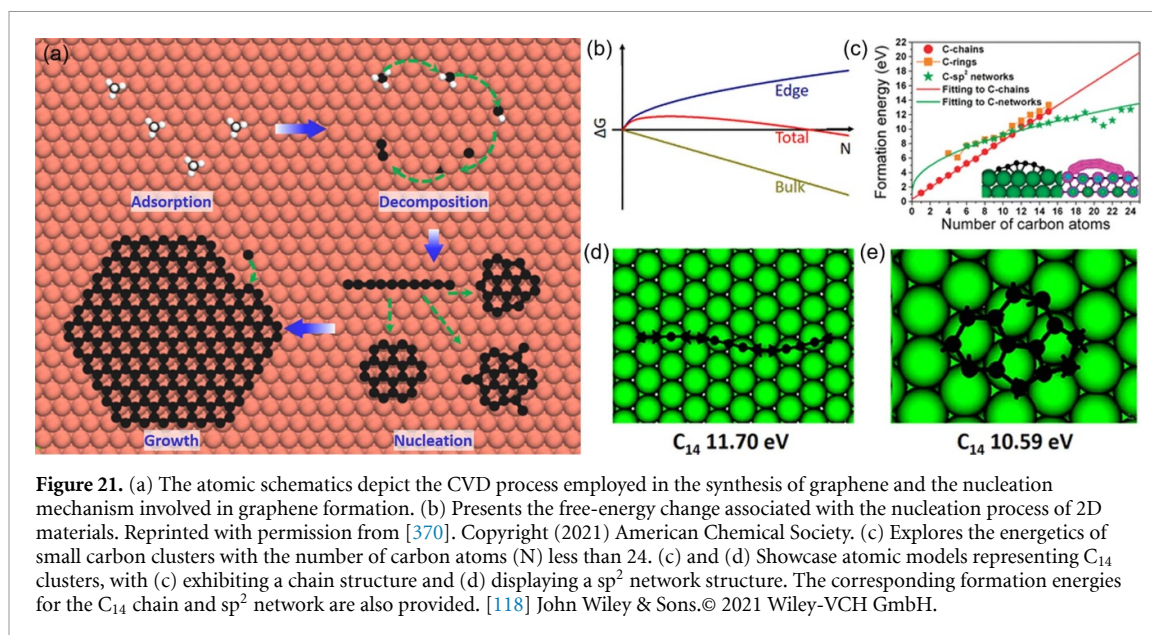
Given the predominantly Edisonian (trial and error) approach in the experimental synthesis of 2D materials, first-principles DFT calculations have made notable contributions to the field.



These studies involve exploring the properties of already synthesized materials and making theoretical predictions for a myriad of new 2D materials. DFT calculations offer insights into a material's energetic stability at absolute zero temperature [356]. This method is commonly employed as an initial step in predicting the feasibility of experimental synthesis. The DFT energy of a compound, along with that of its competing phases in a compositional system, allows for the determination of formation energies. At a specific composition, the formation energy of the convex hull represents the lowest linear combination of energies from competing phases [357]. The disparity between the formation energy of a given compound and that of the convex hull is termed the energy above the convex hull (E_{hull}). This parameter characterizes the material's zero-kelvin thermodynamic stability, where lower E_{hull} values indicate greater stability [357]. Several research efforts have not only identified numerous potential new 2D compounds but have also catalyzed the creation of comprehensive open-access databases like the Computational 2D Materials Database (C2DB) [86, 358], 2D Materials Encyclopedia (2DMatPedia) [359], the MaterialsWeb [360], and the Materials Cloud 2D crystals database [45]. Additionally, specialized high-throughput collections have been developed to explore magnetic properties [361] and spin splitting [362] of 2D materials. Despite these advancements, a notable portion of current theoretical investigations on 2D materials remains centered on manually crafted compounds,

lacking corresponding bulk analogs, and often lacking discussions on their feasibility.

Furthermore, advancements in theoretical studies employing DFT have provided structure-property understanding of different 2D materials. For example, DFT provided a fresh perspective on the morphological aspects of MoS_2 [363]. Notably, findings by Byskov *et al* propose that fully sulfided MoS_2 structures may exhibit a preference for 1010 Mo edges under certain conditions, while 1010 S edges become favored under more reducing conditions [364]. Besides, Schweiger *et al* [365] computed and reported the anticipated shape of MoS_2 clusters under varying conditions. These DFT insights help to understand the formation of highly dispersed single-layer MoS_2 nanoclusters with an average side length of a few nanometers. This DFT achievement was realized through the high-temperature sulfidation of initially deposited Mo on a pristine Au (111) single-crystal surface, maintained in a fully sulfiding atmosphere of H_2S [366]. Further, through a comprehensive analysis that involves comparing the atomic-scale scanning tunneling microscope (STM) images with simulated STM images based on DFT calculations of MoS_2 edges, Lauritsen *et al* reported the structural intricacies of the MoS_2 nanoclusters and establish a connection between their stability and the specific thermodynamic parameters governing their existence. HRTEM and molecular modeling studies of the $\text{MoS}_2\text{-Co}_9\text{S}_8$ interface reveal the formation of open latent vacancy sites on Mo atoms interacting with Co,



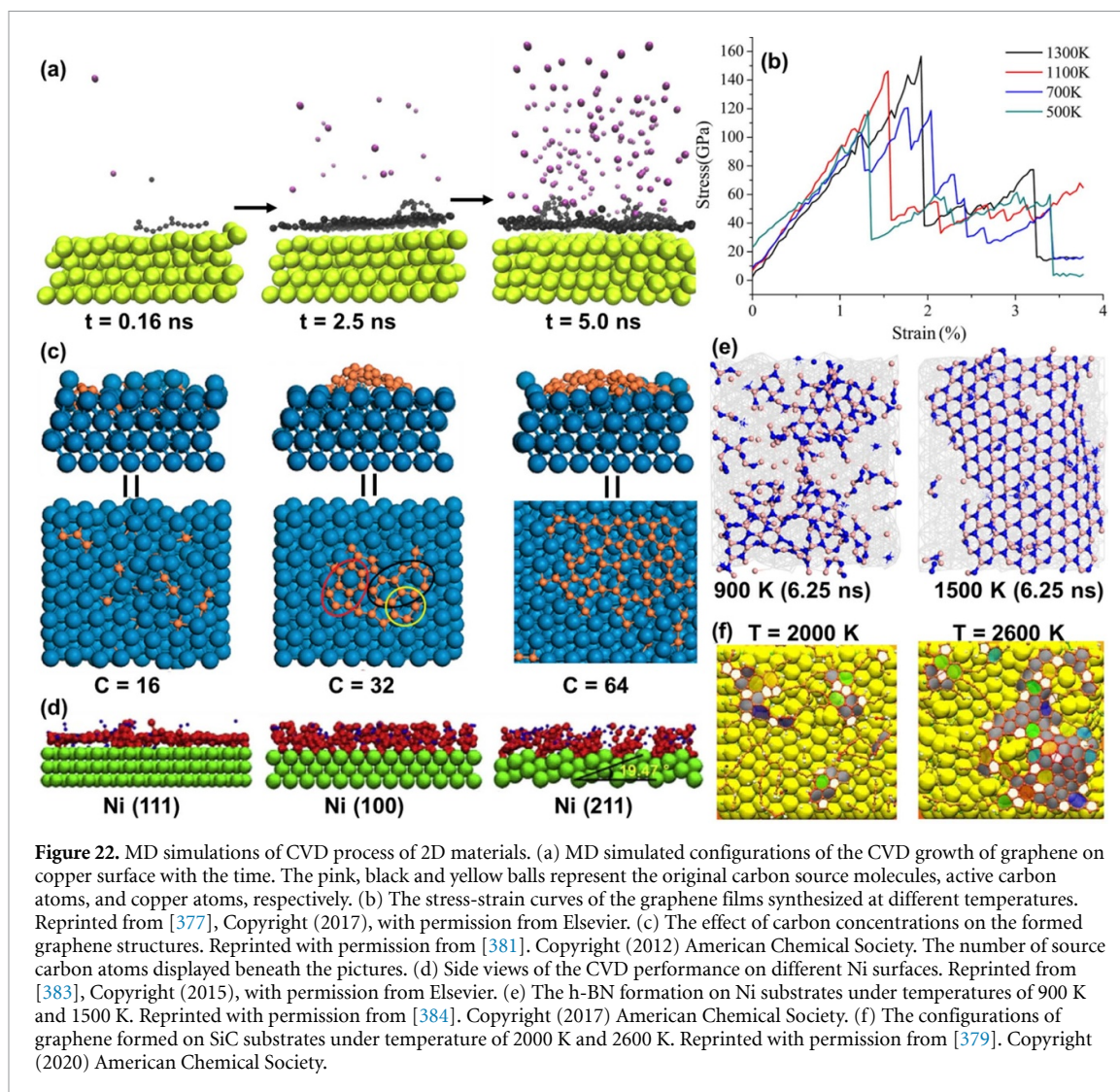
as well as the creation of direct Co–Mo bonds [367]. Additionally, strong electron donation from Co to Mo occurs through the intermediate sulfur atom bonded to both metals, resulting in an enhanced metallic character. These alterations in coordination and electronic properties are anticipated to promote a synergistic effect between Co and Mo at the localized interface region between the two bulk MoS_2 and Co_9S_8 phases, for enhancing the catalytic performance.

In 2D crystals, the electron beam can induce damage to the surface and edges of the extended sheets, resulting in irregular edges or holes caused by high electron beam penetration. However, the mechanisms of radiation damage are highly dependent on the environment and, consequently, the conditions of the radiation exposure [368]. Garcia *et al* conducted an analysis of electron beam damage on exfoliated MoS_2 using aberration-corrected scanning transmission electron microscopy (STEM) with a high angle annular dark field (HAADF) detector. This study also demonstrated that damage to the MoS_2 sheets can be controlled at 80 kV, in accordance with theoretical calculations based on the inelastic scattering of electrons involved in the electron–matter interaction [368].

Among the different synthesizing techniques, CVD is extensively used to produce different classes of 2D materials [332]. In 2012, Artyukov *et al* conducted first-principles calculations on vapor-phase graphene synthesis [369]. Using a step-flow crystal growth model, they investigated carbon atom migration to the nickel catalyst surface and their integration into the lattice. The study elucidated the graphene growth process sequence by calculating energies of intermediate states, highlighting edge attachment, and minimized defect formation in the presence of substrates. This DFT analysis provided key insights into the anisotropic growth, kinetics, and island morphology,

shedding light on experimental results, including carbon nanotube synthesis. The electron localization function (ELF) analysis using DFT can help in identifying the regions of charge localization in the system and thus help in gaining insights on inter-material interactions during synthesis. Furthermore, in most CVD experiments, a multitude of 2D crystals form on a substrate. Subsequent growth of these crystals results in their coalescence. Research indicates that the attainment of large-sized single-crystalline 2D materials involves the seamless coalescence of unidirectionally aligned 2D crystals, contrasting with the formation of polycrystals from misaligned 2D crystals [370]. Clearly, comprehending the mechanisms governing the alignment and coalescence of 2D crystals on substrates is essential for ensuring the quality of CVD-grown 2D material films [371]. The CVD process and nucleation mechanism of graphene synthesis is shown in figure 21. So, theoretical studies can play an important role in providing strategies to improve the reliability and robustness of synthesis methods for 2D materials and more details can be found elsewhere [332].

Although DFT calculations provide insights into the thermodynamic and kinetic barriers during the synthesis of 2D materials, they lack the capability to simulate the explicit temporal evolution of a system. In contrast, kinetic Monte Carlo (kMC) simulations, founded on probabilistic principles, offer the opportunity to explore growth kinetics over extended time scales, spanning minutes to hours [372]. However, whether conducted on a lattice or in an off-lattice manner, kMC simulations consider a finite number of plausible reaction or diffusion events, relying on rates determined through DFT calculations or fitting to experimental data. Moreover, AIMD simulations leverage first-principles potential energy surfaces to calculate forces and atomic velocities, integrating



atomic motion and entropic effects. Despite their computational demands, AIMD simulations provide a detailed understanding. Alternatively, classical MD simulations employing empirical interatomic potentials have been investigated for simulating chemical reactions, offering increased computational speed albeit with lower accuracy compared to AIMD simulations [373].

6.3. MD simulation facilitated synthesis techniques

MD simulations exhibit promising capabilities in streamlining the synthesis and characterization processes of 2D materials. Optimizing the synthesis of 2D materials through the complex CVD process requires a comprehensive understanding of the underlying mechanisms, which are influenced by factors such as temperature, pressure, carrier gas flow rate, and vapor-phase composition. Theoretical insights into the CVD growth of 2D materials have been obtained through the utilization of MD simulations [374, 375], as well as complementary tools like DFT [45] and kinetic Monte Carlo (KMC) simulations [376]. For example, to explore the mechanisms during the CVD

process, the growth of single layer graphene films on copper surface was investigated by MD simulations, as shown in figure 22(a) [377]. In that study, a hybrid potential, which combines AIREBO for the interaction of C_2 atoms [164], EAM potential for the interaction between Cu atoms, and Lennard-Jones potential for the Cu-C interaction [378], was employed. A graphene domain comprising approximately 300 carbon atoms was successfully achieved. It enabled a thorough examination of the influences of CVD parameters, specifically temperature and gas flow rate, on graphene films. Examining the trajectories of graphene growth reveals a consistent presence of graphene structures, where the side chains play a pivotal role in processes such as ring formation, defect healing, and the amalgamation of graphene nuclei. It is anticipated that the insights obtained from computational modeling will provide guidance for the synthesis of high-quality graphene in CVD experiments. Furthermore, the simulation results indicate that a more fully formed single-layer graphene (SLG) film can be attained at elevated temperatures or with a slower cooling rate, and the tensile strength

of SLG films rises with increasing temperature (see figure 22(b)).

Despite the previous efforts, it was claimed that empirical potentials may lack the capability to comprehensively investigate the CVD process [379]. Alternatively, reactive MD simulation is a promising tool for simulating the complicated chemical reactions that occur during CVD. Since the development of the ReaxFF force field for hydrocarbons in 2001 [380], it has been successfully employed to study the growth of various 2D materials. The pioneer reactive MD studies in this realm can be tracked back to 2012, when Meng *et al* [381] investigated the evolution of carbon structures and the growth kinetics of graphene on Ni (111) surface under different temperature conditions, as displayed in figure 22(c). Utilizing the ReaxFF potential specifically parameterized for C-Ni system [382], simulations were carried out, incorporating a maximum of 320 atoms. The study demonstrated a substantial influence of carbon atom concentration on graphene quality, with low concentrations leading to carbon atom dissolution into nickel, and high concentrations fostering the formation of graphene islands. Additionally, the substantial improvement in the quality of graphene islands can be achieved through efficient defect annealing at the optimal temperature of around 1000 K. This work provided insight into the CVD growth of graphene. In 2015, Lu and Yang [383] tried to use naphthalene/fluorene as carbon sources to study the formation and growth of graphene on nickel surfaces. MD simulations, employing the same ReaxFF potential [382], were carried out with a maximum total number of atoms reaching 954 for all models. Fundamental mechanisms were unraveled, including surface-assisted dehydrogenation reaction and coalescence reaction of active molecular species. They also compared the CVD performance on three different Ni surfaces and concluded that Ni (111) promotes the best formation and growth of high-quality graphene-like structure, as shown in figure 22(d). Following this work, Liu *et al* [384] utilized ReaxFF to explore the growth of h-BN on Ni substrates (figure 22(e)). They observed that nucleation begins with the growth of linear BN chains, and this structural evolution was confirmed by DFT calculations. Additionally, they revealed that the continuous, atomically thin h-BN favors forming at high temperature. In 2020, Zhang and van Duin performed MD simulations to study the growth of graphene on silicon carbide (SiC) substrate (figure 22(f)) [379]. A new Si/H/Graphene ReaxFF potential was parameterized and used in these simulations. A temperature range of 2000 K < T < 3000 K was identified to be suitable for formation of high-quality graphene.

MD simulations are applied to unravel the atomistic details regarding the exfoliation of 2D materials,

assisting in refining experimental conditions and actively contributing to the design of innovative materials with tailored properties. A recently published review article [385] extensively covered the mechanisms involved in the exfoliation of 2D materials. This paper, on the other hand, places a specific focus on the use of MD simulation techniques, emphasizing their significance in comprehending the dynamics of exfoliation. Mechanical exfoliation, as illustrated in figure 23(a), is the one of the most successful techniques to obtain high quality single or multi-layer 2D materials from the substrate for growth. This process usually involves interfacial peeling and intralayer tearing. Gao *et al* [386] conducted both theoretical analysis and coarse-grained MD (CGMD) simulations to investigate the peeling and tearing behaviors of 2D materials from a solid substrate. The study revealed that the most influential factors for controlling the peeling process are the peeling angle and adhesive strength, both of which can be readily adjusted in experimental setups (see figures 23(b) and (c)). It is worth emphasizing that CGMD offers a notable improvement in computational efficiency when compared to reactive MD and classical MD. This improvement is demonstrated by its capacity to simulate models of a considerable scale, reaching $6 \times 6 \mu\text{m}^2$ and represented by 17 200 CG beads [386]. In another work utilizing the GraFF forcefield [387], Sinclair *et al* [388] simulated the process of using stick tape to mechanically exfoliate graphene (see figure 23(d)). Depending on the chosen polymer-adhesive, they uncovered a peeling mechanism that involves a combination of shearing and normal modes. Additionally, a mathematical model for the repeated exfoliation of graphite was deliberated. The MD simulation findings indicate that for enhanced graphene production, the use of rigid and viscous substrates is recommended. Moreover, the peeling mechanics of multilayer graphene stacks was studied by classical MD [389] with registry-dependent interlayer potential, i.e. REBO potential [390]. The study underscored the substantial role of corrugation energy in shaping intricate sliding patterns and intralayer shears, as shown in figures 23(e)–(g). Notably, it was observed that peeling proceeds smoothly on a large scale, while smaller scales exhibit complex sliding patterns. This finding suggests that the interplay of peeling and kink formations has the capacity to induce alterations in stacking order, consequently affecting the electronic structure of multilayer solids.

Furthermore, liquid-phase exfoliation emerges as a widely adopted and promising approach for the large-scale synthesis of 2D layered materials. Zhou *et al* [391] examined the exfoliation process of MoS₂ nanosheet in a mixture of water and isopropanol, featuring cavitation bubbles, as schematically outlined in figure 23(h). Leveraging a hybrid force

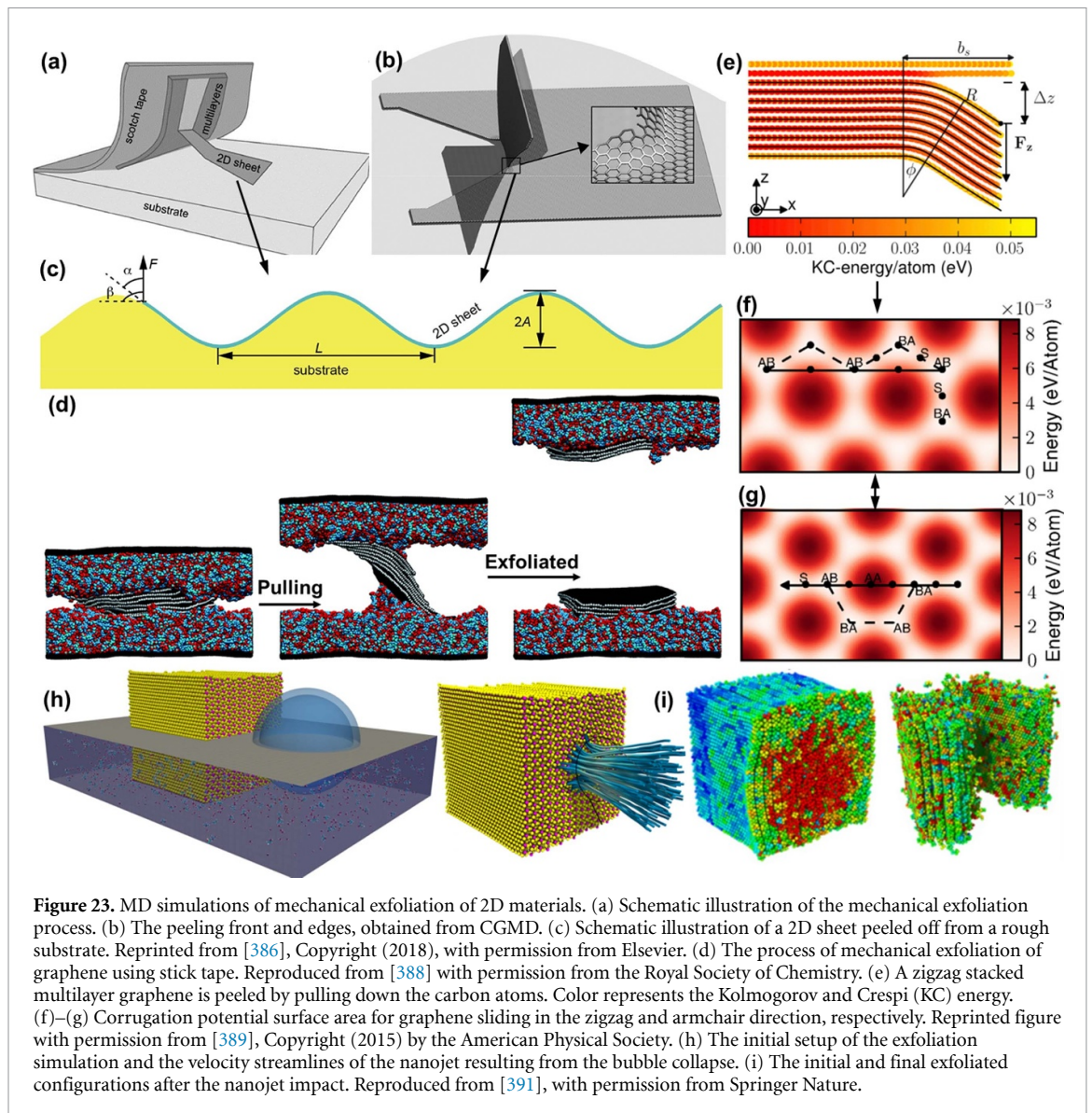


Figure 23. MD simulations of mechanical exfoliation of 2D materials. (a) Schematic illustration of the mechanical exfoliation process. (b) The peeling front and edges, obtained from CGMD. (c) Schematic illustration of a 2D sheet peeled off from a rough substrate. Reprinted from [386], Copyright (2018), with permission from Elsevier. (d) The process of mechanical exfoliation of graphene using stick tape. Reproduced from [388] with permission from the Royal Society of Chemistry. (e) A zigzag stacked multilayer graphene is peeled by pulling down the carbon atoms. Color represents the Kolmogorov and Crespi (KC) energy. (f)–(g) Corrugation potential surface area for graphene sliding in the zigzag and armchair direction, respectively. Reprinted figure with permission from [389], Copyright (2015) by the American Physical Society. (h) The initial setup of the exfoliation simulation and the velocity streamlines of the nanojet resulting from the bubble collapse. (i) The initial and final exfoliated configurations after the nanojet impact. Reproduced from [391], with permission from Springer Nature.

field that integrates TIP4P/2005 potential [392] for water, REBO potential [393] for MoS₂, and OPLS-AA potential [394] for isopropanol, multimillion-atom MD simulations were conducted to investigate the shock-induced collapse of cavitation bubbles and the subsequent exfoliation process of MoS₂, as showcased in figure 23(i). Through the simulation, it was elucidated that the collapse of cavitation bubbles results in high-speed nanojets and shock waves, exerting substantial shear stress on MoS₂ surfaces. This intricate process acts as the driving force for initiating and enhancing exfoliation. The simulation results serve as a valuable resource for experimentalists seeking to optimize and scale the yield of exfoliation.

Furthermore, MD simulations was utilized to study the electrochemical exfoliation of 2D materials, such as MoS₂, as illustrated in figure 24(a) [395]. Ethylene carbonate (EC) and propylene carbonate (PC) are the most common electrolytes for lithium-ion batteries, with different working temperature ranges. MD simulations was employed to study

the exfoliation of electrolyte-intercalated graphene sheets, as shown in figure 24(b) [396]. Their results suggested that the exfoliation diffusion coefficient of the graphene sheet with PC intercalant is ~ 200 times larger than that with EC intercalant. The MD predicted dynamic properties of graphene in two different electrolytes can be used for designing new anode materials with better performance. It is noteworthy that there is a scarcity of MD simulation studies on electrochemical exfoliation of 2D materials compared to the abundance of research on mechanical exfoliation.

MD simulations play an important role in advancing providing fundamental information for guiding the synthesis of 2D materials by elucidating the dynamics of growth processes, providing crucial information about the formation of atomic structures, nucleation, and mechanisms behind material growth. This information is of paramount importance for tailoring material properties and designing novel materials with specific characteristics. With

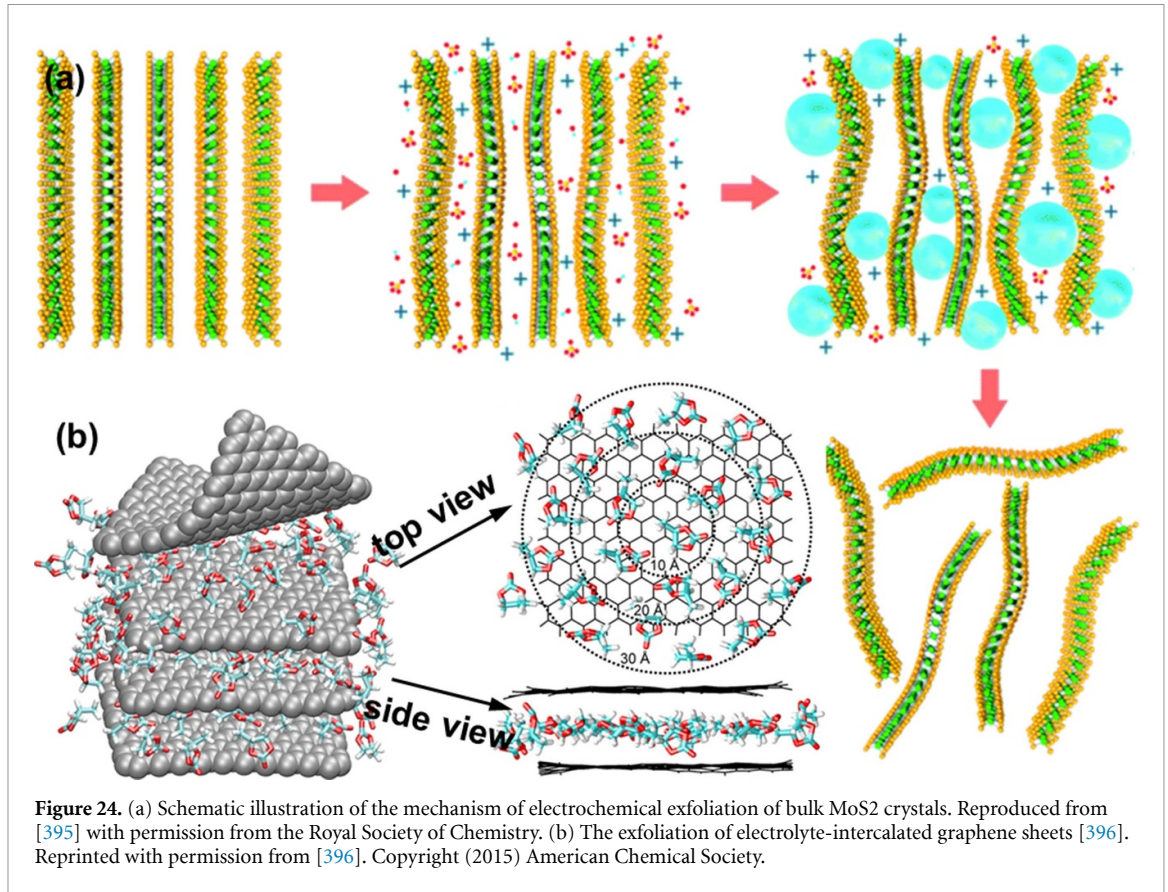


Figure 24. (a) Schematic illustration of the mechanism of electrochemical exfoliation of bulk MoS₂ crystals. Reproduced from [395] with permission from the Royal Society of Chemistry. (b) The exfoliation of electrolyte-intercalated graphene sheets [396]. Reprinted with permission from [396]. Copyright (2015) American Chemical Society.

ongoing developments in algorithms, computational power, and force field accuracy, MD simulations are anticipated to offer even more realistic and reliable predictions of atomic-scale interactions during synthesis.

6.4. Micro/meso scale: PF approach

PF method is a computational approach for simulating and studying the evolution of nano/microstructures and phase transformation [397–401]. It adopts the diffuse interface concept utilizing continuous order parameters for representing phase evolutions without explicitly tracking the interfaces between different phases. The PF model (PFM) uses a scalar field (shown in figure 25(a)) that takes a constant value in each phase and rapidly changes from the value in one phase to another value in the other phase across the diffusive interface [402, 403]. The PF crystal (PFC) model is the extension of PFM to atomistic length scale while maintaining the diffusive time scale; PFC lies between the standard PFM and atomic simulations. As shown in figure 26(a), the crystalline (phase 1) and non-crystalline (phase 2) states in PFC are represented by periodic function of the density field and a constant density value, respectively [404]. PFM and PFC focus on different aspects of material behaviors and have distinct applications. PFM is mostly used to simulate the domain evolution or phase transformation on a microscale to study the

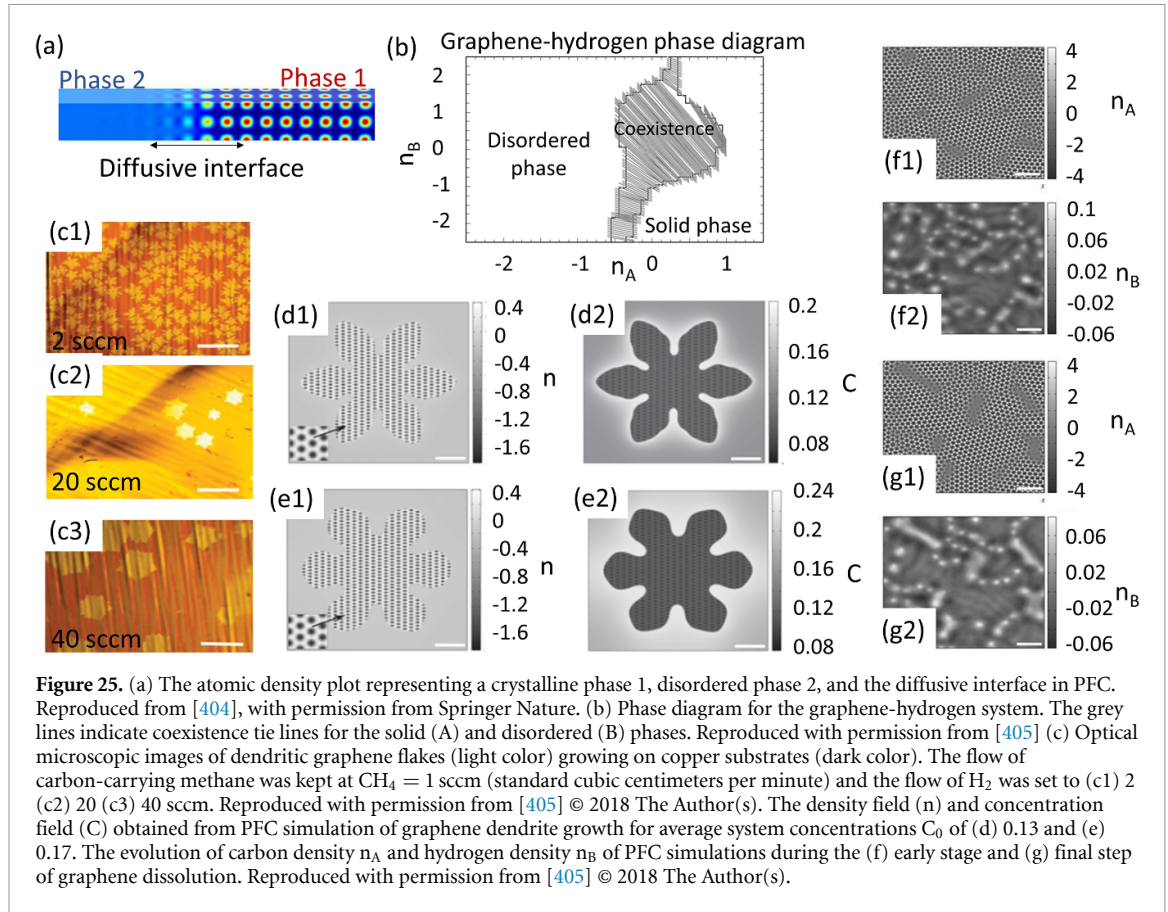
complex interactions between different phases and their boundaries and to understand material's structural evolution. While PFC focuses on the dynamics and structure of atomic arrangements, and it can simulate the behavior of crystalline materials at atomic level such as the nucleation and growth of crystals and defects, without direct investigation of individual atoms [403].

6.4.1. A brief background of PF modeling

The Ginzburg-Landau based free energy in PFM is described by a set of conserved $\{c_i\}$ and non-conserved $\{\varphi_i\}$ field variables that vary continuously across the diffusive interface. The free energy function contains the thermodynamic and kinetic driving forces that govern microstructure evolution, and it has the following form [403]:

$$F = \int d\vec{r} \left[f_0(c_1, \dots, c_n, \varphi_1, \dots, \varphi_m) + \sum_{k=1}^n \alpha_k (\nabla c_k)^2 + \sum_{i,j=1}^3 \sum_{k=1}^m \beta_{ij} \nabla_i \varphi_k \nabla_j \varphi_k \right] \quad (17)$$

First term, f_0 , is the local free energy density of equilibrium phases. The two terms containing gradient of conserved and non-conserved field variables are associated with the excess free energy due to their inhomogeneity across the interface with α_k and β_{ij}



and are related to the interface energy and width. The time evolution of the conserved and non-conserved variables are described by [403, 406]:

$$\frac{\partial \varphi_i}{\partial t} = -L_{ij} \frac{\delta F}{\delta \varphi_j} \quad (18)$$

$$\frac{\partial c_i}{\partial t} = \nabla \cdot \left(M_{ij} \nabla \frac{\delta F}{\delta c_j} \right) + S \quad (19)$$

where L_{ij} and M_{ij} are associated with the mobility and kinetics of the microstructural evolution. S is the source term to incorporate the effect of thermal noise or allow mass transport. Additional terms can be added to the free energy density term in equation (17) depending on different phase transformation phenomena. The contributions of latent heat released during the solidification and the elastic energy are two examples that can be incorporated in equation (17); adding these modifications to the free energy term requires solving the heat equation [407] and the mechanical equilibration term [403, 406]. Furthermore, for simulating polycrystalline microstructures, an additional set of field variables is required to represent the grain orientations [408].

6.4.2. A brief background of PF crystal

The order parameter in PFC method is described by the local-time-averaged density following constant value (periodic function) inside the non-ordered (crystalline) phase [409]. It is important to note

that the periodic function varies with crystal structure of the solid phase. The free energy function described by the order parameter is minimized considering the elastic energy and the symmetric properties of the periodic order parameter [410]. Elasticity, plasticity, formation of dislocations and grain boundaries are inherently incorporated in the PFC model [410]. The free energy function for a single-component PFC is considered as [411–413]:

$$F = \int_V f_0(\phi) d\vec{r} - \frac{1}{2} \iint \phi(\vec{r}) C_2(\vec{r} - \vec{r}') \phi(\vec{r}') d\vec{r} d\vec{r}' \quad (20)$$

ϕ is the normalized density, f_0 is the ideal free energy density, and C_2 is an isotropic two-point correction function consisting of a family of gaussian peaks. Position, width, and the height of the Gaussian peaks are chosen such that it produces the desired crystal structure at the minimum point for energy and stabilizes the multi-phase coexistence. Two-point correction models are mostly suitable to model a simple cubic, fcc, an diamond cubic structures [414]. Higher-order corrections functions are capable of modeling more complex crystal structures [414, 415], however, they may bring additional computational complexity. For a constant volume condition, the order parameter is a conserved field variable, and its dynamic time evolution is given by:

$$\frac{\partial \phi}{\partial t} = \Gamma \nabla^2 \frac{\delta F}{\delta \phi} + \eta \quad (21)$$

η is a Gaussian random variable with zero mean and two-point correction:

$$\langle \eta(\vec{r}, t), \eta(\vec{r}', t') \rangle = \Gamma k_b \nabla^2 \delta(\vec{r} - \vec{r}') \delta(t - t'). \quad (22)$$

Now that we briefly explained how the PFM and PFC approaches work, in the following we summarize their applications in simulating the CVD and PVD processing of 2D materials.

6.4.3. Microscale modeling of chemical vapor deposition

6.4.3.1. PF crystal

2D materials exhibit different crystalline symmetries such as honeycomb, Kagome, triangular, and square lattices. The typical one-point and two-point PFC models can simulate fcc and bcc structures [412, 416, 417], but usually fail to model the highly complex crystal structures. The PFC model for simulating the CVD process should be able to identify the underlying mechanism for selection of the aforementioned distinct crystallization modes along with the nature and growth of the topological defects. Multimode PFC models, with three-point and four-point correction functions, are capable of studying the mechanism governing the formation and dynamics of complex crystalline and stabilized polycrystalline states including honeycomb and Kagome [418]. There are PFC models in literature predicting stabilized single component [418] and binary [419, 420] 2D materials with honeycomb-like and Kagomi-like lattice structures. Various studies in the literature have used these models to simulate complex solid-state phase transformation and to predict the nature of topological defects found in 2D materials [84, 420–424].

The traditional PFC models used to simulate CVD of 2D material contain solid and liquid phases [425] and were developed to simulate the solid-state and liquid to solid phase transformations [409, 426, 427]. To model CVD of 2D material, the free energy functional should also allow the coexistence of solid phase with the vapor phase. PFC models in literature take two different approaches to simulate the coexistence of vapor phase with complex structures such as honeycomb and Kagimi.

The first one considers different field variables for each phase. Schwabach *et al* [428] extended the traditional PFC models containing solid and liquid phases and proposed the first model to simulate the coexistence of solid-liquid-vapor. In addition to the density field variable, they introduced another order parameter. Their model accurately predicts various interfacial properties such as the liquid-vapor interface oscillations and the anisotropic solid-vapor surface energies. Elder *et al* [405] used this approach and extended the two-point PFC model of Greenwood

et al [411] from a single component to a two component system stabilizing the crystal-vapor coexistence with a 2D simulation approach. Compared with the Schwabach's model [428], they used two field variables representing dimensionless atomic density of the solid and vapor phases. As mentioned previously, the two-point PFC models are not very suitable to predict complex structures. For this, Elder *et al* [405] also developed another 2D model by extending the three-point PFC model of Seymour and Provatas [415] to a two component system, each representing the solid and vapor phases.

The second approach for considering the coexistence of solid phase with the vapor phase uses a single continuum field variable. This approach requires higher order correlation functions (up to four-point) to predict three-phase coexistence and transitions including vapor-liquid-solid and the unusual vapor-solid-liquid transition sequences [415, 429–433]. However, obtaining a three-phase coexistence with complex crystal structures is still challenging. Seymour and Provatas developed the first PFC model using a three-point correlation function in the free energy functional to model more structurally complex crystals. Given the phase diagram presented in figure 25(b), their 2D model allows stabilizing the graphene structure and its coexistence with liquid/vapor phases [415, 434].

One application of the PFC modeling is to study the dendritic morphology growth during the CVD. Experimental observations of graphene synthesis using PVD method, shown in figure 25(c), suggested that depending on the flow of CH₄ and H₂ gases inside the chamber, one can produce full coverage graphene or isolated dendritic flakes [405]. To study this phenomena, Elder *et al* [405] applied the 2D two-point PFC model to study the dendritic growth during the CVD of graphene. In comparison to PFC model with three-point correction function, this model is less robust and also leads to some incorrect elastic responses [405]. However, its computational advantage over the three-point models facilitates larger scale simulations for longer periods of time sufficient enough to study the crystallization during CVD. As shown in figures 25(d) and (e), the morphologies of the thin film predicted by PFC were consistent with the experimental observations of CVD [405]. The results suggested that the increase of hydrogen flow rate decreased the dendricity and increases the growth speed [405].

Up to this point, it has been shown how the relative amounts of H₂ and CH₄ gases in the chamber affect the morphology of graphene growth. However, the experimental and PFC studies suggest a high H₂ to CH₄ ratio, even after the partial coverage of surface via graphene flakes interfering with the growth dynamics. This causes dissolution of graphene at grain boundaries, leaving behind a high H₂ concentration at grain boundaries [405, 435]. In

very extreme cases, it can even lead to the disappearance of graphene dendritic flakes. Elder *et al* used the 2D three-point PFC to investigate the role of carbon density on the dynamics of grain boundary [405]. The carbon density (n_a) and hydrogen density (n_b) profiles shown in figures 25(f) and (g) support the experimental observations of graphene dissolution until the hydrogen and carbon densities in the crystallized graphene follow the phase diagram coexistence values.

6.4.3.2. PF model

Synthesizing high-quality single-crystalline 2D material via CVD requires full control of the nucleation and growth processes. CVD synthesis of large-area materials with the desired density of defects and thickness uniformity depends on various synthesis factors such as temperature, pressure, growth time, precursor concentrations, and flow patterns inside the reactor [436, 437]. For instance, studies suggest that tuning the C:H ratio [436], changing the H_2 gas pressure [438], and smoothing the substrate [439] help improve the quality of graphene. However, optimizing the CVD process is challenging because numerous factors affect the dynamics of crystal growth.

2D PFMs of CVD have been developed based on the models of spiral growth [440] and epitaxial growth [441–443]. Ratz and Viogt [441, 442, 444] developed one of the first PFMs that can simulate step flow in epitaxial growth of thin films. They introduced an order parameter, representing the steps or the boundaries of the islands. This order parameter is discrete in the growth direction but continuous in the lateral direction. Meca *et al* [435, 445] developed one of the first PFMs suitable for simulating the growth of a single step during the CVD process of 2D materials. As an alternative to the experimental synthesis of 2D material, PFM of CVD is a powerful tool to investigate various synthesis factors affecting the morphology of the islands, e.g. carbon precursor flux [446, 447], concentration of carbon precursor on the substrate surface [446], and diffusion of the substrate [446].

In general, the free energy term used in these PFMs to simulate the CVD is based on the expression given by Karma and Plapp [440]:

$$F = \int d\vec{r} \left[\kappa^2 (\nabla\psi)^2 - \frac{1}{\pi} \cos(\pi[\psi - \psi_0]) + \lambda\xi \left\{ \psi + \frac{1}{\pi} \sin(\pi[\psi - \psi_0]) \right\} \right] \quad (23)$$

ψ is the order parameter, taking values of -1 and 1 on the substrate and deposited layer, respectively. ξ is the second field variable given by:

$$\xi = \Gamma (u - u_{eq}) \quad (24)$$

where Γ is the atomic area of solid, u represents the concentration of species arriving on the substrate,

and u_{eq} is the equilibrium specie concentration. κ^2 is the gradient step energy term, and the anisotropy of the step energy is considered by assuming:

$$\kappa^2 = \sigma^2 \{1 + \varepsilon_g \cos(n\theta)\} \quad (25)$$

σ^2 is the constant average interface energy density, ε_g is the strength of anisotropy, θ is the angle of the interface normal with x direction, and n corresponds to the symmetry which is considered as 6 for simulating a six-fold crystal symmetry. The minima of free energy are independent from ξ and happen at $\psi - \psi_0 = 2m + 1$, $m = 0, 1, 2, \dots$. λ is a dimensionless constant coupling the evolution equations of ξ and ψ .

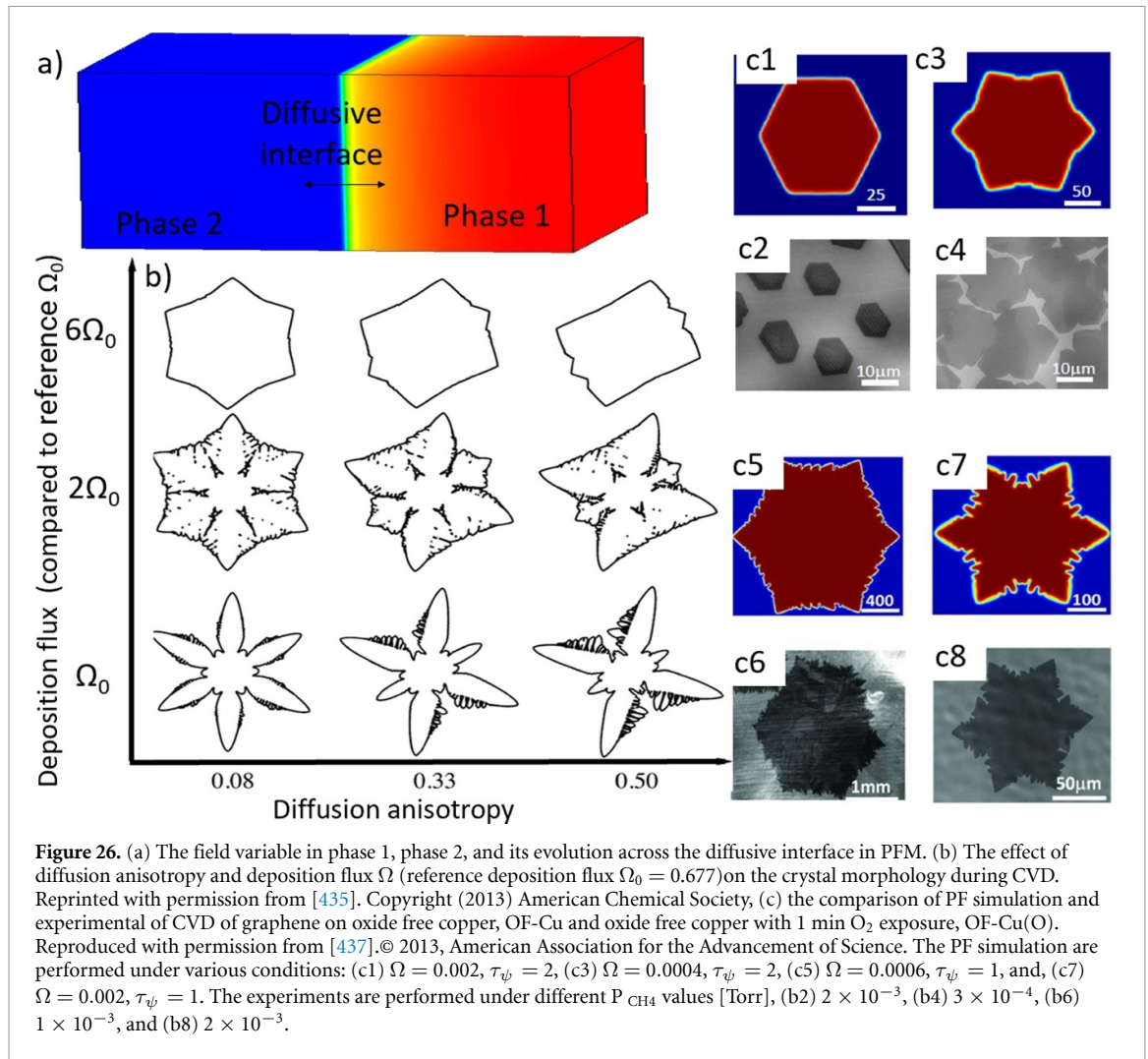
$$\tau_\psi \frac{\partial\psi}{\partial t} = -\frac{\delta F}{\delta\psi} \quad (26)$$

$$\frac{\partial\xi}{\partial t} = D\nabla^2\xi - \frac{\xi}{\tau_s} + \Omega - \frac{1}{2} \frac{\partial\psi}{\partial t} \quad (27)$$

τ_ψ is the characteristic time of attachment of adatom, τ_s is the mean lifetime of adatom on the substrate, Ω is the precursor's flux arriving at the substrate, and D is the diffusion coefficient of adatom.

One of the advantages of PF modeling is its ability to simulate phenomena that are hard to observe or measure through experiments [448, 449]. For instance, the concentration gradient around each graphene island cannot be seen experimentally [446]. However, PF simulation results for CVD of graphene showed the width of the depletion zone, that is, the area with a carbon precursor concentration gradient around the circumference of the growing graphene island, plays a central role in the shape determination of the graphene islands [446]. When the size of the depletion zone is much smaller or much larger than the island, graphene grows in a hexagonal shape. Although an extremely small depletion zone will lead to a graphene island with a regular shape, its edges are found to be rough. However, comparable size between the depletion zone and island promotes fractal-like graphene islands with multi-scaled branches [446].

Another important advantage of PF modeling is its ability to consider anisotropy during the growth process. Some PFMs consider constant values for the diffusion coefficient and kinetic time constant [437, 446]. However, there are other PFMs that account for the anisotropies of these variables [435, 445, 450]. 2D PF simulations of graphene CVD suggest that, as shown in figure 26(b), diffusion anisotropy is the most important anisotropy term impacting the crystal shape. The results show the transition from a six-fold to a four-fold symmetry as the diffusion strength takes a very high value [435, 445]. It should be mentioned that in [435], a systematic investigation on various anisotropy strength values for the diffusion and kinetic term has been performed. However, accurate strength values cannot be



calculated from experiments. MD is a powerful tool with established algorithms for calculating anisotropies of surface energy and kinetic terms [44, 407, 451]. However, the literature lacks an MD-based method and a multiscale framework for a quantitative investigation of the factors affecting domain morphology and growth dynamics during CVD.

PFMs are also capable of simulating how impurities on the substrate alter the nucleation and growth kinetics during CVD. Hao *et al* [437] performed a combined experimental and 2D PF simulation study to identify how oxygen exposure on the substrate surface affects the island morphology and growth rate. Their experimental observations showed oxygen on the copper surface suppresses the nucleation and promotes the growth of large single-crystalline graphene [437]. The change of the graphene domain morphology, as shown in figures 26(c2), (c4), (c6), and (c8), suggests different growth mechanisms are activated under various synthesis conditions. Compact islands in the absence of oxygen impurities suggest the growth is an edge-attachment-limited process. The dendritic shape in oxygen exposure indicates that the growth kinetics are in a diffusion-limited

regime [437]. They also performed PF simulations of CVD that supported their experimental observations. Large energy barriers for the edge attachment, which are experimentally observed in cases with substrate exposed to oxygen, are computationally represented by choosing a large characteristic time of adatom attachment on the substrate. PF simulation results [437] (figures 26(c1) and (c3)) show that as long as the characteristic time of attachment is large, (represented by $\tau_{\psi} = 2$) different values of carbon flux result in compact hexagonal structures. However, for small τ_{ψ} values, shown by figures 26(c5) and (c7), Ω becomes the dominant parameter, and shape of the domain changes to a dendritic. Furthermore, Li *et al* [452] used the same model as Hao *et al* [437] to uncover the growth mechanisms of bilayer and monolayer graphene on copper. This work demonstrates that when graphene was grown by CVD on the surface of clean copper (without impurities), only monolayered graphene islands or graphene films were obtained. While the existing impurity on the substrate assists nucleation. Thus, bi-layered or even few-layered graphene may appear around each impurity particle. It should be mentioned that similar

to all the previous studies on PF modeling of CVD, simulations of [437] were performed in 2D and the multilayer growth is handled by the sin and cos terms in equation (23) which has multiple local minima.

One important factor limiting the reproducibility of CVD is the variability existing between 2D materials grown in different reactors using the same growth conditions. In order to capture the various physics involved in the growth of monolayer materials across different length- and time-scales, Momeni *et al* [453] and Ji *et al* [450] developed a multiscale/multiphysics model based on coupling continuum fluid dynamics (CFD) and PFM for studying CVD growth of 2D materials. This approach correlates the island morphology of the 2D material to macroscopic (such as inlet velocity and temperature) and microscale growth parameters (such as surface diffusion and deposition rates). Their modeling results, as predicted by previous experimental studies [454], suggest that low precursor concentrations result in a more uniform distribution of h-BN islands. Furthermore, Momeni *et al* [455] extended their model by coupling PFM, reactive MD, and CFD to obtain precise control over the coverage, morphology, and properties. This multiscale simulation of WSe₂ synthesis revealed that the uniformity and morphology of 2D materials are strong functions of precursor concentration and its gradient over the substrate, which are also influenced by the growth chamber configuration and flow characteristics. Although this multiscale model takes into account the interplay between the flow inside the reactor and diffusion of precursor, this approach still does not fully solve the reproducibility problem. Because this framework neglects the chemical reactions, breakdown of species, and the effect of substrate defect distribution on the nucleation stage.

6.4.4. Micro scale modeling of physical vapor deposition

In general, the surface morphology and microstructural features formed during the growth of thin film by PVD, such as crystal structure, orientation, grain size, grain shape, chemical composition, phase distribution and surface roughness, depend on deposition conditions and the target materials [456–458]. There is a complex correlation between phenomena associated with synthesis (the vapor transport, surface adhesion and diffusion, phase separation, grain growth, surface roughening), deposition condition, the initial microstructural features of the substrate (grain size, grain boundary type, orientation, temperature,) and microstructural dynamics to deposited thin film [458]. PFM is a powerful tool to simulate the pattern formation and evolution during the PVD.

In general, the field variable ϕ in the PFM ranges between 1 and -1 as it moves from the solid into the vapor phase, respectively. The general form of free

energy in these models is given by:

$$F = \int d\vec{r} \left[f_0(\phi) + \alpha(\phi)(\nabla\phi)^2 + s(\phi)f_{sub} \right] \quad (28)$$

ϕ is the order parameter, f_0 is the symmetric double-well potential with minima at $\phi = -1$ and 1 . f_{sub} represent the driving force for the microstructure evolution during the PVD.

The PFM of PVD describe the kinetics of thin-film growth by two coupled partial differential equations for order parameter ϕ (equation (18)) and a second field variable ρ , describing the incident vapor flux. The evolution of vapor field is given by:

$$\frac{\partial\rho}{\partial t} = \vec{\nabla} \cdot (D\vec{\nabla}\rho) - \vec{\nabla} \cdot (\rho\vec{v}) - S \quad (29)$$

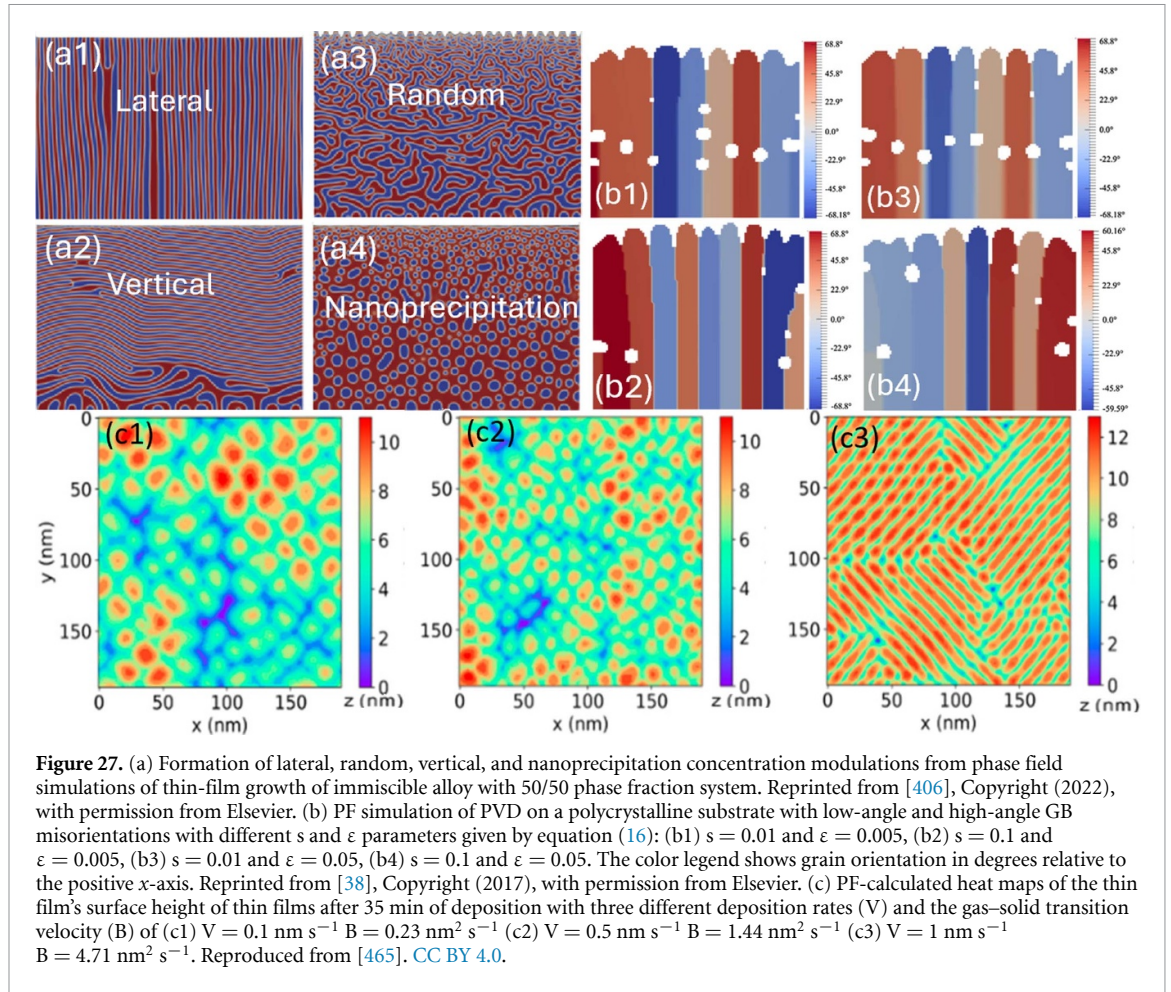
\vec{v} is the velocity field of the incident vapor, S is the source term acting as a sink to remove vapor that has been convert to solid [37, 38, 406, 459, 460].

There are two different PFM approaches in the literature which consider the dynamics of thin-film nucleation and growth along with the evolution microstructure within it. The first approach considers the phase separation happening during the synthesis of immiscible alloys [459–461]. The second approach considers the growth of a single-phase polycrystalline 2D material and studies the deposition of the thin film and the evolution of granular structure during the PVD process [37, 38].

In developing PFM for PVD of a two-phase immiscible alloy system, another field variable c is introduced which describes the local equilibrium composition of phase A or B. In this model, f_{sub} is given by:

$$f_{sub} = f_{elastic} + f_c + \alpha_c(\nabla c)^2 \quad (30)$$

f_c is double-well potential and $f_{elastic}$ is the elastic energy density. The evolution equation c is given by equation (19). Introduction of elastic energy term in the free energy adds elastic strain to the unknown variables and one should also solve the mechanical equilibrium equation. This PFM has been implemented [459, 461] to simulate PVD of various alloy with various two phase-fractions. The results given by figure 27(a) showed that this model is capable of describing the four basic morphologies, known as lateral, vertical, random and nanoprecipitate concentration modulations that are commonly observed by the experiments [462–464]. Despite this PFM's advantages, it still fails to provide a quantitative description of the synthesis process and it is mainly used to investigate how different factors such as phase fraction, incident vapor velocity, and phase kinetics affect the microstructure formation and morphology. In developing PFM for PVD of a polycrystalline



single-phase material, the subsurface free energy contribution is formulated as:

$$f_{sub} = s|\nabla\theta| + \varepsilon|\nabla\theta|^2 \quad (31)$$

θ is a field variable describing the grain orientation with respect to a reference. Evolution equation for θ is also described by an equation similar to equation (18). The parameters s and ε depend on the latent heat of fusion and a characteristic GB thickness [38]. As shown in figure 27(b), PFM is capable of studying how initial microstructural, material properties (e.g. latent heat of fusion) and synthesis factors such as deposition rate and vapor incident vapor affect formation and evolution of polycrystalline microstructure or the surface roughness [37, 38]. Yang *et al* is one the only three-dimensional PF simulations of the 2D material synthesis. Given by figure 27(c), they performed multiple simulations to study the effect of deposition rate and model parameters on the microstructure of deposited thin films [465]. They provided a heat map explaining a quantitative relationship between the surface roughness and the deposition rate and model parameters.

6.5. Continuum modeling and ML in the synthesis of 2D materials

In its conventional form, the PFM accounts for nucleation by adding a term representing thermodynamic fluctuations of field variables [466]. On the other hand, nucleation and growth occur on different time scales. Therefore, observing the nucleation and growth kinetics in real alloys is computationally challenging. As an alternative, the Langevin noise terms in the PFM equations can be replaced with a Poisson seeding algorithm, in which nuclei are introduced in the microstructure with a rate matching the observed nucleation rate [466, 467]. A similar approach was also used in a multiphase field model for simulating the PVD process. This model is capable of studying the role of initial substrate phase and temperature distributions on PVD of a generic allotropic metal with two stable phases [460]. The phase nucleation model explicitly introduces nucleation sites into the PFM via classical nucleation theory and Poisson seeding [466, 467].

Continuum modeling and ML offer significant advantages in the synthesis of 2D materials by enabling efficient and detailed analysis

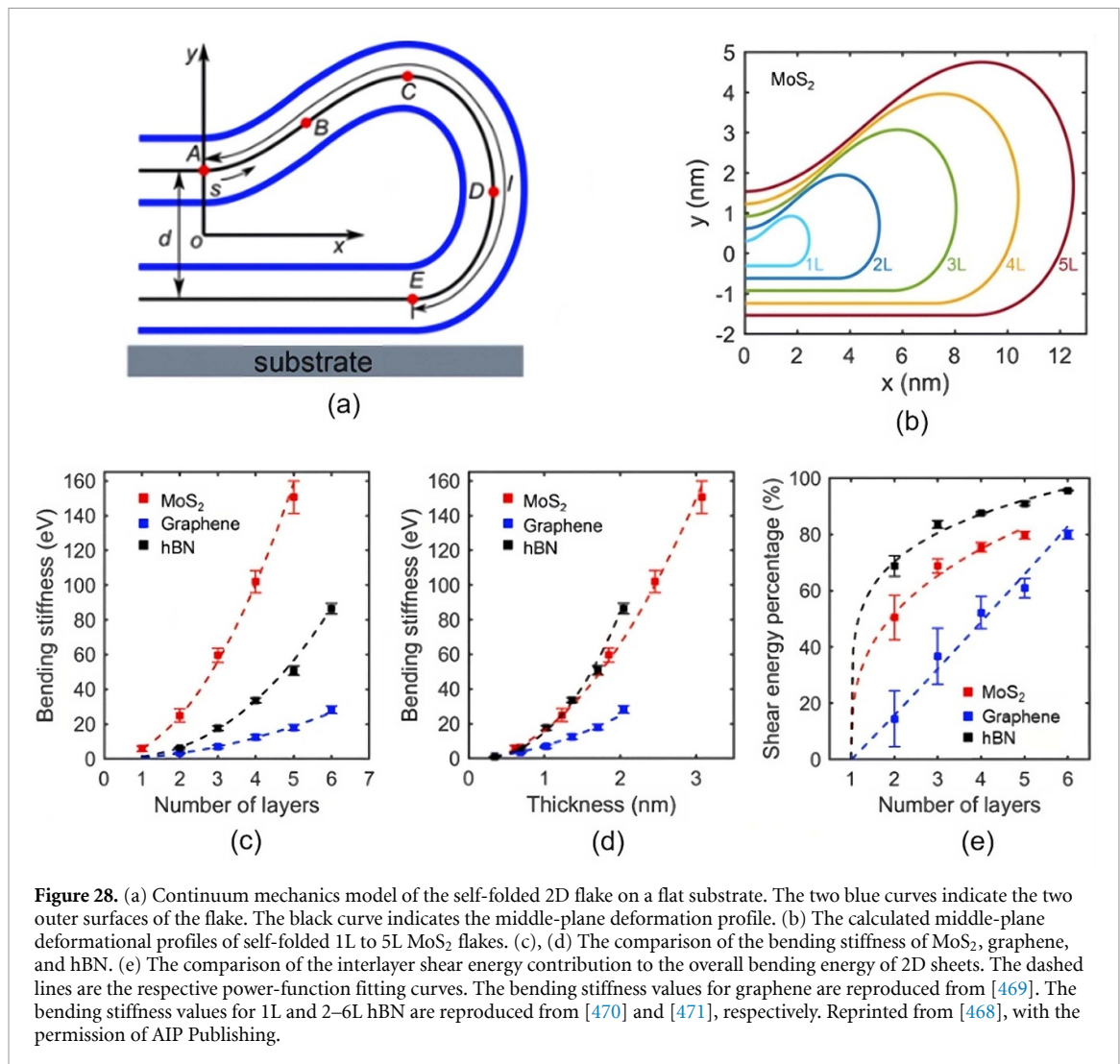


Figure 28. (a) Continuum mechanics model of the self-folded 2D flake on a flat substrate. The two blue curves indicate the two outer surfaces of the flake. The black curve indicates the middle-plane deformation profile. (b) The calculated middle-plane deformation profiles of self-folded 1L to 5L MoS₂ flakes. (c), (d) The comparison of the bending stiffness of MoS₂, graphene, and hBN. (e) The comparison of the interlayer shear energy contribution to the overall bending energy of 2D sheets. The dashed lines are the respective power-function fitting curves. The bending stiffness values for graphene are reproduced from [469]. The bending stiffness values for 1L and 2–6L hBN are reproduced from [470] and [471], respectively. Reprinted from [468], with the permission of AIP Publishing.

of large-scale processes and providing predictive insights. Continuum models are adept at simulating macroscopic phenomena such as stress distribution, heat transfer, and large-scale morphological changes in 2D materials during processes like CVD or exfoliation [468, 472, 473]. Jiang *et al* [468] showed continuum mechanics aids in understanding the mechanical exfoliation of ultrathin 2D materials by analyzing their bending rigidity (refer to figure 28). This approach considers the intricate balance of intra- and inter-layer interactions, particularly in materials like MoS₂, graphene, and hBN, where classical mechanics might not fully capture the nuances of their layered atomic structures and bonding characteristics. They provide a macroscopic view that is critical for scaling up production and ensuring uniformity of material properties.

Along with conventional simulation methods, ML techniques can significantly enhance the synthesis process by predicting optimal synthesis conditions, identifying potential new materials, and optimizing parameters for desired properties [474–476]. Yoshihara *et al* explored the use of ML models to

optimize the CVD process for synthesizing large-area graphene [474]. The study successfully developed an ML model that predicts the size of graphene domains based on CVD growth conditions and surface characteristics of copper substrates. This approach resulted in enhanced graphene growth, demonstrating that ML can significantly improve the efficiency and outcomes of material synthesis processes. By analyzing large datasets from experimental and computational studies, ML algorithms can uncover complex relationships and trends that are not immediately apparent, leading to more efficient and targeted synthesis approaches. For instance, ML can predict the best combination of precursors and process conditions in CVD to obtain high-quality 2D materials with specific properties [477]. Li *et al* presented an ML approach for analyzing optical images of CVD-grown 2D materials [478]. They employed unsupervised learning, combining self-organizing map (SOM) and k-means clustering, to assess the quality of these materials efficiently. This method demonstrates high accuracy and is applicable to various material systems, marking a significant

advance in the efficient evaluation of CVD-grown materials.

ML can be utilized in conjunction with MD simulation results to understand a process. Liu *et al* [296] used reactive MD simulations to study the CVD growth of MoS₂ from MoO₃ and S precursors. Subsequently, the authors used a machine-learning approach involving feedforward neural networks to identify the critical reaction mechanisms. The results from the training of 36 000 simulation data points revealed novel growth mechanisms which turned out to be fundamental for augmenting the experimental CVD growth of MoS₂ [296].

The coupling of continuum models with ML algorithms facilitates a more holistic approach, where the macroscopic insights from continuum models can be combined with the predictive power of ML, leading to an accelerated discovery and optimization process in the synthesis of 2D materials. Along with that, atomistic and molecular level simulation can provide more intricate understanding of the synthesis and process behavior, albeit with higher computational expenses. The overarching research direction would follow integrated, and hybrid atomistic-continuum simulations assisted by ML to harness greater understanding and optimized synthesis processes exploiting the insights across different length scales.

7. Evolving trends and future directions

7.1. Electronic scale calculations

To broaden the capabilities of DFT beyond ground-state properties, extending its reach to accurately depict excited states, non-equilibrium phenomena, and time-dependent processes, advancements in the current methodology is inevitable. This expansion will facilitate a more comprehensive understanding of electronic dynamics. The integration of quantum computing technologies is anticipated to revolutionize DFT simulations. With the rapid progress in both DFT calculations and computational power, accessing basic material properties becomes increasingly straightforward, leading to the creation of numerous materials databases, such as the Materials Project [356]. Quantum computers hold the potential to tackle currently intractable calculations, offering new solutions for complex quantum many-body problems.

Conventional DFT calculations, typically operate within a system size of $<10^3$ atoms, with time scales on the order of picoseconds. To extend length- and timescales, there is a push to develop linear-scaling DFT methods, such as the charge-patching method [479] and the linear scaling 3D fragment method [480]. DFT stands as a cornerstone of the Materials Genome Initiative, and ongoing progress involves crafting efficient workflows for high-throughput screening of materials, accelerating the discovery of novel materials with tailored properties

for specific applications [481]. Research endeavors persist in the development of hybrid functionals that strike a balance between accuracy and computational cost. These functionals aim to overcome limitations associated with describing strongly correlated systems and enhance the treatment of diverse chemical reactions. DFT is anticipated to assume a pivotal role in comprehending and predicting the behavior of complex systems, encompassing biological molecules, interfaces, and materials under extreme conditions [482]. The evolution of more accurate and reliable exchange-correlation functionals is pivotal in this context. The trajectory of DFT involves an unceasing pursuit of accuracy, an expansion of capabilities to address a broader array of electronic phenomena, and an embrace of emerging technologies such as quantum computing and ML to unlock new frontiers in materials science and quantum chemistry.

The accuracy of mesoscale and macroscale models often relies on the parameters and relationships established at the electronic scale. Data obtained from electronic scale simulations can be used to inform and enhance MD simulations at higher scales. Electronic scale simulations also generate vast datasets including atomic coordinates, energies, forces, and electronic properties. These datasets can be leveraged to train ML algorithms for predicting material properties. For example, ML models can be trained to predict mechanical stability, interaction energies, and catalytic activity using electronic scale data as input features. ML models can then be employed to construct surrogate models that approximate potential energy surfaces, enabling accelerated MD simulations. These surrogate models, often referred to as force fields or interatomic potentials, can significantly reduce computational costs while maintaining accuracy. This allows researchers to explore longer time scales and larger system sizes. The insights gained from ML analysis can expedite the materials discovery process, suggesting novel compounds with desirable properties, guiding experimental synthesis efforts, and even predicting new phases of materials.

7.2. MD simulations

MD stands as an exceptional tool for unraveling various behaviors of 2D materials. For the study of mechanical properties, MD simulations offer detailed insights into interactions of nanostructures and defects, revealing material strength, elasticity, and deformation mechanisms with high precision. For investigating thermal properties, MD simulation is capable of capturing atomic motion and heat transfer, improving our understanding of phenomena such as thermal conductivity and phonon dispersion. Additionally, with the advancing of interatomic potentials, MD simulation can be used to elucidate the intricate dynamics of chemical reactions and uncover the pathways and mechanisms of oxidation

[483, 484]. In the context of desalination, MD simulation plays a pivotal role in analyzing the process of ion and water molecule transport through nanoscale pores [485]. Furthermore, in materials synthesis, MD simulations aid in optimizing experimental conditions and understanding the atomistic details of 2D materials growth, as well as guiding the design of novel materials [486]. Overall, the power of MD simulation lies in its ability to bridge atomic and microscopic scales, providing valuable insights into a broad spectrum of material properties and behaviors.

However, it is important to acknowledge the certain challenges and drawbacks of MD simulations. These include the computational demands of simulating large-scale systems, the importance of thorough validation against experimental data, and the potential for discrepancies stemming from limitations in simulation accuracy. While challenges persist, ongoing advancements in simulation methodologies, force fields, and collaboration with experimental studies provide hope for enhancing the effectiveness and trustworthiness of MD simulations in shaping the development of next generation 2D materials.

Advancing MD simulations studies of 2D materials for various purposes and applications involves a multifaceted approach, encompassing considerations from interatomic potentials to multiphysics simulations. Our recommendations for future directions of nanoscale simulations of 2D materials are summarized in the following.

There is an immense need for developing interatomic potentials that are specifically tailored for the unique characteristics of 2D materials, and systematically test the transferability of the potentials across different conditions and materials composition to ensure reliability in diverse simulation scenarios. For example, some empirical and semi-empirical potentials, like Tersoff potential, are popular for studying the mechanical and thermal properties of large-scale 2D materials system that involves millions of atoms [487]. However, these potentials come with limitations in terms of weak transferability and inaccurately capturing the anisotropic features of 2D materials. To address these challenges, we recommend several strategies, such as collaboration with ML approaches to enhance transferability by learning from diverse datasets and incorporating directional bonding and layer-dependent interactions in potential parameterization. On the other hand, while ReaxFF is powerful in simulating chemical reactions, it is confined by the size of the simulation box. To overcome this limit, the suggestion is to incorporate ML methods, and combining ReaxFF with other simulation methods, such as quantum mechanics or classical force fields in order to enable larger scale MD simulations. In general, exploring the integration of ML techniques to accelerate MD simulations, predict material behaviors, and guide the parameterization of interatomic potentials is of great interest.

Integrating MD simulations with other computational techniques, such as DFT and continuum mechanics, is needed to perform multiphysics simulations that capture a broader range of material behaviors like electronic, dielectric, and magnetic properties. An important example of multiphysics studies is the investigation of the chemical reactions induced by mechanical forces, expanding studies beyond thermally driven reactions.

New MD simulation frameworks need to be developed and applied to study the functionalization of 2D materials for specific applications, such as gas sensing, catalysis, or electronic devices. Such models can investigate the effects of functional groups, dopants, or defects on material properties. In addition, MD simulations can be also developed and utilized to study properties of 2D materials for applications in energy storage and conversion, sensors and detectors, electronic and optoelectronic devices, given the accuracy of interatomic potentials.

7.3. Molecular mechanics

The Molecular mechanics-based analytical approach offers a computationally efficient yet accurate method for evaluating the elastic properties of 2D materials, including monolayer (e.g. graphene, h-BN, etc) and multilayer (e.g. MoS₂, MXenes, etc) structures and their heterostructures. Mechanical properties such as Young's moduli, shear modulus, and Poisson's ratios are of utmost importance for accessing the viability of a material's use in various applications of nanoelectromechanical systems. From nano-structural point of view, the 2D materials having hexagonal structural forms are categorized in four different classes. The efficient analytical formulae are applicable to all the classes of material and any of their heterostructures. Good agreement in the results obtained from the analytical expressions and available scientific literature corroborates the validity of these molecular mechanics-based formulae.

An attractive feature of the analytical approach is that it is computationally efficient, insightful, and easy to implement, yet yields accurate results. This has allowed a recent investigation of stochastic characterization concerning the effective elastic properties of 2D materials [488]. Further, the continuum-based approach for analyzing multi-layered 2D material heterostructures has been extended to twisted graphene and other multi-layer 2D materials [283, 489]. Mechanical idealization of the atomic bonds of 2D materials, as discussed in this section, further allows a wide range of efficient dynamic and mechanical stability analysis of single and multi-layered 2D materials, their derivatives and heterostructures following an atomistic finite element approach [27, 490–492]. Further, there exist a range of properties (such as chemo-mechanical properties, electronic characteristics, morphological stability etc) that are

defined at comparatively lower length scales concerning molecular, atomistic, and electronic levels, and such properties cannot be effectively investigated through a continuum-based approach. Thus, the future research direction would follow hybrid multi-scale simulation approaches for an effective, efficient, and comprehensive investigation of a range of 2D materials.

7.4. PF modeling and other microscale models

PF approach is a powerful and versatile tool that can help predict the structure-process-property correlation in the synthesis of 2D materials. Both PFM and PFC models are capable of simulating the vapor deposition (both physical and chemical) synthesis of 2D materials. PFC models can investigate atomic length scale features of materials during temporal evolution over diffusive time scales. In order to predict the triple-phase phase diagram with realistic oscillations of density and anisotropic surface energy at solid-liquid-vapor, the vapor phase should be added to the traditional PFC models of solid-liquid coexistence. Modifications such as using multimode PFC models with three-point and four-point correction functions, or describing the free energy based on three order parameters (for solid, liquid, and vapor phases) help make decent predictions of dendrite morphology and microstructure evolution during CVD. Despite the progress in this field, performing quantitative simulations to improve the understanding of microstructural evolution and surface roughness of deposited thin films still faces different challenges. First, the three-dimensional PFC simulations of the vapor deposition of thin films are challenging due to the computational complexity and resource requirements. Capturing the dynamic evolution of atomic-scale structures in three dimensions over the timescales relevant to 2D material growth requires significant computational power and advanced modeling techniques. For that, the current state often involves simplifications or focuses on 2D simulations to reduce computational demands while still gaining valuable insights into the process. Second, the PFC results depend on model parameters. At a more quantitative level for traditional PFC models of solid-liquid coexistence, studies in the literature use MD results to determine the model parameters by fitting the PFC predictions of various properties (such as peak liquid structure factor properties, solid-density wave amplitudes, and elastic constants) to the MD results [416, 493]. However, the current state of the art sets the PFC parameters such that they can predict the vapor-liquid-solid coexistence. Integrating the current PFC models with MD helps to establish a quantitative relationship between the deposition rate, model parameters, and surface roughness for the optimization of deposition processes.

PFM is a popular simulation technique based on the Ginzburg-Landau theory, providing mesoscale

understanding of phase transitions during vapor deposition. Despite the progress in PFM of PVD and CVD, the current state of the art faces similar challenges as the PFC is a quantitative description of the microstructure evolution during the deposition process. First, very limited studies have performed three-dimensional simulations of the deposition process. It is well known that three-dimensional simulations are essential to ensure the modeling predictions match the physics involved in the thin-film synthesis process. Furthermore, MD is a powerful tool with established algorithms for calculating anisotropies of surface energy and kinetic terms [44, 407, 451]. The literature lacks an MD-based method and a multiscale framework for a quantitative investigation of the factors affecting domain morphology and growth dynamics. Evolving trends and future directions in using PFM for vapor deposition synthesis should focus on enhancing quantitative simulation capabilities by performing three-dimensional simulations of MD-informed PFM. This is essential for quantitative modeling of the synthesis to advance the understanding of the microstructural evolution and surface characteristics of thin films during the deposition process.

7.5. Artificial intelligent and ML

With rapid progress in AI in the areas such as natural language processing (NLP) in the last couple of years, the training data for ML can also be obtained by NLP. In the case of obtaining the training data, text-mining such as Bidirectional Encoder Representations from Transformers (BERT) models can be used. BERT provides promising information extraction tools, but these models may yield suboptimal results when applied to materials domain since they are not trained in materials science specific notations and jargon. In this, the training data generation part for the ML models can be reduced significantly. MatSciBERT [494] and SciBERT [495] are two of the primary candidates in this domain. In the near future, there is a tremendous possibility of exploiting such advancements in ML models for exploring different 2D materials and their heterostructures.

Over the last decade, the necessity of integrating multiple length-scales and respective analysis techniques including DFT, MD, and continuum simulations along with experimental outcomes have become evident for efficient, effective, and comprehensive characterization and innovation in the field of 2D materials. ML based models can be exploited for such scale bridging along with process and growth simulation [17]. These possibilities have led to a strong rationale for creating ML assisted fully functional digital twins in this context for multi-scale design and innovation, synthesis, characterization, and performance monitoring of 2D materials and devices.

One of the major concerns in data-driven ML [496] is related to interpretability and explainability. The materials science community and the ML community are evaluating such issues carefully for a more responsible use of ML [497]. The future trajectory of 2D materials research is poised for an exciting convergence with physics-based ML methodologies [323, 324]. The integration of physics principles into ML models promises a transformative impact on materials science, particularly for 2D materials, by enabling a deeper comprehension of their underlying physics. The development of hybrid models that merge data-driven ML with physics-based constraints is expected to significantly improve the accuracy and interpretability of material property predictions. These advanced methodologies aim to offer insights into material behavior, facilitate the design of materials with specific functionalities, and bridge the theoretical-experimental divide, heralding a new era of precision in materials research at the atomic and nanoscale levels.

8. Concluding remarks


This article provided a comprehensive overview of recent advances, challenges, and opportunities in multiscale computational modeling techniques for the study and design of 2D materials. It discussed the significance of different computational modeling techniques in understanding the structures, multiscale defects, and properties of 2D materials and reviewed various length-scale models aiding in their design and synthesis. The development and integration of multiscale computational techniques, including DFT, MD, PF, continuum-based molecular mechanics, and ML, were presented systematically for the study and design of 2D materials. The study highlighted recent advancements, challenges, and future prospects in modeling techniques tailored for emerging 2D materials, emphasizing the need to accurately capture intricate behaviors across various scales and environments. Opportunities lie in enhancing predictive capabilities through exploiting the tremendous recent advances in numerical algorithm developments and supercomputing capabilities to accelerate materials discovery for applications spanning electronics, photonics, energy storage, catalysis, and nanomechanical devices. This article offered a roadmap for future research in multiscale computational modeling and simulations of 2D materials, emphasizing the importance of integrating physics-based models with data-driven ML methodologies for a deeper comprehension of materials behavior and the design of 2D materials with specific functionalities.

Data availability statement


No new data were created or analyzed in this study.

ORCID iDs

Mohsen Asle Zaeem  <https://orcid.org/0000-0002-5164-6122>

Siby Thomas  <https://orcid.org/0000-0002-7928-4119>

Sepideh Kavousi  <https://orcid.org/0000-0001-7040-237X>

Ning Zhang  <https://orcid.org/0000-0002-4066-1837>

Tanmoy Mukhopadhyay  <https://orcid.org/0000-0002-0778-6515>

Avik Mahata  <https://orcid.org/0000-0002-8723-9414>

References

- [1] Nayir N, Mao Q, Wang T, Kowalik M, Zhang Y, Wang M, Dwivedi S, Jeong G-U, Shin Y K and van Duin A C 2023 Modeling and simulations for 2D materials: a ReaxFF perspective *2D Mater.* **10** 044001
- [2] Fiori G, Bonaccorso F, Iannaccone G, Palacios T, Neumaier D, Seabaugh A, Banerjee S K and Colombo L 2014 Electronics based on two-dimensional materials *Nat. Nanotechnol.* **9** 768–79
- [3] Tang L, Meng X, Deng D and Bao X 2019 Confinement catalysis with 2D materials for energy conversion *Adv. Mater.* **31** 1901996
- [4] Ferrari P F, Kim S and van der Zande A M 2023 Nanoelectromechanical systems from two-dimensional materials *Appl. Phys. Rev.* **10** 031302
- [5] Kanahashi K, Pu J and Takenobu T 2020 2D materials for large-area flexible thermoelectric devices *Adv. Energy Mater.* **10** 1902842
- [6] Dubertret B, Heine T and Terrones M 2015 The rise of two-dimensional materials *Acc. Chem. Res.* **48** 1–2
- [7] Zou X, Xu Y and Duan W 2021 2D materials: rising star for future applications *Innovation* **2** 100115
- [8] Kumbhakar P, Jayan J S, Sreedevi Madhavikutty A, Sreeram P R, Saritha A, Ito T and Tiwary C S 2023 Prospective applications of two-dimensional materials beyond laboratory frontiers: a review *iScience* **26** 106671
- [9] Lin Z et al 2016 2D materials advances: from large scale synthesis and controlled heterostructures to improved characterization techniques, defects and applications *2D Mater.* **3** 042001
- [10] Cai Z, Liu B, Zou X and Cheng H-M 2018 Chemical vapor deposition growth and applications of two-dimensional materials and their heterostructures *Chem. Rev.* **118** 6091–133
- [11] Muratore C, Voevodin A A and Glavin N R 2019 Physical vapor deposition of 2D Van der Waals materials: a review *Thin Solid Films* **688** 137500
- [12] Cai X, Luo Y, Liu B and Cheng H-M 2018 Preparation of 2D material dispersions and their applications *Chem. Soc. Rev.* **47** 6224–66
- [13] Liu X and Hersam M C 2018 Interface characterization and control of 2D materials and heterostructures *Adv. Mater.* **30** 1801586
- [14] Naikoo G A et al 2022 2D materials, synthesis, characterization and toxicity: a critical review *Chem. Biol. Interact.* **365** 110081
- [15] Mitta S B, Choi M S, Nipane A, Ali F, Kim C, Teherani J T, Hone J and Yoo W J 2021 Electrical characterization of 2D materials-based field-effect transistors *2D Mater.* **8** 012002
- [16] Glavin N R, Rao R, Varshney V, Bianco E, Apte A, Roy A, Ringe E and Ajayan P M 2020 Emerging applications of elemental 2D materials *Adv. Mater.* **32** 1904302

- [17] Das S, Kim M, Lee J-W and Choi W 2014 Synthesis, properties, and applications of 2D materials: a comprehensive review *Crit. Rev. Solid State Mater. Sci.* **39** 231–52
- [18] Sinnott S B 2013 Material design and discovery with computational materials science *J. Vac. Sci. Technol. A* **31** 050812
- [19] Li J, Ngan A H and Gumbsch P 2003 Atomistic modeling of mechanical behavior *Acta Mater.* **51** 5711–42
- [20] Er D and Ghatak K 2020—Atomistic modeling by density functional theory of two-dimensional materials *Synthesis, Modeling, and Characterization of 2D Materials, and Their Heterostructures* E-H Yang (Elsevier) pp 113–23
- [21] Mase G E and Mase G 1970 *Continuum Mechanics* vol 970 (McGraw-Hill)
- [22] Taler D and Taler D 2019 Mass, momentum and energy conservation equations *Numerical Modelling and Experimental Testing of Heat Exchangers* (Springer) pp 9–46
- [23] Bergström J 2015 4—Continuum mechanics foundations *Mechanics of Solid Polymers* ed J Bergström (William Andrew Publishing) pp 131–207
- [24] Hirsch C 2007 *Numerical Computation of Internal and External Flows: The Fundamentals of Computational Fluid Dynamics* (Elsevier)
- [25] Mukhopadhyay T, Mahata A, Adhikari S and Asle Zaeem M 2018 Probing the shear modulus of two-dimensional multiplanar nanostructures and heterostructures *Nanoscale* **10** 5280–94
- [26] Mukhopadhyay T, Mahata A, Adhikari S and Asle Zaeem M 2017 Effective mechanical properties of multilayer nano-heterostructures *Sci. Rep.* **7** 15818
- [27] Chandra Y, Mukhopadhyay T, Adhikari S and Figiel Ł 2020 Size-dependent dynamic characteristics of graphene based multi-layer nano hetero-structures *Nanotechnology* **31** 145705
- [28] Nestler B, Garcke H and Stinner B 2005 Multicomponent alloy solidification: phase-field modeling and simulations *Phys. Rev. E* **71** 041609
- [29] Martínez-Pañeda E, Golahmar A and Niordson C F 2018 A phase field formulation for hydrogen assisted cracking *Comput. Methods Appl. Mech. Eng.* **342** 742–61
- [30] Mianroodi J R et al 2022 Modeling and simulation of microstructure in metallic systems based on multi-physics approaches *npj Comput. Mater.* **8** 93
- [31] Dodaran M S, Muhammad M, Shamsaei N and Shao S 2022 Synergistic effect of microstructure and defects on the initiation of fatigue cracks in additively manufactured Inconel 718 *Int. J. Fatigue* **162** 107002
- [32] Anderson M, Grest G and Srolovitz D 1985 Grain growth in three dimensions: a lattice model *Scr. Metall.* **19** 225–30
- [33] Rollett A, Srolovitz D J, Doherty R and Anderson M 1989 Computer simulation of recrystallization in non-uniformly deformed metals *Acta Metall.* **37** 627–39
- [34] Torabi J and Ansari R 2020 Crack propagation in functionally graded 2D structures: a finite element phase-field study *Thin-Walled Struct.* **151** 106734
- [35] Li J, Ni B, Zhang T and Gao H 2018 Phase field crystal modeling of grain boundary structures and growth in polycrystalline graphene *J. Mech. Phys. Solids* **120** 36–48
- [36] Hirvonen P 2019 Phase field crystal modeling of two-dimensional materials
- [37] Stewart J A and Spearot D E 2016 Phase-field models for simulating physical vapor deposition and grain evolution of isotropic single-phase polycrystalline thin films *Comput. Mater. Sci.* **123** 111–20
- [38] Stewart J A and Spearot D E 2017 Phase-field simulations of microstructure evolution during physical vapor deposition of single-phase thin films *Comput. Mater. Sci.* **131** 170–7
- [39] Chen L-Q 2002 Phase-field models for microstructure evolution *Annu. Rev. Mater. Res.* **32** 113–40
- [40] Steinbach I 2013 Phase-field model for microstructure evolution at the mesoscopic scale *Annu. Rev. Mater. Res.* **43** 89–107
- [41] Zhang X, Chen A, Chen L and Zhou Z 2022 2D materials bridging experiments and computations for electro/photocatalysis *Adv. Energy Mater.* **12** 2003841
- [42] Patra L and Pandey R 2022 Mechanical properties of 2D materials: a review on molecular dynamics based nanoindentation simulations *Mater. Today Commun.* **31** 103623
- [43] Monk J, Yang Y, Mendelev M, Asta M, Hoyt J and Sun D 2009 Determination of the crystal-melt interface kinetic coefficient from molecular dynamics simulations *Model. Simul. Mat. Sci. Eng.* **18** 015004
- [44] Kavousi S, Novak B R, Moldovan D and Asle Zaeem M 2021 Quantitative prediction of rapid solidification by integrated atomistic and phase-field modeling *Acta Mater.* **211** 116885
- [45] Mounet N et al 2018 Two-dimensional materials from high-throughput computational exfoliation of experimentally known compounds *Nat. Nanotechnol.* **13** 246–52
- [46] Akinwande D et al 2017 A review on mechanics and mechanical properties of 2D materials—graphene and beyond *Extreme Mech. Lett.* **13** 42–77
- [47] Suter J L, Anderson R L, Greenwell H C and Coveney P V 2009 Recent advances in large-scale atomistic and coarse-grained molecular dynamics simulation of clay minerals *J. Mater. Chem.* **19** 2482–93
- [48] Herriott C, Li X, Kouraytem N, Tari V, Tan W, Anglin B, Rollett A D and Spear A D 2019 A multi-scale, multi-physics modeling framework to predict spatial variation of properties in additive-manufactured metals *Model. Simul. Mat. Sci. Eng.* **27** 025009
- [49] Yan W, Lian Y, Yu C, Kafka O L, Liu Z, Liu W K and Wagner G J 2018 An integrated process–structure–property modeling framework for additive manufacturing *Comput. Methods Appl. Mech. Eng.* **339** 184–204
- [50] Lebensohn R A, Kanjarla A K and Eisenlohr P 2012 An elasto-viscoplastic formulation based on fast Fourier transforms for the prediction of micromechanical fields in polycrystalline materials *Int. J. Plast.* **32** 59–69
- [51] Tari V, Lebensohn R A, Pokharel R, Turner T J, Shade P A, Bernier J V and Rollett A D 2018 Validation of micro-mechanical FFT-based simulations using high energy diffraction microscopy on Ti-7Al *Acta Mater.* **154** 273–83
- [52] Lyngby P and Thygesen K S 2022 Data-driven discovery of 2D materials by deep generative models *npj Comput. Mater.* **8** 232
- [53] Montes de Oca Zapiain D, Stewart J A and Dingreville R 2021 Accelerating phase-field-based microstructure evolution predictions via surrogate models trained by machine learning methods *npj Comput. Mater.* **7** 3
- [54] Vaupel Y, Hamacher N C, Caspari A, Mhamdi A, Kevrekidis I G and Mitsos A 2020 Accelerating nonlinear model predictive control through machine learning *J. Process Control* **92** 261–70
- [55] Alhada-Lahbabi K, Deleruyelle D and Gautier B 2023 Machine learning surrogate model for acceleration of ferroelectric phase-field modeling *ACS Appl. Electron. Mater.* **5** 3894–907
- [56] Wan X, Zhang Z, Yu W and Guo Y 2021 A density-functional-theory-based and machine-learning-accelerated hybrid method for intricate system catalysis *Mater. Rep. Energy* **1** 100046
- [57] Rhone T D, Chen W, Desai S, Torrisi S B, Larson D T, Yacoby A and Kaxiras E 2020 Data-driven studies of magnetic two-dimensional materials *Sci. Rep.* **10** 15795
- [58] Herriott C and Spear A D 2020 Predicting microstructure-dependent mechanical properties in additively manufactured metals with machine- and deep-learning methods *Comput. Mater. Sci.* **175** 109599
- [59] Islam M, Thakur M S H, Mojumder S and Hasan M N 2021 Extraction of material properties through multi-fidelity deep learning from molecular dynamics simulation *Comput. Mater. Sci.* **188** 110187

- [60] Song Y, Siriwardane E M D, Zhao Y and Hu J 2021 Computational discovery of new 2D materials using deep learning generative models *ACS Appl. Mater. Interfaces* **13** 53303–13
- [61] Lew A J, Yu C-H, Hsu Y-C and Buehler M J 2021 Deep learning model to predict fracture mechanisms of graphene *npj 2D Mater. Appl.* **5** 48
- [62] Hohenberg P and Kohn W 1964 Inhomogeneous electron gas *Phys. Rev.* **136** B864
- [63] Kohn W and Sham L J 1965 Self-consistent equations including exchange and correlation effects *Phys. Rev.* **140** A1133
- [64] Yang J and Whitfield J 2023 Machine-learning Kohn–Sham potential from dynamics in time-dependent Kohn–Sham systems *Mach. Learn. Sci. Technol.* **4** 035022
- [65] Engel E 2011 *Density Functional Theory* (Springer)
- [66] Hafner J, Wolvertson C and Ceder G 2006 Toward computational materials design: the impact of density functional theory on materials research *MRS Bull.* **31** 659–68
- [67] Saad Y, Chelikowsky J R and Shontz S M 2010 Numerical methods for electronic structure calculations of materials *SIAM Rev.* **52** 3–54
- [68] Sholl D S and Steckel J A 2022 *Density Functional Theory: A Practical Introduction* (Wiley)
- [69] Perdew J P, Burke K and Ernzerhof M 1996 Generalized gradient approximation made simple *Phys. Rev. Lett.* **77** 3865
- [70] Tao J, Perdew J P, Staroverov V N and Scuseria G E 2003 Climbing the density functional ladder: nonempirical meta-generalized gradient approximation designed for molecules and solids *Phys. Rev. Lett.* **91** 146401
- [71] Tao J, Perdew J, Ruzsinszky A, Scuseria G, Csonka G and Staroverov V 2007 Meta-generalized gradient approximation: non-empirical construction and performance of a density functional *Phil. Mag.* **87** 1071–84
- [72] Cohen A J, Mori-Sánchez P and Yang W 2008 Insights into current limitations of density functional theory *Science* **321** 792–4
- [73] Guo C, Zhou Y, Shi X-Q, Gan L-Y, Jiang H and Zhao Y 2016 Robust half-metallic ferromagnetism and curvature dependent magnetic coupling in fluorinated boron nitride nanotubes *Phys. Chem. Chem. Phys.* **18** 12307–11
- [74] van Gog H, Li W-F, Fang C, Koster R S, Dijkstra M and van Huis M 2019 Thermal stability and electronic and magnetic properties of atomically thin 2D transition metal oxides *npj 2D Mater. Appl.* **3** 18
- [75] Cococcioni M and De Gironcoli S 2005 Linear response approach to the calculation of the effective interaction parameters in the LDA+U method *Phys. Rev. B* **71** 035105
- [76] Li W, Xin X, Wang H, Guo C, Jiang H and Zhao Y 2018 Description of light-element magnetic systems via density functional theory plus U with an example system of fluorinated boron nitride: an efficient alternative to hybrid functional approach *Comput. Mater. Sci.* **146** 84–89
- [77] Lee C and Gonze X 1995 Ab initio calculation of the thermodynamic properties and atomic temperature factors of SiO₂ α -quartz and stishovite *Phys. Rev. B* **51** 8610
- [78] Petretto G, Dwaraknath S, Miranda H P C, Winston D, Giantomassi M, Van Setten M J, Gonze X, Persson K A, Hautier G and Rignanese G-M 2018 High-throughput density-functional perturbation theory phonons for inorganic materials *Sci. Data* **5** 1–12
- [79] Onida G, Reining L and Rubio A 2002 Electronic excitations: density-functional versus many-body Green's-function approaches *Rev. Mod. Phys.* **74** 601
- [80] Hybertsen M S and Louie S G 1986 Electron correlation in semiconductors and insulators: band gaps and quasiparticle energies *Phys. Rev. B* **34** 5390
- [81] Rohlfing M and Louie S G 2000 Electron-hole excitations and optical spectra from first principles *Phys. Rev. B* **62** 4927
- [82] Grimme S, Antony J, Ehrlich S and Krieg H 2010 A consistent and accurate ab initio parametrization of density functional dispersion correction (DFT-D) for the 94 elements H–Pu *J. Chem. Phys.* **132** 154104
- [83] Berland K, Cooper V R, Lee K, Schröder E, Thonhauser T, Hyldgaard P and Lundqvist B I 2015 van der Waals forces in density functional theory: a review of the vdW-DF method *Rep. Prog. Phys.* **78** 066501
- [84] Geim A K and Novoselov K S 2007 The rise of graphene *Nat. Mater.* **6** 183–91
- [85] Manzeli S, Ovchinnikov D, Pasquier D, Yazyev O V and Kis A 2017 2D transition metal dichalcogenides *Nature Rev. Mater.* **2** 1–15
- [86] Gjerding M N, Taghizadeh A, Rasmussen A, Ali S, Bertoldo F, Deilmann T, Knosgaard N R, Kruse M, Larsen A H and Manti S 2021 Recent progress of the computational 2D materials database (C2DB) *2D Mater.* **8** 044002
- [87] Gupta A, Sakthivel T and Seal S 2015 Recent development in 2D materials beyond graphene *Prog. Mater. Sci.* **73** 44–126
- [88] Shin H, Kang S, Koo J, Lee H, Kim J and Kwon Y 2014 Cohesion energetics of carbon allotropes: quantum Monte Carlo study *J. Chem. Phys.* **140** 114702
- [89] Koskinen P, Malola S and Häkkinen H 2008 Self-passivating edge reconstructions of graphene *Phys. Rev. Lett.* **101** 115502
- [90] Ivanovskaya V, Zobelli A, Teillet-Billy D, Rougeau N, Sidis V and Briddon P 2010 Hydrogen adsorption on graphene: a first principles study *Eur. Phys. J. B* **76** 481–6
- [91] Thomas S and Asle Zaeem M 2021 Superior sensing performance of two-dimensional ruthenium carbide (2D-RuC) in detection of NO, NO₂ and NH₃ gas molecules *Appl. Surf. Sci.* **563** 150232
- [92] Hussain G, Asghar M, Iqbal M W, Ullah H and Autieri C 2022 Exploring the structural stability, electronic and thermal attributes of synthetic 2D materials and their heterostructures *Appl. Surf. Sci.* **590** 153131
- [93] Thomas S, Thulaseedasan S and Asle Zaeem M 2022 Surface functionalization effect on physical properties and quantum capacitance of Ca₂C MXenes *FlatChem* **35** 100414
- [94] Pizzi G 2020 Open-science platform for computational materials science: aiiDA and the materials cloud *Handbook of Materials Modeling: Methods: Theory and Modeling* (Springer) pp 1813–35
- [95] Malý O I, Sopiha K V and Persson C 2019 Energy, phonon, and dynamic stability criteria of two-dimensional materials *ACS Appl. Mater. Interfaces* **11** 24876–84
- [96] Chew P Y and Reinhardt A 2023 Phase diagrams—why they matter and how to predict them *J. Chem. Phys.* **158** 030902
- [97] López-Galán O A, Boll T, Nogan J, Chassaing D, Welle A, Heilmaier M and Ramos M 2024 One-step sputtering of MoSSe metastable phase as thin film and predicted thermodynamic stability by computational methods *Sci. Rep.* **14** 7104
- [98] Shanmugam V, Mensah R A, Babu K, Gawusu S, Chanda A, Tu Y, Neisiany R E, Försth M, Sas G and Das O 2022 A review of the synthesis, properties, and applications of 2D materials *Part. Part. Syst. Charact.* **39** 2200031
- [99] Kim J H, Jeong J H, Kim N, Joshi R and Lee G-H 2018 Mechanical properties of two-dimensional materials and their applications *J. Phys. D: Appl. Phys.* **52** 083001
- [100] Born M 1940 On the stability of crystal lattices. I *Mathematical Proceedings of the Cambridge Philosophical Society* (Cambridge University Press)
- [101] Mouhat F and Coudert F-X 2014 Necessary and sufficient elastic stability conditions in various crystal systems *Phys. Rev. B* **90** 224104
- [102] Yorulmaz U, Özden A, Perkgöz N K, Ay F and Sevik C 2016 Vibrational and mechanical properties of single layer MXene structures: a first-principles investigation *Nanotechnology* **27** 335702

- [103] Roldán R, Chirrolli L, Prada E, Silva-Guillén J A, San-Jose P and Guinea F 2017 Theory of 2D crystals: graphene and beyond *Chem. Soc. Rev.* **46** 4387–99
- [104] Xiong Z, Zhong L, Wang H and Li X 2021 Structural defects, mechanical behaviors, and properties of two-dimensional materials *Materials* **14** 1192
- [105] Liu F, Ming P and Li J 2007 Ab initio calculation of ideal strength and phonon instability of graphene under tension *Phys. Rev. B* **76** 064120
- [106] Ibrahim Y, Mohamed A, Abdelgawad A M, Eid K, Abdullah A M and Elzatahry A 2020 The recent advances in the mechanical properties of self-standing two-dimensional MXene-based nanostructures: deep insights into the supercapacitor *Nanomaterials* **10** 1916
- [107] Guo Z, Zhou J, Si C and Sun Z 2015 Flexible two-dimensional $Tin+1Cn$ ($n = 1, 2$ and 3) and their functionalized MXenes predicted by density functional theories *Phys. Chem. Chem. Phys.* **17** 15348–54
- [108] Lee C, Wei X, Kysar J W and Hone J 2008 Measurement of the elastic properties and intrinsic strength of monolayer graphene *Science* **321** 385–8
- [109] Dubois S-M, Rignanese G-M, Pardo T and Charlier J-C 2006 Ideal strength of silicon: an ab initio study *Phys. Rev. B* **74** 235203
- [110] Clatterbuck D, Krenn C, Cohen M L and Morris J Jr 2003 Phonon instabilities and the ideal strength of aluminum *Phys. Rev. Lett.* **91** 135501
- [111] Thomas S, Manju M, Ajith K, Lee S and Asle Zaeem M 2020 Strain-induced work function in h-BN and BCN monolayers *Physica E* **123** 114180
- [112] Pető J, Dobrik G, Kukucska G, Vancsó P, Koós A A, Koltai J, Nemes-Incze P, Hwang C and Tapasztó L 2019 Moderate strain induced indirect bandgap and conduction electrons in MoS₂ single layers *npj 2D Mater. Appl.* **3** 39
- [113] Ibragimova R, Rinke P and Komsa H-P 2022 Native vacancy defects in MXenes at etching conditions *Chem. Mater.* **34** 2896–906
- [114] Banhart F, Kotakoski J and Krasheninnikov A V 2011 Structural defects in graphene *ACS Nano* **5** 26–41
- [115] Thomas S, Ajith K, Chandra S and Valsakumar M 2015 Temperature dependent structural properties and bending rigidity of pristine and defective hexagonal boron nitride *J. Phys.* **27** 315302
- [116] Bertoldo F, Ali S, Manti S and Thygesen K S 2022 Quantum point defects in 2D materials—the QPOD database *npj Comput. Mater.* **8** 56
- [117] Thomas S and Asle Zaeem M 2020 A new planar BCN lateral heterostructure with outstanding strength and defect-mediated superior semiconducting to metallic properties *Phys. Chem. Chem. Phys.* **22** 22066–77
- [118] Thomas S and Asle Zaeem M 2021 Phosgene Gas Sensing of Ti₂CT₂ (T = F–, O–, OH–) MXenes *Adv. Theor. Simul.* **4** 2000250
- [119] Sang X, Xie Y, Lin M-W, Alhabeab M, Van Aken K L, Gogotsi Y, Kent P R, Xiao K and Unocic R R 2016 Atomic defects in monolayer titanium carbide (Ti₃C₂T_x) MXene *ACS Nano* **10** 9193–200
- [120] Thomas S, Mayr F, Madam A K and Gagliardi A 2023 Machine learning and DFT investigation of CO, CO₂ and CH₄ adsorption on pristine and defective two-dimensional magnesene *Phys. Chem. Chem. Phys.* **25** 13170–82
- [121] Kirklin S, Saal J E, Meredig B, Thompson A, Doak J W, Aykol M, Rühl S and Wolverton C 2015 The open quantum materials database (OQMD): assessing the accuracy of DFT formation energies *npj Comput. Mater.* **1** 1–15
- [122] Wang R, Wang S and Wu X 2013 First-principles phonon calculations on the lattice dynamics and thermodynamics of rare-earth intermetallics TbCu and TbZn *Intermetallics* **43** 65–70
- [123] Siao M, Shen W, Chen R, Chang Z, Shih M, Chiu Y and Cheng C-M 2018 Two-dimensional electronic transport and surface electron accumulation in MoS₂ *Nat. Commun.* **9** 1442
- [124] Kurth S, Perdew J P and Blaha P 1999 Molecular and solid-state tests of density functional approximations: LSD, GGAs, and meta-GGAs *Int. J. Quantum Chem.* **75** 889–909
- [125] Heyd J, Peralta J E, Scuseria G E and Martin R L 2005 Energy band gaps and lattice parameters evaluated with the Heyd-Scuseria-Ernzerhof screened hybrid functional *J. Chem. Phys.* **123** 174101
- [126] Mermin N D and Ashcroft N W 2006 Hans Bethe's contributions to solid-state physics *Int. J. Modern Phys. B* **20** 2227–36
- [127] Liechtenstein A, Anisimov V I and Zaanen J 1995 Density-functional theory and strong interactions: orbital ordering in Mott-Hubbard insulators *Phys. Rev. B* **52** R5467
- [128] Carter E A 2008 Challenges in modeling materials properties without experimental input *Science* **321** 800–3
- [129] López-Galán O A, Perez I, Nogan J and Ramos M 2023 Determining the electronic structure and thermoelectric properties of MoS₂/MoSe₂ type-I heterojunction by DFT and the landauer approach *Adv. Mater. Interfaces* **10** 2202339
- [130] Hobbs D, Kresse G and Hafner J 2000 Fully unconstrained noncollinear magnetism within the projector augmented-wave method *Phys. Rev. B* **62** 11556
- [131] Mohn P 2002 *Magnetism in the Solid State: An Introduction* vol 134 (Springer Science & Business Media)
- [132] Zhang W-B, Qu Q, Zhu P and Lam C-H 2015 Robust intrinsic ferromagnetism and half semiconductivity in stable two-dimensional single-layer chromium trihalides *J. Mater. Chem. C* **3** 12457–68
- [133] Wang H, Fan F, Zhu S and Wu H 2016 Doping enhanced ferromagnetism and induced half-metallicity in CrI₃ monolayer *Europhys. Lett.* **114** 47001
- [134] Liu J, Sun Q, Kawazoe Y and Jena P 2016 Exfoliating biocompatible ferromagnetic Cr-trihalide monolayers *Phys. Chem. Chem. Phys.* **18** 8777–84
- [135] Huang B, Clark G, Navarro-Moratalla E, Klein D R, Cheng R, Seyler K L, Zhong D, Schmidgall E, McGuire M A and Cobden D H 2017 Layer-dependent ferromagnetism in a van der Waals crystal down to the monolayer limit *Nature* **546** 270–3
- [136] Jiang X, Liu Q, Xing J, Liu N, Guo Y, Liu Z and Zhao J 2021 Recent progress on 2D magnets: fundamental mechanism, structural design and modification *Appl. Phys. Rev.* **8** 031305
- [137] Kumar V, Dey A, Thomas S, Asle Zaeem M and Roy D R 2021 Hydrogen-induced tunable electronic and optical properties of a two-dimensional penta-Pt₂N₄ monolayer *Phys. Chem. Chem. Phys.* **23** 10409–17
- [138] Lau K W, Cocchi C and Draxl C 2019 Electronic and optical excitations of two-dimensional ZrS₂ and HfS₂ and their heterostructure *Phys. Rev. Mater.* **3** 074001
- [139] He F, Zhou Y, Ye Z, Cho S-H, Jeong J, Meng X and Wang Y 2021 Moiré patterns in 2D materials: a review *ACS Nano* **15** 5944–58
- [140] Ni G, Wang H, Wu J, Fei Z, Goldflam M, Keilmann F, Özyilmaz B, Castro Neto A, Xie X and Fogler M 2015 Plasmons in graphene moiré superlattices *Nat. Mater.* **14** 1217–22
- [141] Ramos M A, Chianelli R, Enriquez-Carrejo J L, Gonzalez G A and Berhault G 2014 Metallic states by angular dependence in 2H-MoS₂ slabs *Comput. Mater. Sci.* **84** 18–22
- [142] Thomas S, Madam A K and Asle Zaeem M 2020 Stone-wales defect induced performance improvement of BC₃ monolayer for high capacity lithium-ion rechargeable battery anode applications *J. Phys. Chem. C* **124** 5910–9
- [143] Moolayadukkam S, Thomas S, Sahoo R C, Lee C H, Lee S U and Matte H R 2020 Role of transition metals in layered double hydroxides for differentiating the oxygen evolution and nonenzymatic glucose sensing *ACS Appl. Mater. Interfaces* **12** 6193–204

- [144] Sahoo R C, Moolayadukkam S, Thomas S, Asle Zaeem M and Matte H R 2021 Solution processed Ni₂Co layered double hydroxides for high performance electrochemical sensors *Appl. Surf. Sci.* **541** 148270
- [145] Abdullahi I M, Thomas S, Gagliardi A, Asle Zaeem M and Nath M 2023 Nanostructured ternary nickel based mixed anionic (telluro)-selenide as a superior catalyst for oxygen evolution reaction *Energy Technol.* **11** 2300177
- [146] Rajput K, Kumar V, Thomas S, Asle Zaeem M and Roy D R 2021 Ca₂C MXene monolayer as a superior anode for metal-ion batteries *2D Mater.* **8** 035015
- [147] Thomas S, Jung H, Kim S, Jun B, Lee C H and Lee S U 2019 Two-dimensional haeckelite h567: a promising high capacity and fast Li diffusion anode material for lithium-ion batteries *Carbon* **148** 344–53
- [148] Wu H, Guo Z, Zhou J and Sun Z 2019 Vacancy-mediated lithium adsorption and diffusion on MXene *Appl. Surf. Sci.* **488** 578–85
- [149] Toyoura K, Koyama Y, Kuwabara A, Oba F and Tanaka I 2008 First-principles approach to chemical diffusion of lithium atoms in a graphite intercalation compound *Phys. Rev. B* **78** 214303
- [150] Li X, Zhu L, Xue Q, Chang X, Ling C and Xing W 2017 Superior selective CO₂ adsorption of C₃N pores: GCMC and DFT simulations *ACS Appl. Mater. Interfaces* **9** 31161–9
- [151] Kumar V, Azhikodan D and Roy D R 2021 2D Sb₂C₃ monolayer: a promising material for the recyclable gas sensor for environmentally toxic nitrogen-containing gases (NCGs) *J. Hazard. Mater.* **405** 124168
- [152] Wang Y, Du Y, Meng Y, Xie B, Ni Z and Xia S 2021 Monatomic Ti doped on defective monolayer boron nitride as an electrocatalyst for the synthesis of ammonia: a DFT study *Appl. Surf. Sci.* **563** 150277
- [153] Kumar S, Lyalin A, Huang Z and Taketsugu T 2022 Catalytic oxidative dehydrogenation of light alkanes over oxygen functionalized hexagonal boron nitride *ChemistrySelect* **7** e202103795
- [154] Gao G, O'Mullane A P and Du A 2017 2D MXenes: a new family of promising catalysts for the hydrogen evolution reaction *ACS Catal.* **7** 494–500
- [155] VahidMohammadi A, Rosen J and Gogotsi Y 2021 The world of two-dimensional carbides and nitrides (MXenes) *Science* **372** eabf1581
- [156] Deng D, Yu L, Pan X, Wang S, Chen X, Hu P, Sun L and Bao X 2011 Size effect of graphene on electrocatalytic activation of oxygen *Chem. Commun.* **47** 10016–8
- [157] Deng J, Li H, Xiao J, Tu Y, Deng D, Yang H, Tian H, Li J, Ren P and Bao X 2015 Triggering the electrocatalytic hydrogen evolution activity of the inert two-dimensional MoS₂ surface via single-atom metal doping *Energy Environ. Sci.* **8** 1594–601
- [158] Plummer G, Thomas S, Asle Zaeem M and Tucker G J 2022 Bond-order potential for the surface-terminated titanium carbide MXene monolayers Ti_{n+1} C_n T_x (n = 1, 2, or 3; T = – O or – F) *Phys. Rev. B* **106** 054105
- [159] Petersilka M, Gossmann U and Gross E 1996 Excitation energies from time-dependent density-functional theory *Phys. Rev. Lett.* **76** 1212
- [160] Runge E and Gross E K 1984 Density-functional theory for time-dependent systems *Phys. Rev. Lett.* **52** 997
- [161] Heyd J, Scuseria G E and Ernzerhof M 2003 Hybrid functionals based on a screened Coulomb potential *J. Chem. Phys.* **118** 8207–15
- [162] Thomas S, Kumar V, Roy D R and Asle Zaeem M 2020 Two-dimensional boron–phosphorus monolayer for reversible NO₂ gas sensing *ACS Appl. Nano Mater.* **3** 10073–81
- [163] Han S S, Kang J K, Lee H M, Van Duin A C and Goddard W A 2005 The theoretical study on interaction of hydrogen with single-walled boron nitride nanotubes. I. The reactive force field ReaxFF/HBN development *J. Chem. Phys.* **123** 114703
- [164] Brenner D W, Shenderova O A, Harrison J A, Stuart S J, Ni B and Sinnott S B 2002 A second-generation reactive empirical bond order (REBO) potential energy expression for hydrocarbons *J. Phys.: Condens. Matter* **14** 783
- [165] Ghaderzadeh S, Ladygin V, Ghorbani-Asl M, Hlawacek G, Schleberger M and Krashennnikov A V 2020 Freestanding and supported MoS₂ monolayers under cluster irradiation: insights from molecular dynamics simulations *ACS Appl. Mater. Interfaces* **12** 37454–63
- [166] Daw M S and Baskes M I 1984 Embedded-atom method: derivation and application to impurities, surfaces, and other defects in metals *Phys. Rev. B* **29** 6443
- [167] Albe K, Möller W and Heinig K-H 1997 Computer simulation and boron nitride *Radiat. Eff. Defects Solids* **141** 85–97
- [168] Los J, Kroes J, Albe K, Gordillo R, Katsnelson M and Fasolino A 2017 Extended Tersoff potential for boron nitride: energetics and elastic properties of pristine and defective h-BN *Phys. Rev. B* **96** 184108
- [169] Mortazavi B and Cuniberti G 2014 Mechanical properties of polycrystalline boron-nitride nanosheets *RSC Adv.* **4** 19137–43
- [170] Lee G-H, Cooper R C, An S J, Lee S, Van Der Zande A, Petrone N, Hammerberg A G, Lee C, Crawford B and Oliver W 2013 High-strength chemical-vapor-deposited graphene and grain boundaries *Science* **340** 1073–6
- [171] Kataria A, Verma A, Sanjay M and Siengchin S 2022 Molecular modeling of 2D graphene grain boundaries: mechanical and fracture aspects *Mater. Today* **52** 2404–8
- [172] Zhang X, Nguyen H, Zhang X, Ajayan P M, Wen J and Espinosa H D 2022 Atomistic measurement and modeling of intrinsic fracture toughness of two-dimensional materials *Proc. Natl Acad. Sci.* **119** e2206756119
- [173] Chen S J, Li C Y, Wang Q and Duan W H 2017 Reinforcing mechanism of graphene at atomic level: Friction, crack surface adhesion and 2D geometry *Carbon* **114** 557–65
- [174] Chaurasia A, Verma A, Parashar A and Mulik R S 2019 Experimental and computational studies to analyze the effect of h-BN nanosheets on mechanical behavior of h-BN/polyethylene nanocomposites *J. Phys. Chem. C* **123** 20059–70
- [175] Xiong S and Cao G 2015 Molecular dynamics simulations of mechanical properties of monolayer MoS₂ *Nanotechnology* **26** 185705
- [176] Hasanian M, Mortazavi B, Ostadhossein A, Rabczuk T and van Duin A C 2018 Hydrogenation and defect formation control the strength and ductility of MoS₂ nanosheets: reactive molecular dynamics simulation *Extreme Mech. Lett.* **22** 157–64
- [177] Luo S, Patole S, Anwer S, Li B, Delclos T, Gogotsi O, Zahorodna V, Balitskyi V and Liao K 2020 Tensile behaviors of Ti₃C₂T_x (MXene) films *Nanotechnology* **31** 395704
- [178] Wyatt B C, Rosenkranz A and Anasori B 2021 2D MXenes: tunable mechanical and tribological properties *Adv. Mater.* **33** 2007973
- [179] Borysiuk V N, Mochalin V N and Gogotsi Y 2015 Molecular dynamic study of the mechanical properties of two-dimensional titanium carbides Ti_{n+1}C_n (MXenes) *Nanotechnology* **26** 265705
- [180] Hatam-Lee S M, Esfandiari A and Rajabpour A 2021 Mechanical behaviors of titanium nitride and carbide MXenes: a molecular dynamics study *Appl. Surf. Sci.* **566** 150633
- [181] Deng Y, Chen Y, Liu H and Yan X 2022 The effects of the temperature and termination (-O) on the friction and adhesion properties of MXenes using molecular dynamics simulation *Nanomaterials* **12** 798
- [182] Plummer G, Anasori B, Gogotsi Y and Tucker G J 2019 Nanoindentation of monolayer Ti_{n+1}C_nT_x MXenes via atomistic simulations: the role of composition and defects on strength *Comput. Mater. Sci.* **157** 168–74

- [183] Wang Y, Zheng Y, Wang Z, Li X, Liang Y, Yan H and Wu F 2023 Theoretical prediction of two-dimensional Cr_3C_2 monolayer and its derivatives as potential electrode of Li-ion batteries *Comput. Mater. Sci.* **226** 112201
- [184] Penev E S, Marzari N and Yakobson B I 2021 Theoretical prediction of two-dimensional materials, behavior, and properties *ACS Nano* **15** 5959–76
- [185] Panico S, Larcher M, Marincioni V, Troi A, Baglivo C and Congedo P M 2023 Identifying key parameters through a sensitivity analysis for realistic hygrothermal simulations at wall level supported by monitored data *Build. Environ.* **229** 109969
- [186] Zhang N and Chen Y 2013 Nanoscale plastic deformation mechanism in single crystal aragonite *J. Mater. Sci.* **48** 785–96
- [187] Hong Y, Zhang N and Asle Zaeem M 2018 Metastable phase transformation and deformation twinning induced hardening-stiffening mechanism in compression of silicon nanoparticles *Acta Mater.* **145** 8–18
- [188] Tiwari S K, Pandey S K, Pandey R, Wang N, Bystrzejewski M, Mishra Y K and Zhu Y 2023 Stone–Wales defect in graphene *Small* **19** 2303340
- [189] Ma J, Alfé D, Michaelides A and Wang E 2009 Stone–Wales defects in graphene and other planar sp²-bonded materials *Phys. Rev. B* **80** 033407
- [190] Huang P Y, Ruiz-Vargas C S, Van Der Zande A M, Whitney W S, Levendof M P, Kevek J W, Garg S, Alden J S, Hustedt C J and Zhu Y 2011 Grains and grain boundaries in single-layer graphene atomic patchwork quilts *Nature* **469** 389–92
- [191] He L, Guo S, Lei J, Sha Z and Liu Z 2014 The effect of Stone–Thrower–Wales defects on mechanical properties of graphene sheets—A molecular dynamics study *Carbon* **75** 124–32
- [192] Park Y and Hyun S 2018 Size effect of defects on the mechanical properties of graphene *J. Korean Phys. Soc.* **72** 681–6
- [193] Zhang C, Zhou J, Zhang C-W and Chen X-F 2021 Effects of Stone–Wales and vacancy defects in fracture behavior of defective graphene *J. Phys.: Conf. Ser.* **2090** 012167
- [194] Carraro G, Savio L and Vattuone L 2022 Influence of defects and heteroatoms on the chemical properties of supported graphene layers *Coatings* **12** 397
- [195] Li M, Chen P, Zheng B, Deng T, Zhang Y, Liao Y and Zhou H 2019 Effect of stone-wales defect on mechanical properties of Gr/epoxy nanocomposites *Polymers* **11** 1116
- [196] Slotman G and Fasolino A 2012 Structure, stability and defects of single layer hexagonal BN in comparison to graphene *J. Phys.: Condens. Matter* **25** 045009
- [197] Sharma B B and Parashar A 2019 Atomistic simulations to study the effect of grain boundaries and hydrogen functionalization on the fracture toughness of bi-crystalline h-BN nanosheets *Phys. Chem. Chem. Phys.* **21** 13116–25
- [198] Islam Z and Haque A 2021 Defects and grain boundary effects in MoS_2 : a molecular dynamics study *J. Phys. Chem. Solids* **148** 109669
- [199] Damasceno D, Rajapakse R, Mesquita E and Pavanello R 2020 Atomistic simulation of tensile strength properties of graphene with complex vacancy and topological defects *Acta Mech.* **231** 3387–404
- [200] Zhang J, Sun R, Ruan D, Zhang M, Li Y, Zhang K, Cheng F, Wang Z and Wang Z-M 2020 Point defects in two-dimensional hexagonal boron nitride: a perspective *J. Appl. Phys.* **128** 100902
- [201] Patra T K, Zhang F, Schulman D S, Chan H, Cherukara M J, Terrones M, Das S, Narayanan B and Sankaranarayanan S K 2018 Defect dynamics in 2D MoS_2 probed by using machine learning, atomistic simulations, and high-resolution microscopy *ACS Nano* **12** 8006–16
- [202] Cui T, Mukherjee S, Sudeep P M, Colas G, Najafi F, Tam J, Ajayan P M, Singh C V, Sun Y and Filletter T 2020 Fatigue of graphene *Nat. Mater.* **19** 405–11
- [203] Liu P, Pei Q-X and Zhang Y-W 2023 Low-cycle fatigue failure of MoS_2 monolayer *Extreme Mech. Lett.* **58** 101942
- [204] Green M S 1954 Markoff random processes and the statistical mechanics of time-dependent phenomena. II. Irreversible processes in fluids *J. Chem. Phys.* **22** 398–413
- [205] Müller-Plathe F 1997 A simple nonequilibrium molecular dynamics method for calculating the thermal conductivity *J. Chem. Phys.* **106** 6082–5
- [206] Sirk T W, Moore S and Brown E F 2013 Characteristics of thermal conductivity in classical water models *J. Chem. Phys.* **138** 064505
- [207] Lv W and Henry A 2016 Direct calculation of modal contributions to thermal conductivity via Green–Kubo modal analysis *New J. Phys.* **18** 013028
- [208] Zhang Y, Pei Q and Wang C 2012 A molecular dynamics investigation on thermal conductivity of graphynes *Comput. Mater. Sci.* **65** 406–10
- [209] Si C, Wang X-D, Fan Z, Feng Z-H and Cao B-Y 2017 Impacts of potential models on calculating the thermal conductivity of graphene using non-equilibrium molecular dynamics simulations *Int. J. Heat Mass Transfer* **107** 450–60
- [210] Hu J, Ruan X and Chen Y P 2009 Thermal conductivity and thermal rectification in graphene nanoribbons: a molecular dynamics study *Nano Lett.* **9** 2730–5
- [211] Zhang H, Lee G and Cho K 2011 Thermal transport in graphene and effects of vacancy defects *Phys. Rev. B* **84** 115460
- [212] Wei N, Xu L, Wang H-Q and Zheng J-C 2011 Strain engineering of thermal conductivity in graphene sheets and nanoribbons: a demonstration of magic flexibility *Nanotechnology* **22** 105705
- [213] Yeo J J, Liu Z and Ng T Y 2012 Comparing the effects of dispersed Stone–Thrower–Wales defects and double vacancies on the thermal conductivity of graphene nanoribbons *Nanotechnology* **23** 385702
- [214] Cao A 2012 Molecular dynamics simulation study on heat transport in monolayer graphene sheet with various geometries *J. Appl. Phys.* **111** 083528
- [215] Ng T Y, Yeo J J and Liu Z 2012 A molecular dynamics study of the thermal conductivity of graphene nanoribbons containing dispersed Stone–Thrower–Wales defects *Carbon* **50** 4887–93
- [216] Yang D, Ma F, Sun Y, Hu T and Xu K 2012 Influence of typical defects on thermal conductivity of graphene nanoribbons: an equilibrium molecular dynamics simulation *Appl. Surf. Sci.* **258** 9926–31
- [217] Yu C and Zhang G 2013 Impacts of length and geometry deformation on thermal conductivity of graphene nanoribbons *J. Appl. Phys.* **113** 044306
- [218] Xu X, Pereira L F, Wang Y, Wu J, Zhang K, Zhao X, Bae S, Tinh Bui C, Xie R and Thong J T 2014 Length-dependent thermal conductivity in suspended single-layer graphene *Nat. Commun.* **5** 3689
- [219] Yang F, Yao Y, Jiang Y, Lu L, Ma Y and Dai W 2016 Sumoylation is important for stability, subcellular localization, and transcriptional activity of SALL4, an essential stem cell transcription factor *J. Biol. Chem.* **291** 428
- [220] Cao B-Y, Yao W-J and Ye Z-Q 2016 Networked nanoconstrictions: an effective route to tuning the thermal transport properties of graphene *Carbon* **96** 711–9
- [221] Wei Z, Ni Z, Bi K, Chen M and Chen Y 2011 In-plane lattice thermal conductivities of multilayer graphene films *Carbon* **49** 2653–8
- [222] Cao H-Y, Guo Z-X, Xiang H and Gong X-G 2012 Layer and size dependence of thermal conductivity in multilayer graphene nanoribbons *Phys. Lett. A* **376** 525–8
- [223] Lee P A and Fisher D S 1981 Anderson localization in two dimensions *Phys. Rev. Lett.* **47** 882
- [224] Ma T, Lin C-T and Wang Y 2020 The dimensionality effect on phonon localization in graphene/hexagonal boron nitride superlattices *2D Mater.* **7** 035029

- [225] Duong T-Q, Massobrio C, Ori G, Boero M and Martin E 2020 Thermal resistance of an interfacial molecular layer by first-principles molecular dynamics *J. Chem. Phys.* **153** 074704
- [226] Le N D, Davier B, Izitounene N, Dollfus P and Saint-Martin J 2022 Study of phonon transport across Si/Ge interfaces using full-band phonon Monte Carlo simulation *J. Comput. Electron.* **21** 744–55
- [227] Xie S, Zhu H, Zhang X and Wang H 2023 A brief review on the recent development of phonon engineering and manipulation at nanoscales *Int. J. Extrem. Manuf.* **6** 012007
- [228] Thomas J A, Turney J E, Iutzi R M, Amon C H and McGaughey A J 2010 Predicting phonon dispersion relations and lifetimes from the spectral energy density *Phys. Rev. B* **81** 081411
- [229] Wang G, Pandey R and Karna S P 2017 Physics and chemistry of oxidation of two-dimensional nanomaterials by molecular oxygen *Wiley Interdiscip. Rev.-Comput. Mol. Sci.* **7** e1280
- [230] Lotfi R, Naguib M, Yilmaz D E, Nanda J and Van Duin A C 2018 A comparative study on the oxidation of two-dimensional Ti_3C_2 MXene structures in different environments *J. Mater. Chem. A* **6** 12733–43
- [231] Osti N C, Naguib M, Ostadhossein A, Xie Y, Kent P R, Dyatkin B, Rother G, Heller W T, Van Duin A C and Gogotsi Y 2016 Effect of metal ion intercalation on the structure of MXene and water dynamics on its internal surfaces *ACS Appl. Mater. Interfaces* **8** 8859–63
- [232] Hou P, Tian Y, Xie Y, Du F, Chen G, Vojvodic A, Wu J and Meng X 2023 Unraveling the oxidation behaviors of MXenes in aqueous systems by active-learning-potential molecular-dynamics simulation *Angew. Chem.* **135** e202304205
- [233] Jiao Y, Kang Y, Yang C and Li D 2015 *Osmosis and Its Applications* (Springer) pp 2622–33
- [234] Dervin S, Dionysiou D D and Pillai S C 2016 2D nanostructures for water purification: graphene and beyond *Nanoscale* **8** 15115–31
- [235] Wang Y, He Z, Gupta K M, Shi Q and Lu R 2017 Molecular dynamics study on water desalination through functionalized nanoporous graphene *Carbon* **116** 120–7
- [236] Xu M, Liang T, Shi M and Chen H 2013 Graphene-like two-dimensional materials *Chem. Rev.* **113** 3766–98
- [237] Gupta K K, Mukhopadhyay T, Roy A and Dey S 2020 Probing the compound effect of spatially varying intrinsic defects and doping on mechanical properties of hybrid graphene monolayers *J. Mater. Sci. Technol.* **50** 44–58
- [238] Das S, Robinson J A, Dubey M, Terrones H and Terrones M 2015 Beyond graphene: progress in novel two-dimensional materials and van der Waals solids *Annu. Rev. Mater. Res.* **45** 1–27
- [239] Houssa M, van den Broek B, Iordanidou K, Lu A K A, Pourtois G, Locquet J-P, Afanas'ev V and Stesmans A 2016 Topological to trivial insulating phase transition in stanene *Nano Res.* **9** 774–8
- [240] Mahata A and Mukhopadhyay T 2018 Probing the chirality-dependent elastic properties and crack propagation behavior of single and bilayer stanene *Phys. Chem. Chem. Phys.* **20** 22768–82
- [241] Mukhopadhyay T, Mahata A, Adhikari S and Asle Zaeem M 2017 Effective elastic properties of two dimensional multiplanar hexagonal nanostructures *2D Mater.* **4** 025006
- [242] Geim A K 2009 Graphene: status and prospects *Science* **324** 1530–4
- [243] Bhimanapati G R, Kozuch D and Robinson J A 2014 Large-scale synthesis and functionalization of hexagonal boron nitride nanosheets *Nanoscale* **6** 11671–5
- [244] Raidongia K, Nag A, Hembam K, Waghmare U V, Datta R and Rao C 2010 BCN: a graphene analogue with remarkable adsorptive properties *Chemistry* **16** 149–57
- [245] Kara A, Enriquez H, Seitsonen A P, Voon L L Y, Vizzini S, Aufray B and Oughaddou H 2012 A review on silicene—new candidate for electronics *Surf. Sci. Rep.* **67** 1–18
- [246] Acun A, Zhang L, Bampoulis P, Farmanbar M V, van Houselt A, Rudenko A, Lingenfelder M, Brocks G, Poelsema B and Katsnelson M 2015 Germanene: the germanium analogue of graphene *J. Phys.: Condens. Matter* **27** 443002
- [247] Carvalho A, Wang M, Zhu X, Rodin A S, Su H and Castro Neto A H 2016 Phosphorene: from theory to applications *Nat. Rev. Mater.* **1** 1–16
- [248] Zhu F-F, Chen W-J, Xu Y, Gao C-L, Guan D-D, Liu C-H, Qian D, Zhang S-C and Jia J-F 2015 Epitaxial growth of two-dimensional stanene *Nat. Mater.* **14** 1020–5
- [249] Ranjan P, Lee J M, Kumar P and Vinu A 2020 Borophene: new sensation in flatland *Adv. Mater.* **32** 2000531
- [250] Lembke D, Bertolazzi S and Kis A 2015 Single-layer MoS₂ electronics *Acc. Chem. Res.* **48** 100–10
- [251] Rothschild A, Sloan J and Tenne R 2000 Growth of WS₂ nanotubes phases *J. Am. Chem. Soc.* **122** 5169–79
- [252] Eftekhari A 2017 Molybdenum diselenide (MoSe₂) for energy storage, catalysis, and optoelectronics *Appl. Mater. Today* **8** 1–17
- [253] Zhao W, Ghorannevis Z, Chu L, Toh M, Kloc C, Tan P-H and Eda G 2013 Evolution of electronic structure in atomically thin sheets of WS₂ and WSe₂ *ACS Nano* **7** 791–7
- [254] Ruppert C, Aslan B and Heinz T F 2014 Optical properties and band gap of single- and few-layer MoTe₂ crystals *Nano Lett.* **14** 6231–6
- [255] Zolyomi V, Wallbank J and Fal'ko V 2014 Silicene and germanene: tight-binding and first-principles studies (arXiv:1401.2365)
- [256] Lorenz T, Joswig J-O and Seifert G 2014 Stretching and breaking of monolayer MoS₂—an atomistic simulation *2D Mater.* **1** 011007
- [257] Debbichi L, Kim H, Björkman T, Eriksson O and Lebegue S 2016 First-principles investigation of two-dimensional trichalcogenide and sesquichalcogenide monolayers *Phys. Rev. B* **93** 245307
- [258] Lebegue S and Eriksson O 2009 Electronic structure of two-dimensional crystals from ab initio theory *Phys. Rev. B* **79** 115409
- [259] Cherukara M J, Narayanan B, Kinaci A, Sasikumar K, Gray S K, Chan M K and Sankaranarayanan S K 2016 *Ab initio*-based bond order potential to investigate low thermal conductivity of stanene nanostructures *J. Phys. Chem. Lett.* **7** 3752–9
- [260] Grantab R, Shenoy V B and Ruoff R S 2010 Anomalous strength characteristics of tilt grain boundaries in graphene *Science* **330** 946–8
- [261] Chang T and Gao H 2003 Size-dependent elastic properties of a single-walled carbon nanotube via a molecular mechanics model *J. Mech. Phys. Solids* **51** 1059–74
- [262] Scarpa F, Adhikari S and Phani A S 2009 Effective elastic mechanical properties of single layer graphene sheets *Nanotechnology* **20** 065709
- [263] Boldrin L, Scarpa F, Chowdhury R and Adhikari S 2011 Effective mechanical properties of hexagonal boron nitride nanosheets *Nanotechnology* **22** 505702
- [264] Shokrieh M M and Rafiee R 2010 Prediction of Young's modulus of graphene sheets and carbon nanotubes using nanoscale continuum mechanics approach *Mater. Des.* **31** 790–5
- [265] Gelin B R 1994 *Molecular Modeling of Polymer Structures and Properties* (Hanser-Gardner Publications)
- [266] Mukhopadhyay T and Adhikari S 2017 Effective in-plane elastic moduli of quasi-random spatially irregular hexagonal lattices *Int. J. Eng. Sci.* **119** 142–79
- [267] Sinha P and Mukhopadhyay T 2023 Programmable multi-physical mechanics of mechanical metamaterials *Mater. Sci. Eng. R* **155** 100745
- [268] Cornell W D, Cieplak P, Bayly C I, Gould I R, Merz K M, Ferguson D M, Spellmeyer D C, Fox T, Caldwell J W and Kollman P A 1995 A second generation force field for the

- simulation of proteins, nucleic acids, and organic molecules *J. Am. Chem. Soc.* **117** 5179–97
- [269] Brunier T M, Drew M G and Mitchell P C 1992 Molecular mechanics studies of molybdenum disulphide catalysts parameterisation of molybdenum and sulphur *Mol. Simul.* **9** 143–59
- [270] Radisavljevic B, Radenovic A, Brivio J, Giacometti V and Kis A 2011 Single-layer MoS₂ transistors *Nat. Nanotechnol.* **6** 147–50
- [271] Bronsema K D, De Boer J and Jellinek F 1986 On the structure of molybdenum diselenide and disulfide *Z. Anorg. Allg. Chem.* **540** 15–17
- [272] Schönfeld B, Huang J and Moss S 1983 Anisotropic mean-square displacements (MSD) in single-crystals of 2H- and 3R-MoS₂ *Acta Crystallogr. B* **39** 404–7
- [273] Wieting T and Verble J 1971 Infrared and Raman studies of long-wavelength optical phonons in hexagonal MoS₂ *Phys. Rev. B* **3** 4286
- [274] Ma X Z and Dai S S 1989 Ab initio studies on the electronic structure of the complexes containing Mo–S bond using relativistic effective core potentials *Acta Chim. Sin. English Ed.* **7** 201–8
- [275] Jiang J-W, Wang J-S and Li B 2009 Young's modulus of graphene: a molecular dynamics study *Phys. Rev. B* **80** 113405
- [276] Brenner D W 1990 Empirical potential for hydrocarbons for use in simulating the chemical vapor deposition of diamond films *Phys. Rev. B* **42** 9458–71
- [277] Alzebdeh K 2012 Evaluation of the in-plane effective elastic moduli of single-layered graphene sheet *Int. J. Mech. Mater. Des.* **8** 269–78
- [278] Alzebdeh K I 2014 An atomistic-based continuum approach for calculation of elastic properties of single-layered graphene sheet *Solid State Commun.* **177** 25–28
- [279] Sakhaee-Pour A 2009 Elastic properties of single-layered graphene sheet *Solid State Commun.* **149** 91–95
- [280] Woo S, Park H C and Son Y-W 2016 Poisson's ratio in layered two-dimensional crystals *Phys. Rev. B* **93** 075420
- [281] Mukhopadhyay T and Adhikari S 2016 Effective in-plane elastic properties of auxetic honeycombs with spatial irregularity *Mech. Mater.* **95** 204–22
- [282] Naskar S, Mukhopadhyay T, Sriramula S and Adhikari S 2017 Stochastic natural frequency analysis of damaged thin-walled laminated composite beams with uncertainty in micromechanical properties *Compos. Struct.* **160** 312–34
- [283] Saumya K, Naskar S and Mukhopadhyay T 2023 'Magic' of twisted multi-layered graphene and 2D nano-heterostructures *Nano Futures* **7** 032005
- [284] Singh A and Li Y 2023 Reliable machine learning potentials based on artificial neural network for graphene *Comput. Mater. Sci.* **227** 112272
- [285] Senfle T P, Hong S, Islam M M, Kylasa S B, Zheng Y, Shin Y K, Junkermeier C, Engel-Herbert R, Janik M J and Aktulga H M 2016 The ReaxFF reactive force-field: development, applications and future directions *npj Comput. Mater.* **2** 1–14
- [286] Rajasekaran G, Kumar R and Parashar A 2016 Tersoff potential with improved accuracy for simulating graphene in molecular dynamics environment *Mater. Res. Express* **3** 035011
- [287] Rowe P, Csányi G, Alfe D and Michaelides A 2018 Development of a machine learning potential for graphene *Phys. Rev. B* **97** 054303
- [288] Berger E, Lv Z-P and Komsa H-P 2023 Raman spectra of 2D titanium carbide MXene from machine-learning force field molecular dynamics *J. Mater. Chem. C* **11** 1311–9
- [289] Chan H, Narayanan B, Cherukara M J, Sen F G, Sasikumar K, Gray S K, Chan M K and Sankaranarayanan S K 2019 Machine learning classical interatomic potentials for molecular dynamics from first-principles training data *J. Phys. Chem. C* **123** 6941–57
- [290] Thiemann F L, Rowe P, Müller E A and Michaelides A 2020 Machine learning potential for hexagonal boron nitride applied to thermally and mechanically induced rippling *J. Phys. Chem. C* **124** 22278–90
- [291] Mortazavi B, Podryabinkin E V, Roche S, Rabczuk T, Zhuang X and Shapeev A V 2020 Machine-learning interatomic potentials enable first-principles multiscale modeling of lattice thermal conductivity in graphene/borophene heterostructures *Mater. Horiz.* **7** 2359–67
- [292] Tawfik S A, Isayev O, Stampfl C, Shapter J, Winkler D A and Ford M J 2019 Efficient prediction of structural and electronic properties of hybrid 2D materials using complementary DFT and machine learning approaches *Adv. Theor. Simul.* **2** 1800128
- [293] Eivari H A, Ghasemi S A, Tahmasbi H, Rostami S, Faraji S, Rasoulkhani R, Goedecker S and Amsler M 2017 Two-dimensional hexagonal sheet of TiO₂ *Chem. Mater.* **29** 8594–603
- [294] Miyazato I, Tanaka Y and Takahashi K 2018 Accelerating the discovery of hidden two-dimensional magnets using machine learning and first principle calculations *J. Phys.: Condens. Matter* **30** 06LT01
- [295] Zhang Z, Hong Y, Hou B, Zhang Z, Negahban M and Zhang J 2019 Accelerated discoveries of mechanical properties of graphene using machine learning and high-throughput computation *Carbon* **148** 115–23
- [296] Liu J, Zhang Y, Zhang Y, Kitipornchai S and Yang J 2022 Machine learning assisted prediction of mechanical properties of graphene/aluminium nanocomposite based on molecular dynamics simulation *Mater. Des.* **213** 110334
- [297] Wang X, Hong Y, Wang M, Xin G, Yue Y and Zhang J 2019 Mechanical properties of molybdenum diselenide revealed by molecular dynamics simulation and support vector machine *Phys. Chem. Chem. Phys.* **21** 9159–67
- [298] Malakar P, Thakur M S H, Nahid S M and Islam M M 2022 Data-driven machine learning to predict mechanical properties of monolayer transition-metal dichalcogenides for applications in flexible electronics *ACS Appl. Nano Mater.* **5** 16489–99
- [299] Wang X, Han D, Hong Y, Sun H, Zhang J and Zhang J 2019 Machine learning enabled prediction of mechanical properties of tungsten disulfide monolayer *ACS Omega* **4** 10121–8
- [300] Xu Y, Shi Q, Zhou Z, Xu K, Lin Y, Li Y, Zhang Z and Wu J 2022 Machine learning assisted insights into the mechanical strength of nanocrystalline graphene oxide *2D Mater.* **9** 035002
- [301] Mousavi S A and Montazeri A 2023 Predicting mechanical properties of defective h-BN nanosheets using data-driven models *Comput. Mater. Sci.* **228** 112380
- [302] Ramanathan E S and Chowdhury C 2023 Structural and electronic properties of two-dimensional materials: a machine-learning-guided prediction *ChemPhysChem* **24** e202300308
- [303] Zheng J, Sun X, Hu J, Wang S, Yao Z, Deng S, Pan X, Pan Z and Wang J 2021 Symbolic transformer accelerating machine learning screening of hydrogen and deuterium evolution reaction catalysts in MA₂Z₄ materials *ACS Appl. Mater. Interfaces* **13** 50878–91
- [304] Rajan A C, Mishra A, Satsangi S, Vaish R, Mizuseki H, Lee K-R and Singh A K 2018 Machine-learning-assisted accurate band gap predictions of functionalized MXene *Chem. Mater.* **30** 4031–8
- [305] Sterbentz R M, Haley K L and Island J O 2021 Universal image segmentation for optical identification of 2D materials *Sci. Rep.* **11** 5808
- [306] Willhelm D, Wilson N, Arroyave R, Qian X, Cagin T, Pachter R and Qian X 2022 Predicting van der Waals heterostructures by a combined machine learning and density functional theory approach *ACS Appl. Mater. Interfaces* **14** 25907–19

- [307] Shen Y and Zhu S 2023 Machine learning mechanical properties of defect-engineered hexagonal boron nitride *Comput. Mater. Sci.* **220** 112030
- [308] Yankovich A B, Röding M, Skärström V W, Ranjan A and Olsson E 2023 Convolution neural networks and position averaged convergent beam electron diffraction for determining the structure of 2D materials *Microsc. Microanal.* **29** 691–3
- [309] Saito Y, Shin K, Terayama K, Desai S, Onga M, Nakagawa Y, Itahashi Y M, Iwasa Y, Yamada M and Tsuda K 2019 Deep-learning-based quality filtering of mechanically exfoliated 2D crystals *npj Comput. Mater.* **5** 124
- [310] Lu B, Xia Y, Ren Y, Xie M, Zhou L, Vinai G, Morton S A, Wee A T, van der Wiel W G and Zhang W 2024 When machine learning meets 2D materials: a review *Adv. Sci.* **11** 2305277
- [311] Das S, Pegu H, Sahu K K, Nayak A K, Ramakrishna S, Datta D and Swayamjyoti S 2020 Machine learning in materials modeling—fundamentals and the opportunities in 2D materials *Synthesis, Modeling, and Characterization of 2D Materials, and Their Heterostructures* (Elsevier) pp 445–68
- [312] Gupta K, Mukhopadhyay T, Roy L and Dey S 2022 Hybrid machine-learning-assisted quantification of the compound internal and external uncertainties of graphene: towards inclusive analysis and design *Mater. Adv.* **3** 1160–81
- [313] Singh A, Chen X, Li Y, Koric S and Guleryuz E 2020 Development of artificial neural network potential for graphene *AIAA Scitech 2020 Forum*
- [314] Gupta K K, Mukhopadhyay T, Roy L and Dey S 2022 High-velocity ballistics of twisted bilayer graphene under stochastic disorder *Adv. Nano Res.* **12** 529–47
- [315] Gupta K, Roy A, Mukhopadhyay T, Roy L and Dey S 2022 Probing the stochastic fracture behavior of twisted bilayer graphene: efficient ANN based molecular dynamics simulations for complete probabilistic characterization *Mater. Today Commun.* **32** 103932
- [316] Gupta K, Mukhopadhyay T, Roy A, Roy L and Dey S 2021 Sparse machine learning assisted deep computational insights on the mechanical properties of graphene with intrinsic defects and doping *J. Phys. Chem. Solids* **155** 110111
- [317] Geim A K and Grigorieva I V 2013 Van der Waals heterostructures *Nature* **499** 419–25
- [318] Choudhary K, Garrity K F, Hartman S T, Pilania G and Tavazza F 2023 Efficient computational design of two-dimensional van der Waals heterostructures: band alignment, lattice mismatch, and machine learning *Phys. Rev. Mater.* **7** 014009
- [319] Choudhary K, Garrity K F, Reid A C, DeCost B, Biacchi A J, Hight Walker A R, Trautt Z, Hatrick-Simpers J, Kusne A G and Centrone A 2020 The joint automated repository for various integrated simulations (JARVIS) for data-driven materials design *npj Comput. Mater.* **6** 173
- [320] Dong R, Jacob A, Bourdais S and Sanvito S 2021 High-throughput bandstructure simulations of van der Waals hetero-bilayers formed by 1T and 2H monolayers *npj 2D Mater. Appl.* **5** 26
- [321] Mahata A, Mukhopadhyay T, Chakraborty S and Asle Zaeem M 2024 Atomistic simulation assisted error-inclusive Bayesian machine learning for probabilistically unraveling the mechanical properties of solidified metals *npj Comput. Mater.* **10** 22
- [322] Gupta S, Mukhopadhyay T and Kushvaha V 2023 Microstructural image based convolutional neural networks for efficient prediction of full-field stress maps in short fiber polymer composites *Def. Technol.* **24** 58–82
- [323] Chen C T and Gu G X 2023 Physics-informed deep-learning for elasticity: forward, inverse, and mixed problems *Adv. Sci.* **10** 2300439
- [324] Chew A K, Sender M, Kaplan Z, Chandrasekaran A, Browning A R, Kwak H S, Halls M D and Afzal M A F 2024 Advancing material property prediction: using physics-informed machine learning models for viscosity *J. Cheminform.* **16** 31
- [325] Sinha S and Arora S K 2020 van der Waals heterostructures based on liquid phase exfoliated MoS₂ and WS₂ nanosheets *Mater. Today* **21** 1840–5
- [326] Zhao S Y F et al 2018 Controlled electrochemical intercalation of graphene/h-BN van der Waals heterostructures *Nano Lett.* **18** 460–6
- [327] Novoselov K S, Geim A K, Morozov S V, Jiang D, Zhang Y, Dubonos S V, Grigorieva I V and Firsov A A 2004 Electric field effect in atomically thin carbon films *Science* **306** 666–9
- [328] Puthirath Balan A, Radhakrishnan S, Woellner C F, Sinha S K, Deng L, Reyes C D L, Rao B M, Paulose M, Neupane R and Apte A 2018 Exfoliation of a non-van der Waals material from iron ore hematite *Nat. Nanotechnol.* **13** 602–9
- [329] Wang D et al 2018 Mass production of large-sized, nonlayered 2D nanosheets: their directed synthesis by a rapid “Gel-Blowing” strategy, and applications in Li/Ni storage and catalysis *Adv. Mater.* **30** 1803569
- [330] Tran R, Xu Z, Radhakrishnan B, Winston D, Sun W, Persson K A and Ong S P 2016 Surface energies of elemental crystals *Sci. Data* **3** 1–13
- [331] Balan A P et al 2022 Non-van der Waals quasi-2D materials; recent advances in synthesis, emergent properties and applications *Mater. Today* **58** 164–200
- [332] Bhowmik S and Govind Rajan A 2022 Chemical vapor deposition of 2D materials: a review of modeling, simulation, and machine learning studies *iScience* **25** 103832
- [333] Nicolosi V, Chhowalla M, Kanatzidis M G, Strano M S and Coleman J N 2013 Liquid exfoliation of layered materials *Science* **340** 1226419
- [334] Backes C, Higgins T M, Kelly A, Boland C, Harvey A, Hanlon D and Coleman J N 2017 Guidelines for exfoliation, characterization and processing of layered materials produced by liquid exfoliation *Chem. Mater.* **29** 243–55
- [335] Huo C, Yan Z, Song X and Zeng H 2015 2D materials via liquid exfoliation: a review on fabrication and applications *Sci. Bull.* **60** 1994–2008
- [336] Hu C-X, Shin Y, Read O and Casiraghi C 2021 Dispersant-assisted liquid-phase exfoliation of 2D materials beyond graphene *Nanoscale* **13** 460–84
- [337] Yang S, Zhang P, Nia A S and Feng X 2020 Emerging 2D materials produced via electrochemistry *Adv. Mater.* **32** 1907857
- [338] Zhang X, Li Y, Mu W, Bai W, Sun X, Zhao M, Zhang Z, Shan F and Yang Z 2021 Advanced tape-exfoliated method for preparing large-area 2D monolayers: a review *2D Mater.* **8** 032002
- [339] Jayasena B, Reddy C and Subbiah S 2013 Separation, folding and shearing of graphene layers during wedge-based mechanical exfoliation *Nanotechnology* **24** 205301
- [340] Lee D, Lee B, Park K H, Ryu H J, Jeon S and Hong S H 2015 Scalable exfoliation process for highly soluble boron nitride nanoplatelets by hydroxide-assisted ball milling *Nano Lett.* **15** 1238–44
- [341] Anasori B, Lukatskaya M R and Gogotsi Y 2017 2D metal carbides and nitrides (MXenes) for energy storage *Nat. Rev. Mater.* **2** 1–17
- [342] Sokol M, Natu V, Kota S and Barsoum M W 2019 On the chemical diversity of the MAX phases *Trends Chem.* **1** 210–23
- [343] Naguib M, Mashtalir O, Carle J, Presser V, Lu J, Hultman L, Gogotsi Y and Barsoum M W 2012 Two-dimensional transition metal carbides *ACS Nano* **6** 1322–31
- [344] Zhou C, Zhao X, Xiong Y, Tang Y, Ma X, Tao Q, Sun C and Xu W 2022 A review of etching methods of MXene and applications of MXene conductive hydrogels *Eur. Polym. J.* **167** 111063

- [345] Wang J-B, Ren Z, Hou Y, Yan X-L, Liu P-Z, Zhang H, Zhang H-X and Guo J-J 2020 A review of graphene synthesis at low temperatures by CVD methods *New Carbon Mater.* **35** 193–208
- [346] Sun J, Lu C, Song Y, Ji Q, Song X, Li Q, Zhang Y, Zhang L, Kong J and Liu Z 2018 Recent progress in the tailored growth of two-dimensional hexagonal boron nitride via chemical vapour deposition *Chem. Soc. Rev.* **47** 4242–57
- [347] Zhang Y, Yao Y, Sendeku M G, Yin L, Zhan X, Wang F, Wang Z and He J 2019 Recent progress in CVD growth of 2D transition metal dichalcogenides and related heterostructures *Adv. Mater.* **31** 1901694
- [348] Liu H, Neal A T, Zhu Z, Luo Z, Xu X, Tománek D and Ye P D 2014 Phosphorene: an unexplored 2D semiconductor with a high hole mobility *ACS Nano* **8** 4033–41
- [349] Li L, Yu Y, Ye G J, Ge Q, Ou X, Wu H, Feng D, Chen X H and Zhang Y 2014 Black phosphorus field-effect transistors *Nat. Nanotechnol.* **9** 372–7
- [350] Ci L et al 2010 Atomic layers of hybridized boron nitride and graphene domains *Nat. Mater.* **9** 430–5
- [351] Nagashima A, Tejima N, Gamou Y, Kawai T and Oshima C 1996 Electronic states of monolayer hexagonal boron nitride formed on the metal surfaces *Surf. Sci.* **357** 307–11
- [352] Wang Q H, Kalantar-Zadeh K, Kis A, Coleman J N and Strano M S 2012 Electronics and optoelectronics of two-dimensional transition metal dichalcogenides *Nat. Nanotechnol.* **7** 699–712
- [353] Houssa M, Dimoulas A and Molle A 2015 Silicene: a review of recent experimental and theoretical investigations *J. Phys.: Condens. Matter* **27** 253002
- [354] Wang Y, Li J, Xiong J, Pan Y, Ye M, Guo Y, Zhang H, Quhe R and Lu J 2016 Does the Dirac cone of germanene exist on metal substrates? *Phys. Chem. Chem. Phys.* **18** 19451–6
- [355] Yadav A, Acosta C M, Dalpian G M and Malyi O I 2023 First-principles investigations of 2D materials: challenges and best practices *Matter* **6** 2711–34
- [356] Jain A, Ong S P, Hautier G, Chen W, Richards W D, Dacek S, Cholia S, Gunter D, Skinner D and Ceder G 2013 Commentary: the materials project: a materials genome approach to accelerating materials innovation *APL Mater.* **1** 011002
- [357] Lee A, Sarker S, Saal J E, Ward L, Borg C, Mehta A and Wolverton C 2022 Machine learned synthesizability predictions aided by density functional theory *Commun. Mater.* **3** 73
- [358] Haastrup S, Strange M, Pandey M, Deilmann T, Schmidt P S, Hinsche N F, Gjerding M N, Torelli D, Larsen P M and Riis-Jensen A C 2018 The computational 2D materials database: high-throughput modeling and discovery of atomically thin crystals *2D Mater.* **5** 042002
- [359] Zhou J, Shen L, Costa M D, Persson K A, Ong S P, Huck P, Lu Y, Ma X, Chen Y and Tang H 2019 2DMatPedia, an open computational database of two-dimensional materials from top-down and bottom-up approaches *Sci. Data* **6** 86
- [360] Ashton M, Paul J, Sinnott S B and Hennig R G 2017 Topology-scaling identification of layered solids and stable exfoliated 2D materials *Phys. Rev. Lett.* **118** 106101
- [361] Kabiraj A, Kumar M and Mahapatra S 2020 High-throughput discovery of high Curie point two-dimensional ferromagnetic materials *npj Comput. Mater.* **6** 35
- [362] Nascimento G M, Ogoshi E, Fazzio A, Acosta C M and Dalpian G M 2022 High-throughput inverse design and Bayesian optimization of functionalities: spin splitting in two-dimensional compounds *Sci. Data* **9** 195
- [363] Lauritsen J, Bollinger M, Lægsgaard E, Jacobsen K W, Nørskov J K, Clausen B, Topsøe H and Besenbacher F 2004 Atomic-scale insight into structure and morphology changes of MoS₂ nanoclusters in hydrotreating catalysts *J. Catal.* **221** 510–22
- [364] Byskov L S, Nørskov J K, Clausen B S and Topsøe H 2000 Edge termination of MoS₂ and CoMoS catalyst particles *Catal. Lett.* **64** 95–99
- [365] Schweiger H, Raybaud P, Kresse G and Toulhoat H 2002 Shape and edge sites modifications of MoS₂ catalytic nanoparticles induced by working conditions: a theoretical study *J. Catal.* **207** 76–87
- [366] Helveg S, Lauritsen J V, Lægsgaard E, Stensgaard I, Nørskov J K, Clausen B, Topsøe H and Besenbacher F 2000 Atomic-scale structure of single-layer MoS₂ nanoclusters *Phys. Rev. Lett.* **84** 951
- [367] Ramos M, Berhaut G, Ferrer D A, Torres B and Chianelli R R 2012 HRTEM and molecular modeling of the MoS₂-Co₉S₈ interface: understanding the promotion effect in bulk HDS catalysts *Catal. Sci. Technol.* **2** 164–78
- [368] Garcia A, Raya A M, Mariscal M M, Esparza R, Herrera M, Molina S I, Scavello G, Galindo P L, Jose-Yacamán M and Ponce A 2014 Analysis of electron beam damage of exfoliated MoS₂ sheets and quantitative HAADF-STEM imaging *Ultramicroscopy* **146** 33–38
- [369] Artyukhov V I, Liu Y and Yakobson B I 2012 Equilibrium at the edge and atomistic mechanisms of graphene growth *Proc. Natl Acad. Sci.* **109** 15136–40
- [370] Dong J, Zhang L, Wu B, Ding F and Liu Y 2021 Theoretical study of chemical vapor deposition synthesis of graphene and beyond: challenges and perspectives *J. Phys. Chem. Lett.* **12** 7942–63
- [371] Yang P, Zhang S, Pan S, Tang B, Liang Y, Zhao X, Zhang Z, Shi J, Huan Y and Shi Y 2020 Epitaxial growth of centimeter-scale single-crystal MoS₂ monolayer on Au (111) *ACS Nano* **14** 5036–45
- [372] Momeni K, Ji Y, Wang Y, Paul S, Neshani S, Yilmaz D E, Shin Y K, Zhang D, Jiang J-W and Park H S 2020 Multiscale computational understanding and growth of 2D materials: a review *npj Comput. Mater.* **6** 22
- [373] Mao Q, Feng M, Jiang X Z, Ren Y, Luo K H and van Duin A C 2023 Classical and reactive molecular dynamics: principles and applications in combustion and energy systems *Prog. Energy Combust. Sci.* **97** 101084
- [374] Paul S and Momeni K 2019 Mechanochemistry of stable diamane and atomically thin diamond films synthesis from bi- and multilayer graphene: a computational study *J. Phys. Chem. C* **123** 15751–60
- [375] Sangiovanni D G, Georgiev G and Kakanakova-Georgieva A 2018 *Ab initio* molecular dynamics of atomic-scale surface reactions: insights into metal organic chemical vapor deposition of AlN on graphene *Phys. Chem. Chem. Phys.* **20** 17751–61
- [376] Nie Y, Liang C, Cha P-R, Colombo L, Wallace R M and Cho K 2017 A kinetic Monte Carlo simulation method of van der Waals epitaxy for atomistic nucleation-growth processes of transition metal dichalcogenides *Sci. Rep.* **7** 2977
- [377] Zhang L, Zhu Y, Teng W, Xia T, Rong Y, Li N and Ma H 2017 A molecular dynamics simulation of the graphene growth on Cu (1 1 1) surface *Comput. Mater. Sci.* **130** 10–15
- [378] Toprak K and Bayazitoglu Y 2013 Numerical modeling of a CNT-Cu coaxial nanowire in a vacuum to determine the thermal conductivity *Int. J. Heat Mass Transfer* **61** 172–5
- [379] Zhang W and Van Duin A C 2020 Atomistic-scale simulations of the graphene growth on a silicon carbide substrate using thermal decomposition and chemical vapor deposition *Chem. Mater.* **32** 8306–17
- [380] Van Duin A C, Dasgupta S, Lorant F and Goddard W A 2001 ReaxFF: a reactive force field for hydrocarbons *J. Phys. Chem. A* **105** 9396–409
- [381] Meng L, Sun Q, Wang J and Ding F 2012 Molecular dynamics simulation of chemical vapor deposition graphene growth on Ni (111) surface *J. Phys. Chem. C* **116** 6097–102
- [382] Mueller J E, Van Duin A C and Goddard W A III 2010 Development and validation of ReaxFF reactive force field

- for hydrocarbon chemistry catalyzed by nickel *J. Phys. Chem. C* **114** 4939–49
- [383] Lu Y and Yang X 2015 Molecular simulation of graphene growth by chemical deposition on nickel using polycyclic aromatic hydrocarbons *Carbon* **81** 564–73
- [384] Liu S, Van Duin A C, Van Duin D M, Liu B and Edgar J H 2017 Atomistic insights into nucleation and formation of hexagonal boron nitride on nickel from first-principles-based reactive molecular dynamics simulations *ACS Nano* **11** 3585–96
- [385] Islam M A, Serles P, Kumral B, Demingos P G, Qureshi T, Meiyazhagan A, Puthirath A B, Abdullah M S B, Faysal S R and Ajayan P M 2022 Exfoliation mechanisms of 2D materials and their applications *Appl. Phys. Rev.* **9** 041301
- [386] Gao E, Lin S-Z, Qin Z, Buehler M J, Feng X-Q and Xu Z 2018 Mechanical exfoliation of two-dimensional materials *J. Mech. Phys. Solids* **115** 248–62
- [387] Sinclair R C, Suter J L and Coveney P V 2018 Graphene–graphene interactions: friction, superlubricity, and exfoliation *Adv. Mater.* **30** 1705791
- [388] Sinclair R C, Suter J L and Coveney P V 2019 Micromechanical exfoliation of graphene on the atomistic scale *Phys. Chem. Chem. Phys.* **21** 5716–22
- [389] Korhonen T and Koskinen P 2015 Peeling of multilayer graphene creates complex interlayer sliding patterns *Phys. Rev. B* **92** 115427
- [390] Tersoff J 1988 New empirical approach for the structure and energy of covalent systems *Phys. Rev. B* **37** 6991
- [391] Zhou G, Rajak P, Susarla S, Ajayan P M, Kalia R K, Nakano A and Vashishta P 2018 Molecular simulation of MoS₂ exfoliation *Sci. Rep.* **8** 16761
- [392] Abascal J L and Vega C 2005 A general purpose model for the condensed phases of water: TIP4P/2005 *J. Chem. Phys.* **123** 234505
- [393] Liang T, Phillpot S R and Sinnott S B 2009 Parametrization of a reactive many-body potential for Mo–S systems *Phys. Rev. B* **79** 245110
- [394] Ferrando N, Lachet V, Teuler J-M and Boutin A 2009 Transferable force field for alcohols and polyalcohols *J. Phys. Chem. A* **113** 5985–95
- [395] Fang Y, Li X, Li J, Yao C, Hoh H Y, Hai X, Lu J and Su C 2019 Janus electrochemical exfoliation of two-dimensional materials *J. Mater. Chem. A* **7** 25691–711
- [396] Lee O-S and Carignano M A 2015 Exfoliation of electrolyte-intercalated graphene: molecular dynamics simulation study *J. Phys. Chem. C* **119** 19415–22
- [397] Kavousi S and Asle Zaeem M 2021 Quantitative phase-field modeling of solute trapping in rapid solidification *Acta Mater.* **205** 116562
- [398] Gameiro M, Mischaikow K and Wanner T 2005 Evolution of pattern complexity in the Cahn–Hilliard theory of phase separation *Acta Mater.* **53** 693–704
- [399] Moelans N, Wendler F and Nestler B 2009 Comparative study of two phase-field models for grain growth *Comput. Mater. Sci.* **46** 479–90
- [400] Lotfolahpour A, Huber W and Asle Zaeem M 2023 A phase-field model for interactive evolution of phase transformation and cracking in superelastic shape memory ceramics *Comput. Mater. Sci.* **216** 111844
- [401] Mamivand M, Asle Zaeem M and El Kadiri H 2013 A review on phase field modeling of martensitic phase transformation *Comput. Mater. Sci.* **77** 304–11
- [402] DeWitt S and Thornton K 2017 *Phase Field Modeling of Microstructural Evolution*
- [403] Provatas N and Elder K 2011 *Phase-field Methods in Materials Science and Engineering* (Wiley)
- [404] Asadi E, Asle Zaeem M and Baskes M I 2014 Phase-field crystal model for Fe connected to MEAM molecular dynamics simulations *JOM* **66** 429–36
- [405] Elder K L M, Seymour M, Lee M, Hille M and Provatas N 2018 Two-component structural phase-field crystal models for graphene symmetries *Phil. Trans. R. Soc. A* **376** 20170211
- [406] Stewart J A 2022 Recent progress on the mesoscale modeling of architected thin-films via phase-field formulations of physical vapor deposition *Comput. Mater. Sci.* **211** 111503
- [407] Kavousi S, Novak B R, Asle Zaeem M and Moldovan D 2019 Combined molecular dynamics and phase field simulation investigations of crystal–melt interfacial properties and dendritic solidification of highly undercooled titanium *Comput. Mater. Sci.* **163** 218–29
- [408] Asle Zaeem M, El Kadiri H, Wang P T and Horstemeyer M F 2011 Investigating the effects of grain boundary energy anisotropy and second-phase particles on grain growth using a phase-field model *Comput. Mater. Sci.* **50** 2488–92
- [409] Asadi E and Asle Zaeem M 2015 A review of quantitative phase-field crystal modeling of solid–liquid structures *JOM* **67** 186–201
- [410] Elder K and Grant M 2004 Modeling elastic and plastic deformations in nonequilibrium processing using phase field crystals *Phys. Rev. E* **70** 051605
- [411] Greenwood M, Rottler J and Provatas N 2011 Phase-field-crystal methodology for modeling of structural transformations *Phys. Rev. E* **83** 031601
- [412] Greenwood M, Provatas N and Rottler J 2010 Free energy functionals for efficient phase field crystal modeling of structural phase transformations *Phys. Rev. Lett.* **105** 045702
- [413] Elder K R, Provatas N, Berry J, Stefanovic P and Grant M 2007 Phase-field crystal modeling and classical density functional theory of freezing *Phys. Rev. B* **75** 064107
- [414] Alster E, Montiel D, Thornton K and Voorhees P W 2017 Simulating complex crystal structures using the phase-field crystal model *Phys. Rev. Mater.* **1** 060801
- [415] Seymour M and Provatas N 2016 Structural phase field crystal approach for modeling graphene and other two-dimensional structures *Phys. Rev. B* **93** 035447
- [416] Wu K-A, Adland A and Karma A 2010 Phase-field-crystal model for fcc ordering *Phys. Rev. E* **81** 061601
- [417] Wu K-A, Plapp M and Voorhees P W 2010 Controlling crystal symmetries in phase-field crystal models *J. Phys.: Condens. Matter* **22** 364102
- [418] Mkhonta S K, Elder K R and Huang Z-F 2013 Exploring the complex world of two-dimensional ordering with three modes *Phys. Rev. Lett.* **111** 035501
- [419] Taha D, Mkhonta S K, Elder K R and Huang Z-F 2017 Grain boundary structures and collective dynamics of inversion domains in binary two-dimensional materials *Phys. Rev. Lett.* **118** 255501
- [420] Ankudinov V and Galenko P K 2022 Structure diagram and dynamics of formation of hexagonal boron nitride in phase-field crystal model *Phil. Trans. R. Soc. A* **380** 20200318
- [421] Jo G-B, Guzman J, Thomas C K, Hosur P, Vishwanath A and Stamper-Kurn D M 2012 Ultracold atoms in a tunable optical kagome lattice *Phys. Rev. Lett.* **108** 045305
- [422] Osterman N, Babič D, Poberaj I, Dobnikar J and Zihler P 2007 Observation of condensed phases of quasiplanar core-softened colloids *Phys. Rev. Lett.* **99** 248301
- [423] Vogt P, De Padova P, Quaresima C, Avila J, Frantzeskakis E, Asensio M C, Resta A, Ealet B and Le Lay G 2012 Silicene: compelling experimental evidence for graphenelike two-dimensional silicon *Phys. Rev. Lett.* **108** 155501
- [424] Chen Q, Bae S C and Granick S 2011 Directed self-assembly of a colloidal kagome lattice *Nature* **469** 381–4
- [425] Guo C, Wang J, Wang Z, Li J, Guo Y and Tang S 2015 Modified phase-field-crystal model for solid-liquid phase transitions *Phys. Rev. E* **92** 013309
- [426] Asadi E, Asle Zaeem M, Nouranian S and Baskes M I 2015 Quantitative modeling of the equilibration of two-phase

- solid-liquid Fe by atomistic simulations on diffusive time scales *Phys. Rev. B* **91** 024105
- [427] Emdadi A, Asle Zaeem M and Asadi E 2016 Revisiting phase diagrams of two-mode phase-field crystal models *Comput. Mater. Sci.* **123** 139–47
- [428] Schwalbach E J, Warren J A, Wu K-A and Voorhees P W 2013 Phase-field crystal model with a vapor phase *Phys. Rev. E* **88** 023306
- [429] Kocher G and Provatas N 2015 New density functional approach for solid-liquid-vapor transitions in pure materials *Phys. Rev. Lett.* **114** 155501
- [430] Jreidini P, Pinomaa T, Wiezorek J M K, McKeown J T, Laukkanen A and Provatas N 2021 Orientation gradients in rapidly solidified pure aluminum thin films: comparison of experiments and phase-field crystal simulations *Phys. Rev. Lett.* **127** 205701
- [431] Wang Z-L, Liu Z, Huang Z-F and Duan W 2020 Minimal phase-field crystal modeling of vapor-liquid-solid coexistence and transitions *Phys. Rev. Mater.* **4** 103802
- [432] Wang Z-L, Liu Z, Duan W and Huang Z-F 2022 Control of phase ordering and elastic properties in phase field crystals through three-point direct correlation *Phys. Rev. E* **105** 044802
- [433] Frick M J, Wilson E and Provatas N 2023 Consistent representation of vapor phases in phase field crystal dynamics *Phys. Rev. Mater.* **7** 023405
- [434] Seymour M 2018 *Study of Multi-point Interactions in PFC Models for Complex Structural Transformations* (McGill University)
- [435] Meca E, Lowengrub J, Kim H, Mattevi C and Shenoy V B 2013 Epitaxial graphene growth and shape dynamics on copper: phase-field modeling and experiments *Nano Lett.* **13** 5692–7
- [436] Bhaviripudi S, Jia X, Dresselhaus M S and Kong J 2010 Role of kinetic factors in chemical vapor deposition synthesis of uniform large area graphene using copper catalyst *Nano Lett.* **10** 4128–33
- [437] Hao Y *et al* 2013 The role of surface oxygen in the growth of large single-crystal graphene on copper *Science* **342** 720–3
- [438] Vlassiok I, Regmi M, Fulvio P, Dai S, Datskos P, Eres G and Smirnov S 2011 Role of hydrogen in chemical vapor deposition growth of large single-crystal graphene *ACS Nano* **5** 6069–76
- [439] Yan Z, Lin J, Peng Z, Sun Z, Zhu Y, Li L, Xiang C, Samuel E L, Kittrell C and Tour J M 2012 Toward the synthesis of wafer-scale single-crystal graphene on copper foils *ACS Nano* **6** 9110–7
- [440] Karma A and Plapp M 1998 Spiral surface growth without desorption *Phys. Rev. Lett.* **81** 4444–7
- [441] Rätz A and Voigt A 2005 *Edge Diffusion in Phase-Field Models for Epitaxial Growth* (Birkhäuser Basel)
- [442] Rätz A and Voigt A 2004 Phase-field model for island dynamics in epitaxial growth *Appl. Anal.* **83** 1015–25
- [443] Hu Z, Lowengrub J S, Wise S M and Voigt A 2012 Phase-field modeling of epitaxial growth: applications to step trains and island dynamics *Physica D* **241** 77–94
- [444] Otto F, Penzler P, Rätz A, Rump T and Voigt A 2003 A diffuse-interface approximation for step flow in epitaxial growth *Nonlinearity* **17** 477
- [445] Meca E, Shenoy V B and Lowengrub J 2013 Phase-field modeling of two-dimensional crystal growth with anisotropic diffusion *Phys. Rev. E* **88** 052409
- [446] Zhuang J, Zhao W, Qiu L, Xin J, Dong J and Ding F 2019 Morphology evolution of graphene during chemical vapor deposition growth: a phase-field theory simulation *J. Phys. Chem. C* **123** 9902–8
- [447] Xu X *et al* 2016 Ultrafast growth of single-crystal graphene assisted by a continuous oxygen supply *Nat. Nanotechnol.* **11** 930–5
- [448] Liu F, Li P, An H, Peng P, McLean B and Ding F 2022 Achievements and challenges of graphene chemical vapor deposition growth *Adv. Funct. Mater.* **32** 2203191
- [449] Wang Z-J, Weinberg G, Zhang Q, Lunkenbein T, Klein-Hoffmann A, Kurnatowska M, Plodinec M, Li Q, Chi L and Schlögl R 2015 Direct observation of graphene growth and associated copper substrate dynamics by in situ scanning electron microscopy *ACS Nano* **9** 1506–19
- [450] Ji Y, Momeni K and Chen L-Q 2021 A multiscale insight into the growth of h-BN: effect of the enclosure *2D Mater.* **8** 035033
- [451] Kavousi S, Novak B R, Hoyt J and Moldovan D 2020 Interface kinetics of rapid solidification of binary alloys by atomistic simulations: application to Ti-Ni alloys *Comput. Mater. Sci.* **184** 109854
- [452] Li J *et al* 2016 Impurity-induced formation of bilayered graphene on copper by chemical vapor deposition *Nano Res.* **9** 2803–10
- [453] Momeni K, Ji Y and Chen L-Q 2022 Computational synthesis of 2D materials grown by chemical vapor deposition *J. Mater. Res.* **37** 114–23
- [454] Azizi A, Gadinski M R, Li Q, AlSaud M A, Wang J, Wang Y, Wang B, Liu F, Chen L Q and Alem N 2017 High-performance polymers sandwiched with chemical vapor deposited hexagonal boron nitrides as scalable high-temperature dielectric materials *Adv. Mater.* **29** 1701864
- [455] Momeni K *et al* 2022 A computational framework for guiding the MOCVD-growth of wafer-scale 2D materials *npj Comput. Mater.* **8** 240
- [456] Habig K H 1986 Chemical vapor deposition and physical vapor deposition coatings: properties, tribological behavior, and applications *J. Vac. Sci. Technol. A* **4** 2832–43
- [457] Petrov I, Barna P, Hultman L and Greene J 2003 Microstructural evolution during film growth *J. Vac. Sci. Technol. A* **21** S117–28
- [458] Wadley H, Zhou X, Johnson R and Neurock M 2001 Mechanisms, models and methods of vapor deposition *Prog. Mater. Sci.* **46** 329–77
- [459] Stewart J A and Dingreville R 2020 Microstructure morphology and concentration modulation of nanocomposite thin-films during simulated physical vapor deposition *Acta Mater.* **188** 181–91
- [460] Stewart J A and Spearot D E 2018 Physical vapor deposition of multiphase materials with phase nucleation via a coupled phase-field approach *Comput. Mater. Sci.* **143** 71–79
- [461] Powers M, Stewart J A, Dingreville R, Derby B K and Misra A 2021 Compositionally-driven formation mechanism of hierarchical morphologies in co-deposited immiscible alloy thin films *Nanomaterials* **11** 2635
- [462] Adams C, Atzmon M, Cheng Y and Srolovitz D J 1992 Phase separation during co-deposition of Al-Ge thin films *J. Mater. Res.* **7** 653–66
- [463] Cui Y, Derby B, Li N and Misra A 2019 Design of bicontinuous metallic nanocomposites for high-strength and plasticity *Mater. Des.* **166** 107602
- [464] Mei F and Meng W 2010 Microstructural characteristic of vapor-phase sputter co-deposited Al-Ge nanocomposite thin films *Thin Solid Films* **518** 4299–303
- [465] Yang S, Zhong J, Chen M and Zhang L 2019 A parametric three-dimensional phase-field study of the physical vapor deposition process of metal thin films aiming at quantitative simulations *Coatings* **9** 607
- [466] Simmons J P, Wen Y, Shen C and Wang Y Z 2004 Microstructural development involving nucleation and growth phenomena simulated with the phase field method *Mater. Sci. Eng.* **365** 136–43
- [467] Simmons J, Shen C and Wang Y 2000 Phase field modeling of simultaneous nucleation and growth by explicitly incorporating nucleation events *Scr. Mater.* **43** 935–42
- [468] Jiang Y, Sridhar S, Liu Z, Wang D, Zhou H, Deng J, Chew H B and Ke C 2023 The interplay of intra- and inter-layer interactions in bending rigidity of ultrathin 2D materials *Appl. Phys. Lett.* **122** 153101

- [469] Chen X, Yi C and Ke C 2015 Bending stiffness and interlayer shear modulus of few-layer graphene *Appl. Phys. Lett.* **106** 101907
- [470] Guo Y, Qiu J and Guo W 2016 Mechanical and electronic coupling in few-layer graphene and hBN wrinkles: a first-principles study *Nanotechnology* **27** 505702
- [471] Qu W, Bagchi S, Chen X, Chew H B and Ke C 2019 Bending and interlayer shear moduli of ultrathin boron nitride nanosheet *J. Phys. D: Appl. Phys.* **52** 465301
- [472] Jabbour M E and Bhattacharya K 2003 A continuum theory of multispecies thin solid film growth by chemical vapor deposition *J. Elast.* **73** 13–74
- [473] Marcus M S, Simmons J M, Baker S E, Hamers R J and Eriksson M A 2009 Predicting the results of chemical vapor deposition growth of suspended carbon nanotubes *Nano Lett.* **9** 1806–11
- [474] Yoshihara N, Tahara Y and Noda M 2023 Machine learning method for determining chemical vapor deposition conditions for large-area graphene growth *Asia-Pac. J. Chem. Eng.* **18** e2911
- [475] Zeng Q, Gao Y, Guan K, Liu J and Feng Z 2021 Machine learning and a computational fluid dynamic approach to estimate phase composition of chemical vapor deposition boron carbide *J. Adv. Ceram.* **10** 537–50
- [476] Costine A, Delsa P, Li T, Reinke P and Balachandran P V 2020 Data-driven assessment of chemical vapor deposition grown MoS₂ monolayer thin films *J. Appl. Phys.* **128** 235303
- [477] Lu M, Ji H, Zhao Y, Chen Y, Tao J, Ou Y, Wang Y, Huang Y, Wang J and Hao G 2022 Machine learning-assisted synthesis of two-dimensional materials *ACS Appl. Mater. Interfaces* **15** 1871–8
- [478] Li Z, Lee J, Yao F and Sun H 2021 Quantifying the CVD-grown two-dimensional materials via image clustering *Nanoscale* **13** 15324–33
- [479] Wang L-W 2002 Charge-density patching method for unconventional semiconductor binary systems *Phys. Rev. Lett.* **88** 256402
- [480] Wang L-W, Zhao Z and Meza J 2008 Linear-scaling three-dimensional fragment method for large-scale electronic structure calculations *Phys. Rev. B* **77** 165113
- [481] White A 2012 The materials genome initiative: one year on *MRS Bull.* **37** 715–6
- [482] Cohen A J, Mori-Sánchez P and Yang W 2012 Challenges for density functional theory *Chem. Rev.* **112** 289–320
- [483] Jiang X Z, Feng M, Zeng W and Luo K H 2019 Study of mechanisms for electric field effects on ethanol oxidation via reactive force field molecular dynamics *Proc. Combust. Inst.* **37** 5525–35
- [484] Shen F, Liu G, Liu C, Zhang Y and Yang L 2024 Corrosion and oxidation on iron surfaces in chloride contaminated electrolytes: insights from ReaxFF molecular dynamic simulations *J. Mater. Res. Technol.* **29** 1305–12
- [485] Günay M G, Kemerli U, Karaman C, Karaman O, Güngör A and Karimi-Maleh H 2023 Review of functionalized nano porous membranes for desalination and water purification: MD simulations perspective *Environ. Res.* **217** 114785
- [486] Lin Y-C, Torsi R, Younas R, Hinkle C L, Rigosi A F, Hill H M, Zhang K, Huang S, Shuck C E and Chen C 2023 Recent advances in 2D material theory, synthesis, properties, and applications *ACS Nano* **17** 9694–747
- [487] Pan X, Jin H, Ku X and Fan J 2023 The atom sampling method for mesoscale molecular dynamics and its application to graphene assemblies *Phys. Chem. Chem. Phys.* **25** 19727–39
- [488] Trinh M-C and Mukhopadhyay T 2021 Semi-analytical atomic-level uncertainty quantification for the elastic properties of 2D materials *Mater. Today Nano* **15** 100126
- [489] Mukhopadhyay T, Mahata A, Naskar S and Adhikari S 2020 Probing the effective Young's Modulus of 'Magic Angle' inspired multi-functional twisted nano-heterostructures *Adv. Theor. Simul.* **3** 2000129
- [490] Chandra Y, Adhikari S, Mukherjee S and Mukhopadhyay T 2022 Unfolding the mechanical properties of buckypaper composites: nano- to macro-scale coupled atomistic-continuum simulations *Eng. Comput.* **38** 5199–229
- [491] Chandra Y, Saavedra Flores E I and Adhikari S 2020 Buckling of 2D nano hetero-structures with moire patterns *Comput. Mater. Sci.* **177** 109507
- [492] Chandra Y, Adhikari S, Saavedra Flores E I and Figiel E 2020 Advances in finite element modelling of graphene and associated nanostructures *Mater. Sci. Eng. R* **140** 100544
- [493] Asadi E and Asle Zaeem M 2015 Quantifying a two-mode phase-field crystal model for BCC metals at melting point *Comput. Mater. Sci.* **105** 101–9
- [494] Gupta T, Zaki M and Krishnan N M A 2022 MatSciBERT: a materials domain language model for text mining and information extraction *npj Comput. Mater.* **8** 102
- [495] Beltagy I, Lo K and Cohan A 2019 SciBERT: a pretrained language model for scientific text (arXiv:1903.10676)
- [496] Singh V, Patra S, Murugan N A, Toncu D-C and Tiwari A 2022 Recent trends in computational tools and data-driven modeling for advanced materials *Mater. Adv.* **3** 4069–87
- [497] Kobayashi K and Alam S B 2024 Explainable, interpretable, and trustworthy AI for an intelligent digital twin: a case study on remaining useful life *Eng. Appl. Artif. Intell.* **129** 107620